1188

TRANSPORTATION RESEARCH RECORD

Effects of Geosynthetics on Soil Properties and of Environment on Pavement Systems

TRANSPORTATION RESEARCH BOARD
NATIONAL RESEARCH COUNCIL
WASHINGTON, D.C. 1988

Transportation Research Record 1188
Price: $12.00
Editor: Elizabeth W. Kaplan

modes
1 highway transportation
2 public transit
3 rail transportation

subject areas
24 pavement design and performance
62 soil foundations
63 soil and rock mechanics

Transportation Research Board publications are available by ordering directly from TRB. They may also be obtained on a regular basis through organizational or individual affiliation with TRB; affiliates or library subscribers are eligible for substantial discounts. For further information, write to the Transportation Research Board, National Research Council, 2101 Constitution Avenue, N.W., Washington, D.C. 20418.

Printed in the United States of America

Library of Congress Cataloging-in-Publication Data
National Research Council. Transportation Research Board.

Effects of geosynthetics on soil properties and of environment on pavement systems.

(Transportation research record, ISSN 0361-1981 ; 1188)
ISBN 0-309-04757-9
1. Roads—Subgrades. 2. Soil stabilization. 3. Geosynthetics. 4. Pavements—Environmental aspects. I. National Research Council (U.S.). Transportation Research Board. II. Series.
TE7.H5 no. 1188 [TE210.4] 380.5 s—dc20 [625.7'35] 89-12859 CIP

Sponsorship of Transportation Research Record 1188

GROUP 2—DESIGN AND CONSTRUCTION OF TRANSPORTATION FACILITIES
Chairman: David S. Gedney, Harland Bartholomew & Associates

Geology and Properties of Earth Materials Section
Chairman: C. William Lovell, Purdue University

Committee on Soil and Rock Properties
Chairman: James J. Schnabel, Schnabel Engineering Associates
Robert C. Bachus, S. S. Bandyopadhyay, Robert K. Barrett, Roy H. Borden, Timothy Bowen, Carl D. Ealy, William H. Highter, Robert D. Holtz, Richard H. Howe, Robert B. Johnson, Ernest Jonas, C. William Lovell, Priscilla P. Nelson, Gerald P. Raymond, Surendra K. Saxena, J. Allan Tice, Mehmet T. Tumay, John L. Walkinshaw, Gary C. Whited

Committee on Environmental Factors Except Frost
Chairman: Malcolm L. Steinberg, Texas State Department of Highways and Public Transportation
S. S. Bandyopadhyay, Warren T. Bennett, Michael L. Bunting, Fu Hua Chen, Barry J. Dempsey, Donald G. Fohs, Donald J. Janssen, Badru M. Kiggundu, Amos Komornik, C. William Lovell, Robert L. Lytton, Said Ossama Mazen, R. Gordon McKeen, James B. Nevels, Jr., Zvi Ofer, Thomas M. Petry, Rogel H. Prysock, Albert C. Ruckman, Larry A. Scofield, Joe P. Sheffield, Shiraz D. Tayabji, T. Paul Teng, John L. Walkinshaw, William G. Weber, Jr., Gdalyah Wiseman

G. P. Jayaprakash, Transportation Research Board staff

Sponsorship is indicated by a footnote at the end of each paper. The organizational units, officers, and members are as of December 31, 1987.

Transportation Research Record 1188

Contents

Foreword

Pull-out interaction properties are the fundamental design parameters for reinforced soil systems. Because of the importance of understanding these properties, many studies of nonextensible reinforcements have been conducted. Similar studies on extensible reinforcements are needed because of the rapid development of a large number of geosynthetic reinforcements. The first five papers in this Record are on the effects of geosynthetics on soil properties.

Bonczkiewicz et al. describe a laboratory evaluation of the interaction between soil and various types of reinforcements such as geotextiles, geogrids, and metal and fiber strips. They discuss the observed stress-strain behavior. The laboratory study by Haas et al. is on geogrid reinforcement of granular base layers of flexible pavements. Bathurst and Jarrett present data from a large-scale test program conducted to evaluate prefabricated flexible polymeric soil confinement systems that are used to improve the trafficability and load-bearing capacity of thin granular bases placed over highly compressible subgrades. Juran and Chen present a soil-reinforcement load transfer model and an interpretation procedure for pull-out tests on extensible reinforcements. Lentz and Pyatt describe a mechanism of soil-geogrid interaction that they used to explain the results of their laboratory pull-out tests.

Cedergren describes damage to pavements caused by water and the benefits of providing internal drainage to rapidly remove all water that enters. Fan and Lovell describe field soil erosion tests that were conducted to extend the applicability of the Universal Soil Loss Equation to highway slopes that are steeper than 18 percent.

Evaluation of Soil-Reinforcement Interaction by Large-Scale Pull-Out Tests

C. BONCZKIEWICZ, B. R. CHRISTOPHER, AND D. K. ATMATZIDIS

Pull-out tests were conducted to evaluate soil-reinforcement interaction for various types of geotextiles and geogrids under varying normal load and soil conditions. All tests were performed using a 4.4 ft × 2.3 ft × 1.5 ft pull-out box and consistent test procedures. Iterative strain measurements were made using wire extensometers mounted along the length of the material to evaluate in-soil strain response and stress transfer. In all, 10 different reinforcement materials were evaluated, including slit-film and coarse woven geotextiles, needle-punched and heat-bonded nonwoven geotextiles, and two types of geogrid. In addition, comparative results were obtained for metal and fiber strip reinforcements. Pull-out resistance was reported as a function of applied normal load. Soil-reinforcement resistance coefficients were found by several methods and are presented as shear stress versus normal stress plots. Load transfer behavior is discussed in terms of observed stress-strain behavior.

Soil reinforcement with geosynthetics has been practiced for about two decades, and substantial research has been conducted to evaluate the interaction between soils and geosynthetic reinforcement in order to determine resistance of the material to sliding. Until now it has been difficult to compare various methods of evaluating sliding resistance because of inconsistencies among test methods, equipment, and interpretive methods. To alleviate this situation, large-scale pull-out tests were performed as part of an extensive laboratory and field investigation of reinforced soil behavior.

The study, sponsored by the FHWA, included reinforcement materials representing all types currently available. The portion of the results concerning geosynthetics and strip reinforcements is presented here.

Using a uniform pull-out test procedure, pull-out resistance and coefficient of resistance were found for 10 types of reinforcement. The materials included geotextiles, geogrids, and strip-type reinforcements. A series of tests was performed at varying normal stresses using gravel, sand, silt, and clay as the test medium.

Results are presented as plots of maximum pull-out resistance versus test normal stress. A soil-reinforcement resistance angle in sand was also determined for each type of reinforcement. Iterative strain information obtained during testing was used to examine different methods of evaluating this parameter. Examples of plots of maximum pull-out force versus embedment length and maximum shear stress versus normal stress are presented. Finally, an attempt to define the in-soil stress-strain response, along with the stress distribution in reinforcements during the pull-out test, is discussed.

C. Bonczkiewicz, Northwestern University, Evanston, Ill. and STS Consultants Ltd., 111 Phingsten Road, Northbrook, Ill. B. R. Christopher, STS Consultants Ltd., 111 Phingsten Road, Northbrook, Ill. D. K. Atmatzidis, Department of Civil Engineering, University of Patras, Patras, Greece.

BACKGROUND

Pull-out testing generally consists of measuring the force necessary to pull a specimen out of a soil mass. This force expressed per unit width of reinforcing material is commonly referred to as pull-out resistance. Pull-out stress is the force expressed per area of material.

Some researchers have concentrated on developing a method of obtaining a soil-reinforcement resistance coefficient (δ), which could be used in the shear strength relation

$$\tau = n \tan \delta \quad (1)$$

where τ is shear (or pull-out) stress and n is normal stress.

If the load distribution on the test material is unknown, the pull-out force is often assumed to be evenly distributed over the total area of reinforcement. The total area coefficient (δ) then is the slope of a maximum pull-out stress versus normal stress plot. Often this coefficient is approximated to be equal to $\frac{2}{3}\ \phi_{soil}$ (*1*).

Solomone et al. (*2*) presented another methodology for obtaining a pull-out coefficient by finding an interaction parameter designated K_r where K_r was the slope of the relationship between a pull-out force and the mobilized embedded length of reinforcement. K_r was related to a soil/reinforcement resistance angle δ by

$$K_r/2b = N \tan \delta \quad (2)$$

where

b = reinforcement width,
N = normal pressure, and
K_r = interaction parameter.

The stress distribution in extensible reinforcements during a pull-out test has been studied by several investigators who obtained deformation measurements along the length

TABLE 1 PULL-OUT TEST PROGRAM

Reinforcement Type	Gravel	Sand	Silt	Clay
Geotextiles				
Coarse woven		5,10,15		
Smooth woven	1,2,5	1,2,5	2,5	5
Needled nonwoven		1,5	5,15	5
Heat-bonded nonwoven		4,2,5		
Geogrids				
Extruded 1 × 1		3,4,6		
Extruded 1 × 4	2,4,8	2,4,8	15	5,15
Welded 3 × 3		3,4,6		
Welded 1.5 × 4	2,4,8	2,4,8		
Strips				
Fiber		5,15,37	5,15	
Metal		5,15,37		

NOTE: Values are normal stress used for test (psi).

of pull-out specimens. Most [*3–5* and R. D. Holtz, Laboratory Studies of Reinforced Earth Using a Woven Plastic Material (unpublished technical report), October 1973] concluded that stress is maximum near the application point and decreases with some function to zero at or before the end of the pull-out sample.

One complication in determining the distribution of stresses is the apparent increase in stress-strain modulus of geosynthetics with confinement. Loads up to twice the unconfined strength values for nonwoven geotextiles were reported (*3, 6, 7*). Increased modulus values for woven geotextiles have also been found (*8*).

Because the analysis methods presented have been used on data from a variety of pull-out test procedures, comparisons of the findings are limited. This study attempted to employ the latest equipment studies (*9, 10*) in the design of the pull-out box and the modification of basic test procedures. The procedures used are described, and, because they were consistent throughout the test program, results can be compared.

EXPERIMENTAL INVESTIGATION

Throughout this test program, test conditions varied only with normal stress, soil type, and reinforcement type. A description of procedures and reinforcement conditions tested follows.

Test Program

The test program was developed to test a wide range of reinforcement materials under a wide range of test conditions. Most of the research was conducted with sand-type soil as the standard; some tests were performed in soils with larger and smaller grain sizes for comparison. Tests using a number of normal loads were performed with the same sample-soil combination to develop a relationship between maximum pull-out force and normal stress. The test program is given in Table 1.

Materials

Reinforcements

The reinforcing materials in this program included geotextiles, polymer grids, and two types of strips. Select physical characteristics are summarized in Table 2. All are considered extensible materials with the exception of the metal strips. The samples were oriented in their machine or warp direction for pull-out.

TABLE 2 PROPERTIES OF REINFORCEMENT MATERIALS

Reinforcement Type	Tensile Strength[a] Peak Strength (lb/in.) Machine Dir.	Peak Strength (lb/in.) Cross Dir.	Elongation at Max. Load (%) Machine Dir.	Elongation at Max. Load (%) Cross Dir.	Thickness[b] (in.)	Opening Size (in.)
Geotextiles						
Coarse woven	569	459	20	13	0.06	0.023[c]
Smooth woven	211	212	26	16	0.03	0.012[c]
Needled nonwoven	108	104	94	49	0.11	0.005–0.007[c]
Heat-bonded nonwoven	61	76	60	69	0.024	0.003[c]
Geogrids						
Extruded 1 × 1	106	175	12	–	0.04–0.1	1 × 1.5
Extruded 1 × 4	424	57	16	–	0.06–0.2	0.9 × 4.4
Welded 3 × 3	271	170	8	11	0.01–0.08	3 × 3
Welded 1.5 × 4	553	225	7	–	0.01–0.08	1.5 × 4
Strips						
Fiber	3,300[c]	–	3[b]	–	0.14	–
Metal	7,200[c]	–	–	–	0.2–0.3	–

NOTE: Dash indicates not available or not applicable.
[a]Tested according to ASTM D-4595.
[b]Tested according to ASTM D-1777.
[c]From Geotechnical Fabrics Report (1986) or other manufacturers' literature.

TABLE 3 PROPERTIES OF SOILS USED IN PULL-OUT TESTS

Soil Type	Test Density (pcf)	Reference Density (%)	Water Content (%)	Liquid Limit	Plasticity Index	Angle of Internal Friction[a] (degrees)
Fine sand	104	96[b]	Air dry	–	–	35
Gravel	112	–	Air dry	–	–	43[c]
Silt	107	95[d]	4	24	6	21
Clay	106	95[d]	18.5	45	31	15

[a]From triaxial tests.
[b]Relative density.
[c]Estimated.
[d]Percentage of maximum standard Proctor value.

Both coarse and smooth woven geotextiles were tested. The coarse woven geotextile chosen for the test program was a polypropylene multifilament (14 oz/yd^2) geotextile of relatively high strength (569 lb/in.). The smooth woven geotextile was a polypropylene slit film woven (7 oz/yd^2) with less than half the tensile strength of the coarse fabric.

A medium-weight (8 oz/yd^2) continuous filament polyester needle-punched fabric was used as the needled nonwoven geotextile representative. It had a high elongation capacity in the testing direction and necked considerably during the tests. The weakest material tested was the heat-bonded nonwoven geotextile with a wide width strength of 61 lb/in. The material was a polypropylene heat-bonded geotextile (6 oz/yd^2) with relatively smooth sides.

The polymer grids tested were of two different types distinguished by polymer, shape, and manufacturing process. Two different products of each type were tested. The welded-strip geogrids were made of orthogonally placed 0.5-in.-wide strips of highly oriented polyester welded together at the crossover points. This material had a thin metal screen attached at the nodes along each cross direction strip. The 3 × 3 welded strip grid consisted of strips placed 3 in. apart in both directions. A 1.5 × 4 welded strip grid with strips placed every 1.5 in. in the machine direction and at 4-in. intervals in the cross direction was also tested.

The extruded geogrids were made by stretching a punched polymer sheet in the preferred direction. The 1 × 4 extruded grid (27 oz/yd^2) was made from a high-density polyethylene sheet and had oval openings about 1 in. wide by 4 in. long oriented in the machine direction. The 1 × 1 extruded grid was a biaxially oriented polypropylene 9 oz/yd^2 geogrid with openings 1 in. by 1.5 in. and 0.1-in.-wide ribs.

The strip reinforcements were made of metal and fibers. The fiber strips were made of polyester fibers arranged in bundles covered with a black polyethylene thermoplastic. The strips were 3.4 in. wide and 0.14 in. thick. The other strips were 2 in. wide, 0.2 in. thick galvanized steel with ridges 0.1 in. high in the cross direction at intervals.

Soils

Four different types of soil were used to conduct the pull-out tests: sand, gravel, silt, and clay. The characteristics of these soils are given in Table 3 and shown in Figure 1.

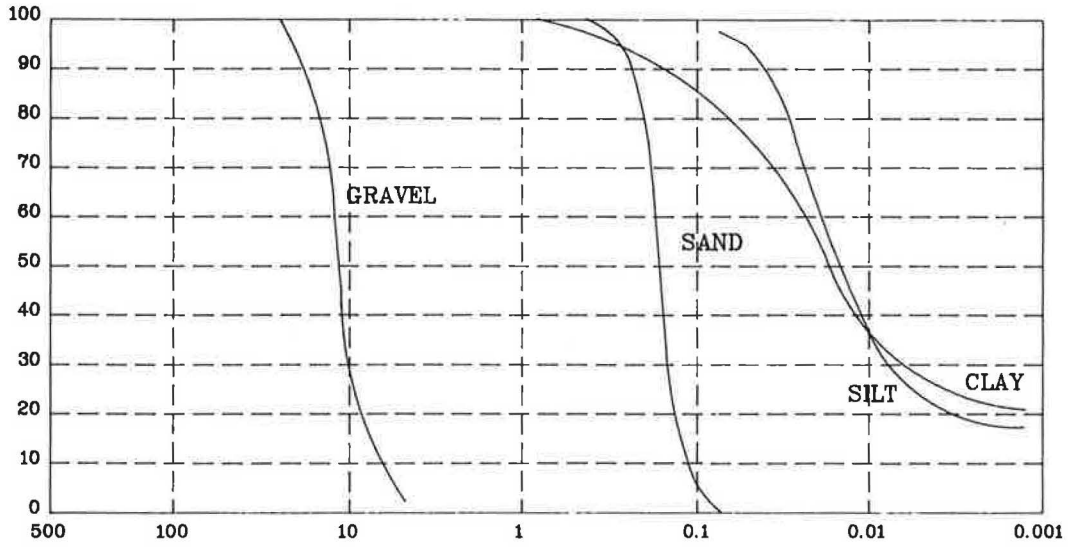

FIGURE 1 Grain size distribution of soils used in test program.

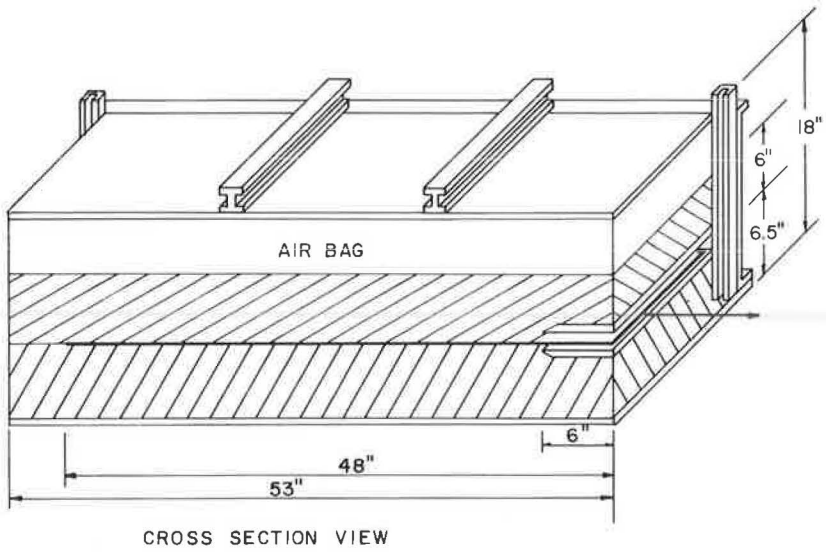

FIGURE 2 Cross section of pull-out box.

Most of the tests were conducted with the soil identified as sand—a poorly graded Fontainebleu sand.

The gravel consisted of subrounded particles ranging in size from 0.75 in. to 0.2 in. with almost no sand or smaller-sized particles. The silt was slightly cohesive with a relatively high angle of internal friction (35 degrees). A low-plasticity silty clay was used as the fourth type of soil.

Equipment

The methodology for determining pull-out resistance was based on measurement of horizontal forces used in pull-out of reinforcement materials embedded in aggregate in a large pull-out box.

The pull-out box (Figure 2), which was designed and built by STS Consultants Ltd., consisted of two 18-in. channel sections for sides, a bottom plate, a removable back wall, and a horizontally split door. Inside dimensions were 53 × 27 × 18 in. (length × width × depth). A horizontal metal sleeve 6 in. long was located over the full width of the box in an attempt to decrease the horizontal stress near the door face during pull-out.

Pull-out was performed by a hydraulic cylinder mounted horizontally 40 in. in front of the door of the pull-out box. The cylinder was 0.5 in. above the bottom half of the door to allow a level pull of reinforcement placed on a 6.5-in. layer of aggregate. The ram was attached to the reinforcement sample and was retracted to provide the force for the test. Pull-out force was measured by a load cell attached between the reinforcement and the hydraulic ram.

The normal loads for the pull-out tests were supplied by inflating an air bag fitted in the pull-out box to act as a diaphragm. The bag was placed between a 0.2-in.-thick flexible metal plate, which rested on the aggregate, and the 0.55-in.-thick metal pull-out box cover plate. Two 3-in. H-sections were bolted across the width of the top of the box to provide a reaction for the cover plate. Constant

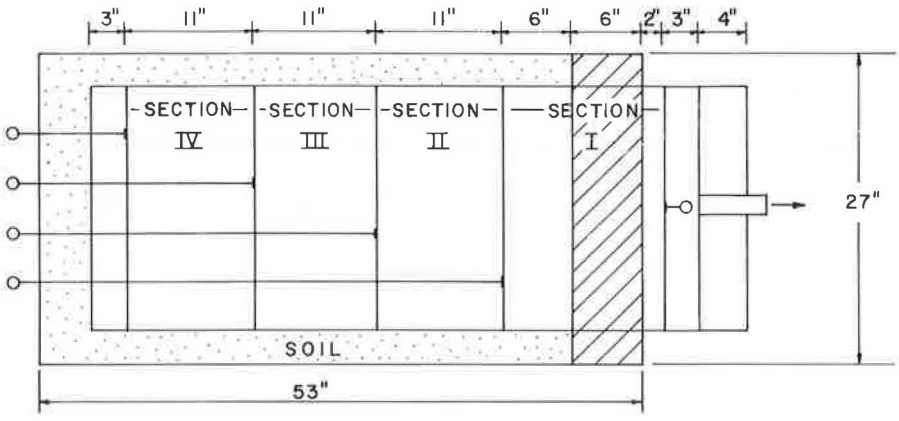

FIGURE 3 Plan view and typical gauge placements.

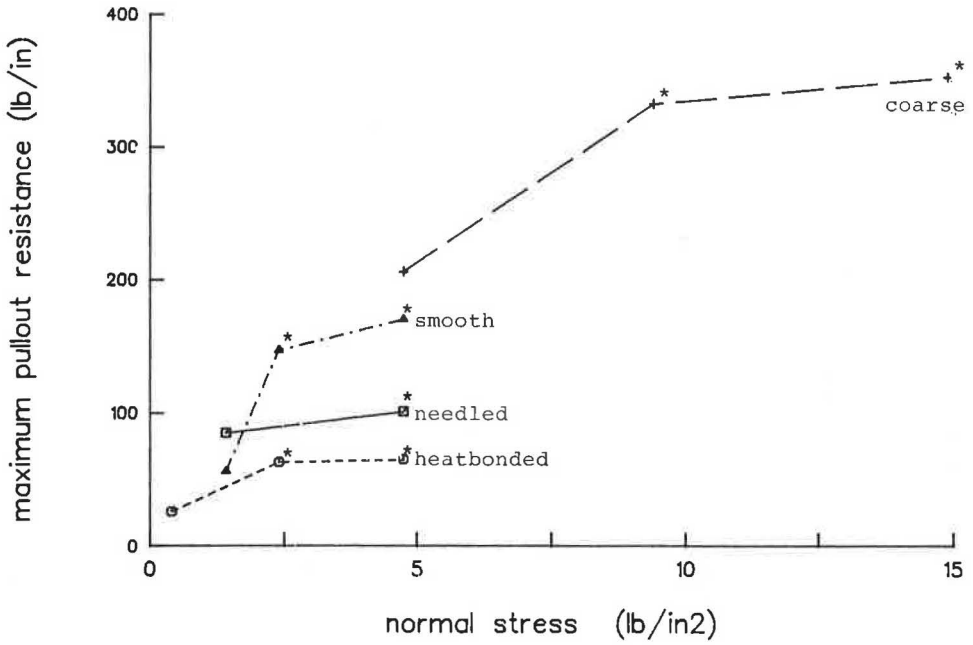

FIGURE 4 Pull-out resistance versus normal stress for geotextiles.

pressure was maintained throughout the test by a regulator connected to the air bag.

Horizontal displacement of the reinforcements was measured by several extensometers. One dial extensometer was mounted on the reinforcement outside the box near the door, and four wire extensometers measured displacements of the specimen inside the pull-out box. The wire gauges consisted of inextensible wire that was connected to a spring-loaded dial extensometer mounted outside the pull-out box and attached to a metal ring on the reinforcement sample. The wires were attached to the specimen at four different distances from the pull-out box door. They were encased in stiff tubing to enable free movement under normal loading. Figure 3 is a diagram of extensometer locations.

Reinforcements were gripped in a simple clamp made of a series of bolts holding the material between metal angle pieces. The clamp was 24 in. wide and 4 in. long with two rows of bolts. It was attached to the hydraulic load piston by a swivel connection. When slippage was a problem, the material was epoxy coated or held in the clamp by looping it over a metal rod behind the clamp, or both.

Procedures

Pull-out testing was previously described as measuring the force necessary to pull a specimen out of a soil mass. More specifically, at the beginning of the tests, half the soil mass was placed in the box and compacted with a vibratory compactor (hand placement of silt and clay). The reinforcement sample was then placed on the soil, slipped into the 6-in.-long metal sleeve, and connected to the pulling ram. Next the gauges were attached, the front door of the box replaced, and the remaining 6 in. of soil placed. A normal load was applied by positioning the air bag with its cover and then pressurizing the bag. A pulling force was applied so that the test rate was 0.04 in./min as monitored by the extensometer mounted just outside the box door. Loading continued until the geosynthetic ruptured or until pull-out occurred.

RESULTS AND OBSERVATIONS

The results of this test program were evaluated in terms of pull-out resistance (P) and soil reinforcement resistance angle (δ). Pull-out resistance, as previously noted, is an expression of the horizontal force per unit width opposing mobilization of a reinforcing material in soil. Comparison of pull-out resistance under different test conditions is presented to illustrate the effect of normal stress, reinforcement tensile strength, and soil type. Four methods were used to calculate soil reinforcement resistance coefficients from the test data in sand. The use of extensometer data to obtain a confined stress-strain relationship is also demonstrated.

Reinforcement Pull-Out Resistance

Figures 4–6 show the maximum pull-out resistance values obtained for the different reinforcements in sand under a series of normal load conditions. An increase in maximum pull-out resistance with increasing normal load is evident in the figures. The cases in which rupture of the reinforcement occurred before pull-out are exceptions and are indicated by an asterisk in the graphs.

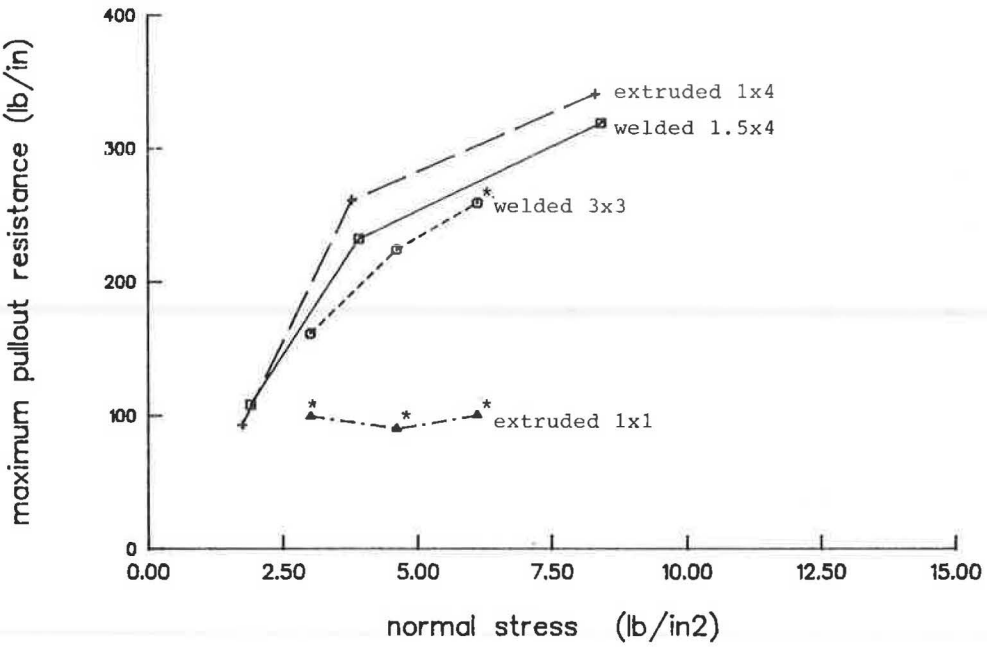

FIGURE 5 Pull-out resistance versus normal stress for geogrids.

Most materials that failed before pull-out showed pull-out resistance values close to their wide width tensile strength. This was anticipated because the materials were unconfined outside the pull-out box where failure actually occurred. The case of coarse woven geotextiles is an exception with observed pull-out values of less than 60 percent of tensile strength. This result was most probably due to weakening of the fabric at the clamp during the clamping procedure.

Influence of Soil Type

The effect of soil type on pull-out resistance was also studied, and comparative graphs are shown in Figures 7–11. Pull-out resistance in gravel was found to be greater than in sand; however, in some cases this difference was minimal. The pull-out resistance results in noncohesive silt were slightly lower than in sand for the geotextiles, geogrids, and strip reinforcements tested.

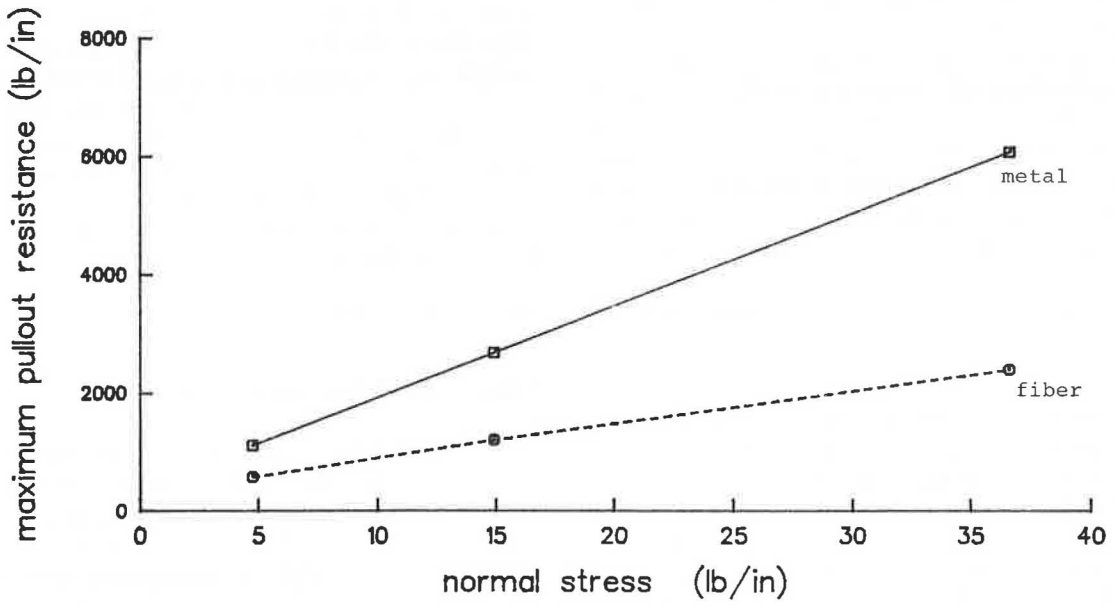

FIGURE 6 Pull-out resistance versus normal stress for strip reinforcements.

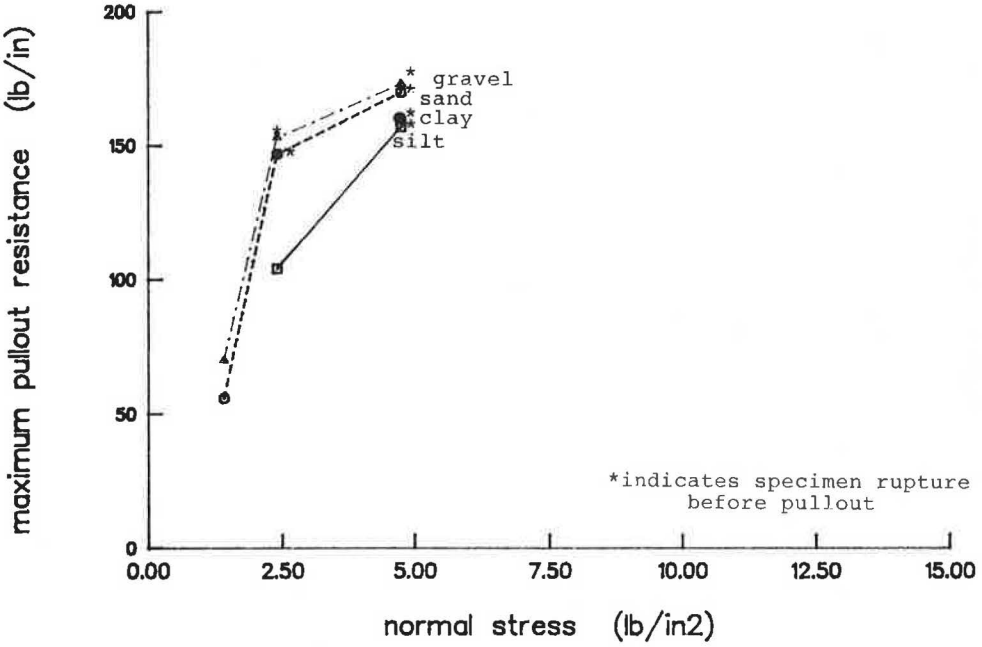

FIGURE 7 Pull-out resistance with various soil types— smooth woven geotextile.

A limited number of tests in a low-plasticity clay resulted in pull-out resistance values that were slightly less than the values in sand for the smooth woven geotextile and slightly greater than the values in sand for nonwoven geotextiles and geogrids. It should be noted that these data were from short-term testing and one moisture/density relation. They provide only an initial indication of pull-out resistance in cohesive soil. The influences of moisture, density, pore pressure, soil creep, and other characteristics of clay were not evaluated in this study.

Soil-Reinforcement Interaction

As previously indicated, pull-out resistance is often evaluated by comparing the ϕ angle of the soil with a soil-reinforcement resistance angle (δ), which can be obtained by a variety of methods. Values of δ obtained by four methods for a sampling of the test materials are given in Table 4. The table includes only tests performed using sand in the pull-out box in order to eliminate the soil as a variable.

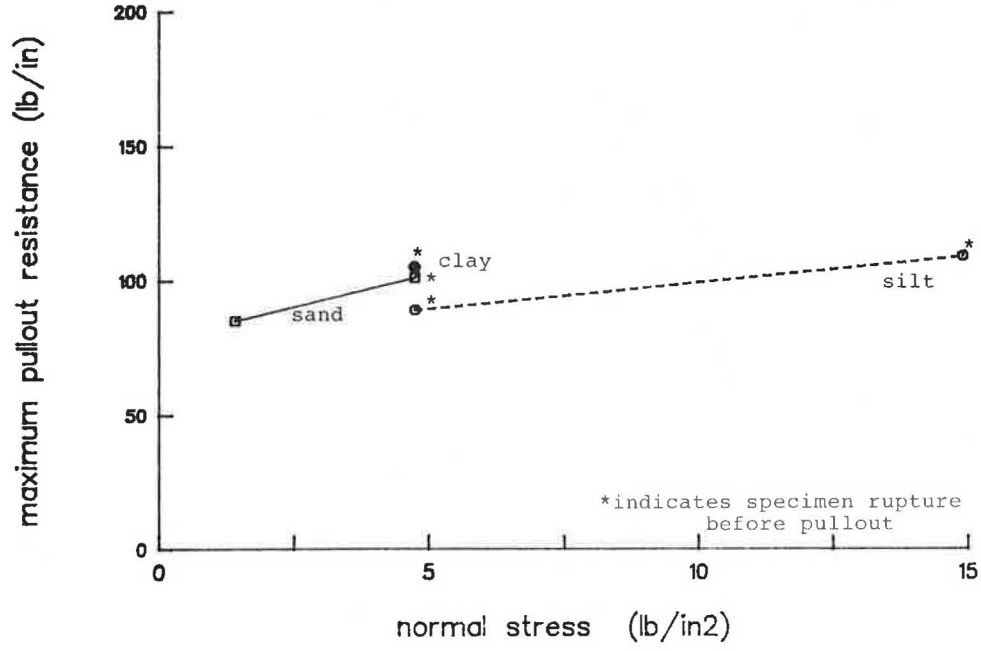

FIGURE 8 Pull-out resistance with various soil types— needled nonwoven geotextile.

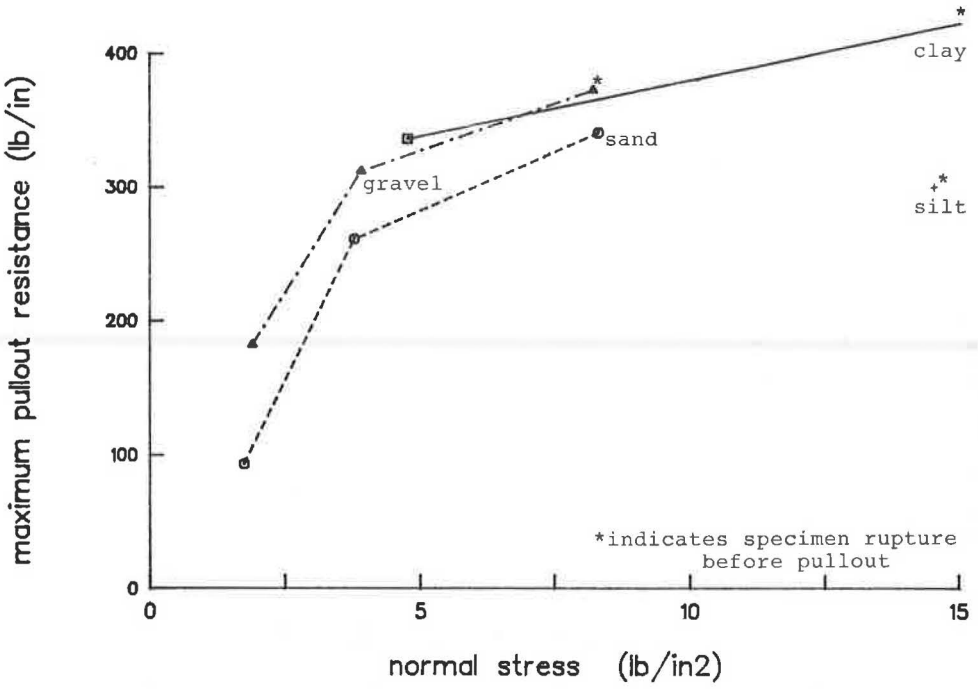

FIGURE 9 Pull-out resistance with various soil types—1 × 4 extruded geogrid.

The first two methods used were the $\frac{2}{3}\ \phi_{soil}$ approach and the area method. For the area method, δ was found from a plot of maximum pull-out stress versus normal stress. Because resistance is developed by both sides of the reinforcement, pull-out stress was defined as the ultimate pull-out load divided by two times the embedded area of the reinforcement.

Knowledge of specimen movements in the pull-out box provided another way to find a soil-reinforcement resistance angle. It appears that the wire extensometers can be used to determine the length of geosynthetic sliding as the pull-out test progresses. By using only the portion of the sample that is actually moving and the specimen width, a corrected area can be calculated for the portion of the sample that is being stressed. This method is referred to as the "corrected area method" in Table 4, where pull-

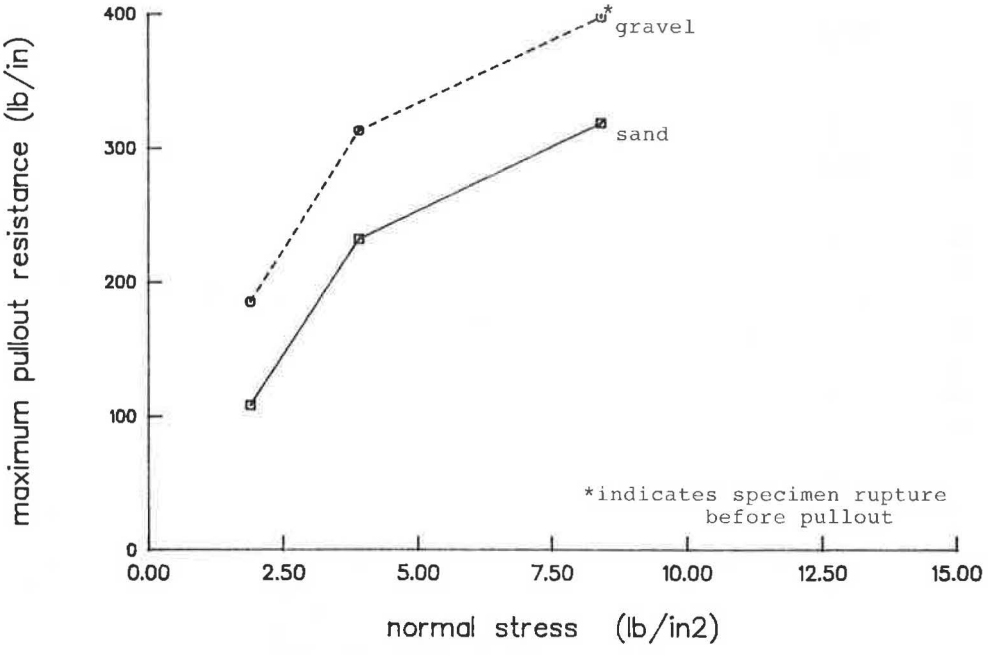

FIGURE 10 Pull-out resistance with various soil types— 1.5 × 4 welded geogrid.

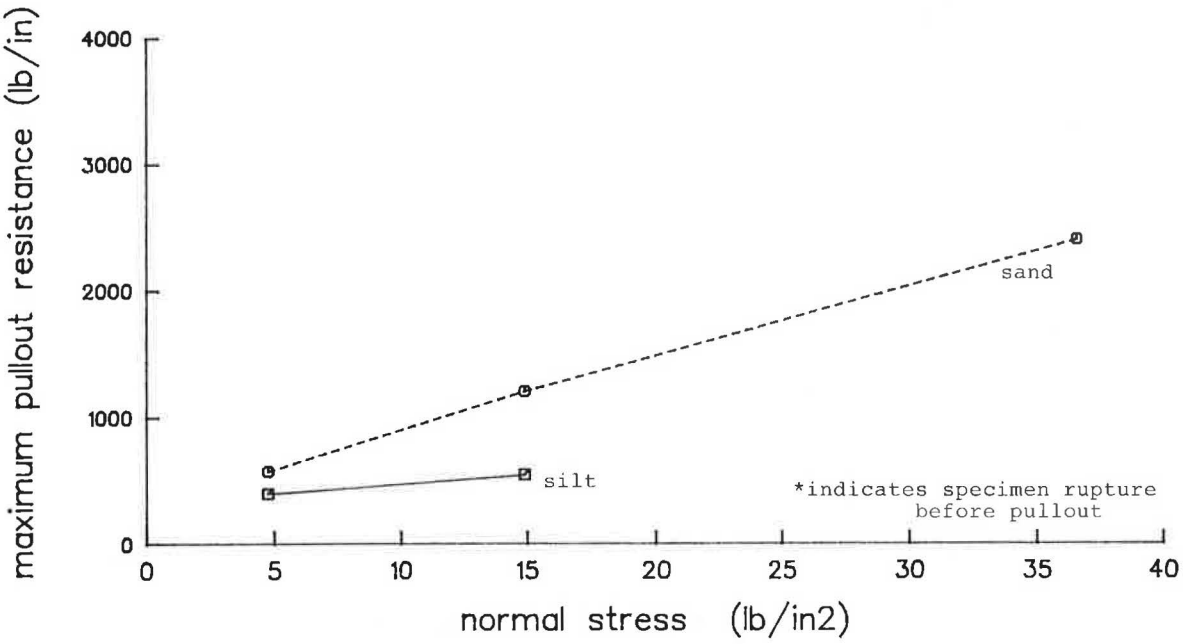

FIGURE 11 Pull-out resistance with various soil types— fiber strip reinforcement.

out stress is obtained from

$$\text{Pull-out stress} = \frac{\text{Load to mobilize reinforcement section}}{\text{Corrected area of section} \times 2} \tag{3}$$

The pull-out stress versus normal stress relation was then used to determine a δ angle. The values presented in Table 4 were found by using the wire gauge readings from Section II of Figure 3. For most extensible materials, δ values determined by using this method were found to be greater than those determined previously with the area method, as shown in plots of shear stress versus normal stress (Figures 12–16). A best fit line using the corrected area results implied a pseudo-cohesion intercept for the geogrid materials. This may be due to the bearing resistance provided by the cross members of these materials.

Another value of δ was calculated using the K_r method proposed by Holtz and Solomone et al. (*2*). The slope of the force versus mobilized length relation was called K_r and is shown for a sample of cases in Figures 17–19. The mobilized length of the reinforcements was found by assuming that movement at a wire gauge location indicated pull-out at that point. This assumption proved valid when pull-out results from geogrids of different lengths were compared with results obtained by using wire gauge movement to determine embedded length. A soil-reinforcement resistance angle (δ) was found using Equation 2, as suggested by Solomone et al., for each test; the range of values

TABLE 4 COMPARISON OF δ VALUES

Reinforcement	Soil Reinforcement Resistance Angle δ[a]			
	$\frac{2}{3}\Phi_{soil}$	Area Method[b]	K_r Method[c]	Corrected Area Method
Coarse woven	22	28	23–27	29
Smooth woven	22	31	21–29	34
Needled nonwoven	22	14	28	27
Heat-bonded nonwoven	22	37	25–31	37
Extruded grid 1 × 1	22	33	11–23	33
Extruded grid 1.5 × 4	22	23	N/A	N/A
Welded grid 3 × 3	22	22	29–32	23
Welded grid 1.5 × 4	22	23	N/A	N/A
Fiber strip	22	34	33–46	47
Metal strip	22	63	N/A	N/A

NOTE: N/A = not applicabe because iterative strain data not available.
[a]δ calculated from pull-out tests in sand and expressed in degrees.
[b]From plots of ultimate pull-out load/2 × area.
[c]Range of δ calculated using K_r (Equation 2).

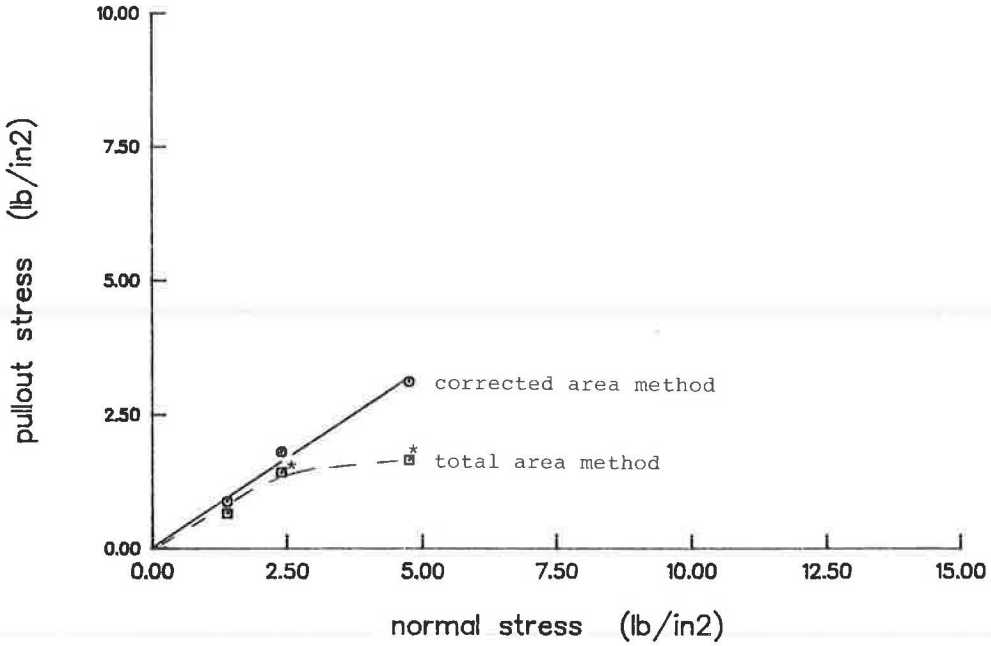

FIGURE 12 Resistance angle determination for smooth woven geotextile.

is reported for each reinforcement in Table 4. These calculations assume no cohesion-type intercept.

The data in Table 4 indicate that it is possible to obtain a wide range of values for δ depending on the method used. Comparisons of the corrected area and the K_r determination methods were limited because of the small number of extensometers on the specimens, which resulted in rough approximations for the corrected area and sliding areas. Inaccuracies in these coarse measurements may have affected the K_r relation, which was not in all cases found to be linear as expected by Holtz. One limitation of the total area method was lack of valid data as the result of test specimen failure. Also, many research results indicate that, in extensible materials, the total area is not uniformly stressed in the pull-out test as is assumed in the calculations.

Stress-Strain Behavior

Wire extensometers attached to the specimen allowed determination of stress on separate sections of reinforcement during the pull-out test. Strain was found by subtracting the movement measured at one location from the

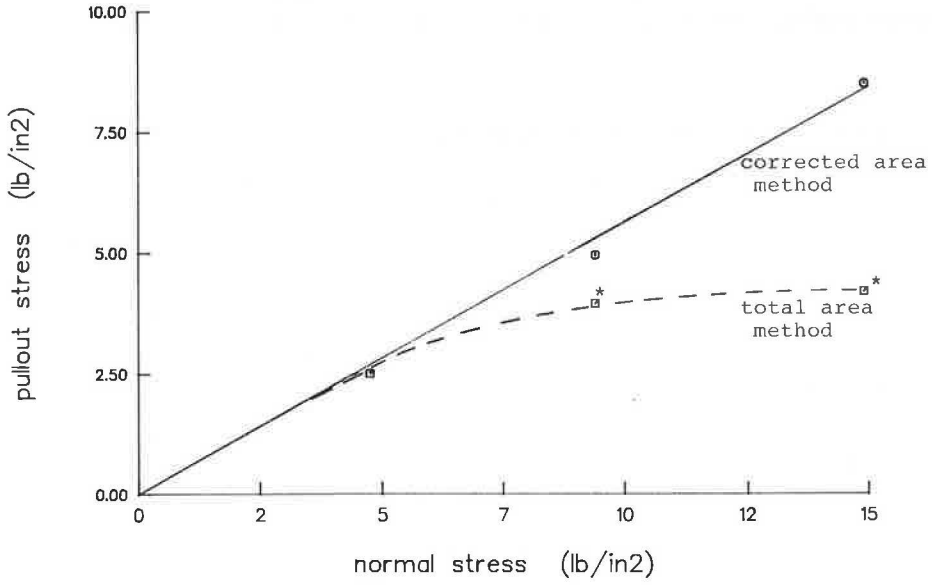

FIGURE 13 Resistance angle determination for coarse woven geotextile.

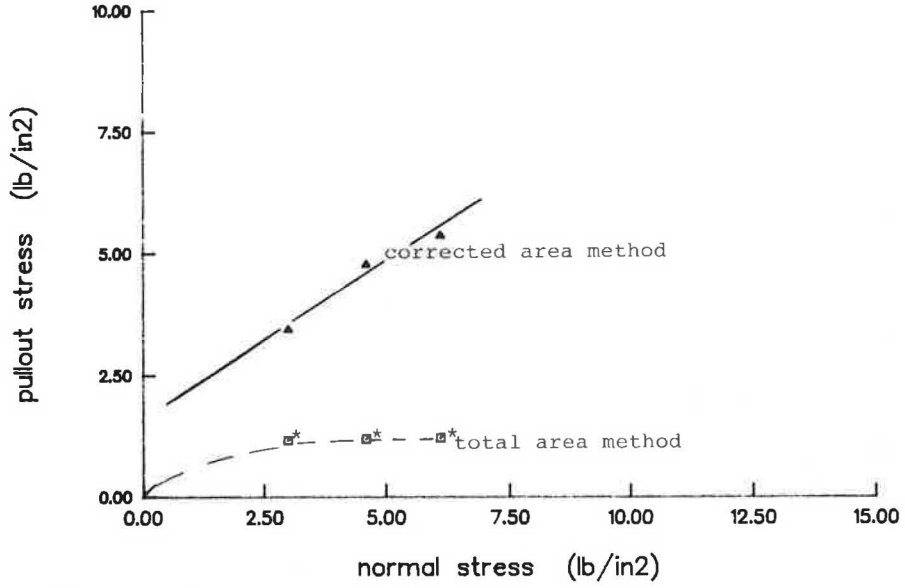

FIGURE 14 Resistance angle determination for 1 × 1 extruded geogrid.

movement measured by an adjacent gauge and dividing by the distance between gauges. Elongation values are plotted versus pull-out resistance in Figures 20 and 21 for geotextiles and in Figure 22 for one of the geogrids. If change in pull-out resistance versus elongation is plotted as in Figures 23 and 24, it can be seen that the confined sections of a needled nonwoven geotextile and geogrid behave quite similarly and have moduli that are higher than those determined from their respective unconfined behavior. Figure 25, however, shows that the elongation of a coarse woven geotextile was variable along its length and not substantially greater than that of an unconfined sample. This behavior was anticipated from the work of Christopher et al. (*7*).

A confined load/elongation curve was assumed as an average of the curves from gauged Sections II, III, and IV in Figures 23–25. Figures 26–28 are approximations of stress distribution on the reinforcements during pull-out. The stress values were obtained by choosing pull-out resistance values from the average confined load/elongation curve corresponding to the displacements measured in the reinforcement sections. The different load levels presented

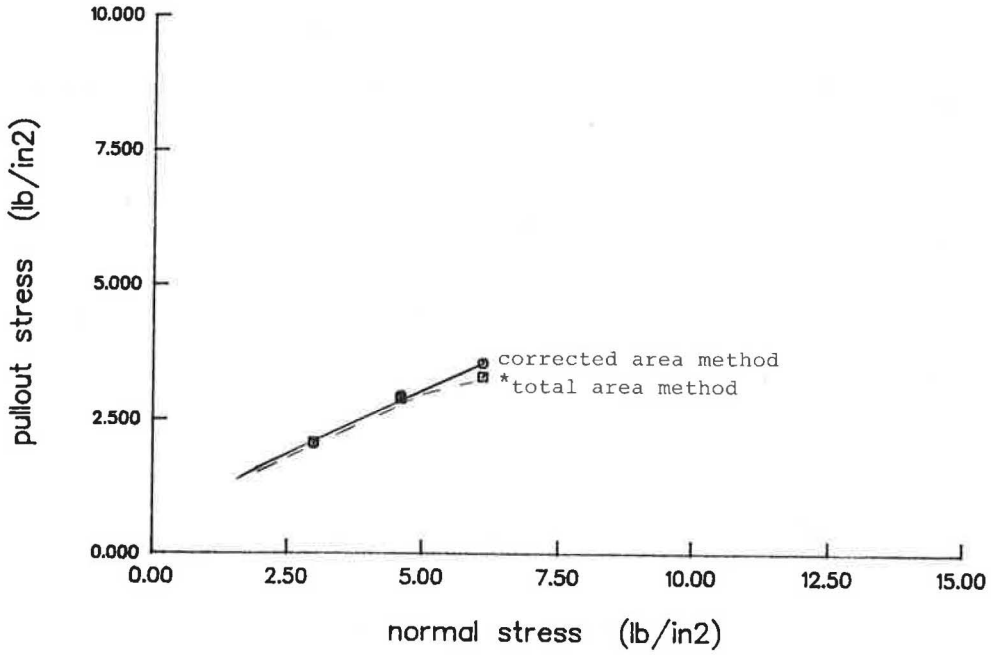

FIGURE 15 Resistance angle determination for 3 × 3 welded geogrid.

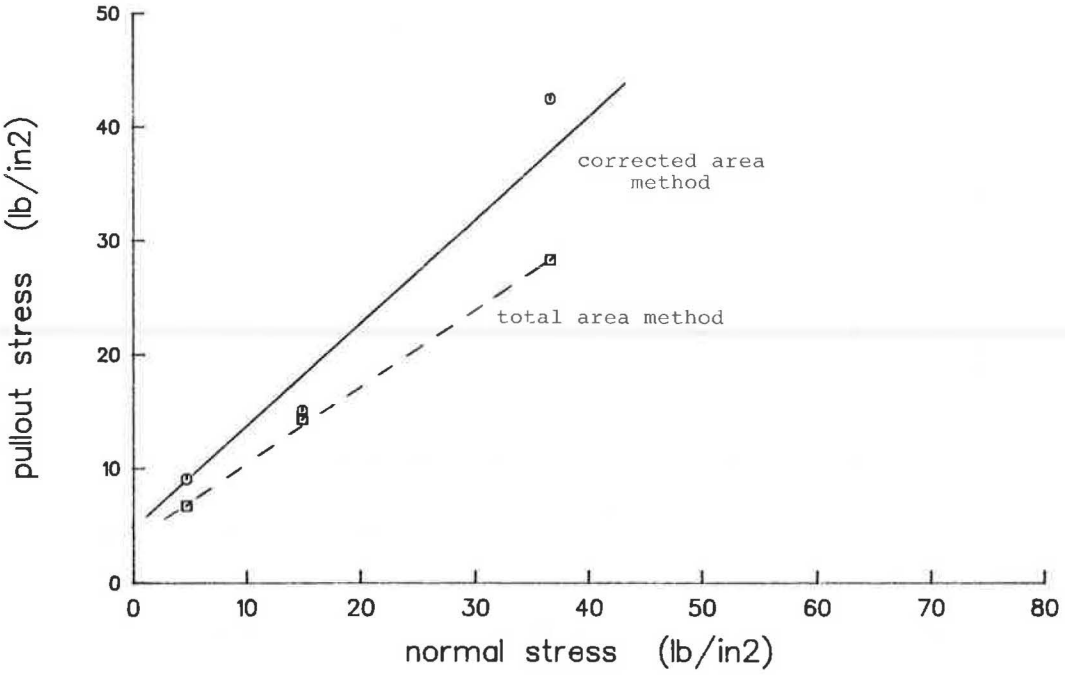

FIGURE 16 Resistance angle determination for fiber strip reinforcement.

indicate that stress distribution changes as loading progresses. This approximation yields stresses that are not uniformly distributed but decrease away from the applied load with some parabolic function as anticipated for extensible materials.

SUMMARY AND CONCLUSIONS

The considerable variation in pull-out resistance observed can be attributed to material and soil type without the influence of testing differences. This test program thus

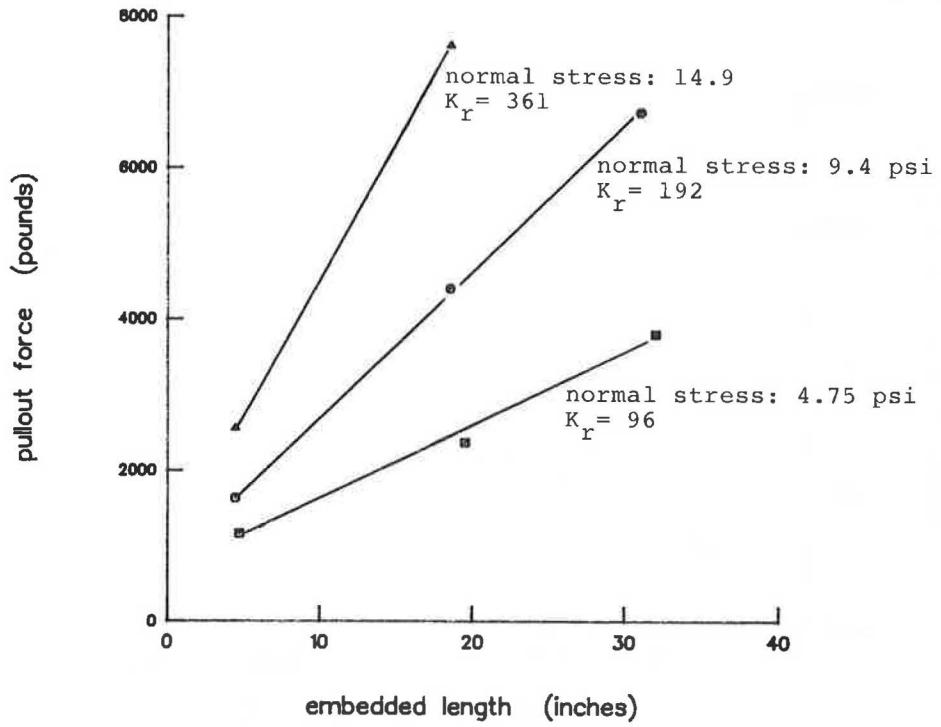

FIGURE 17 K_r plots—coarse woven geotextile.

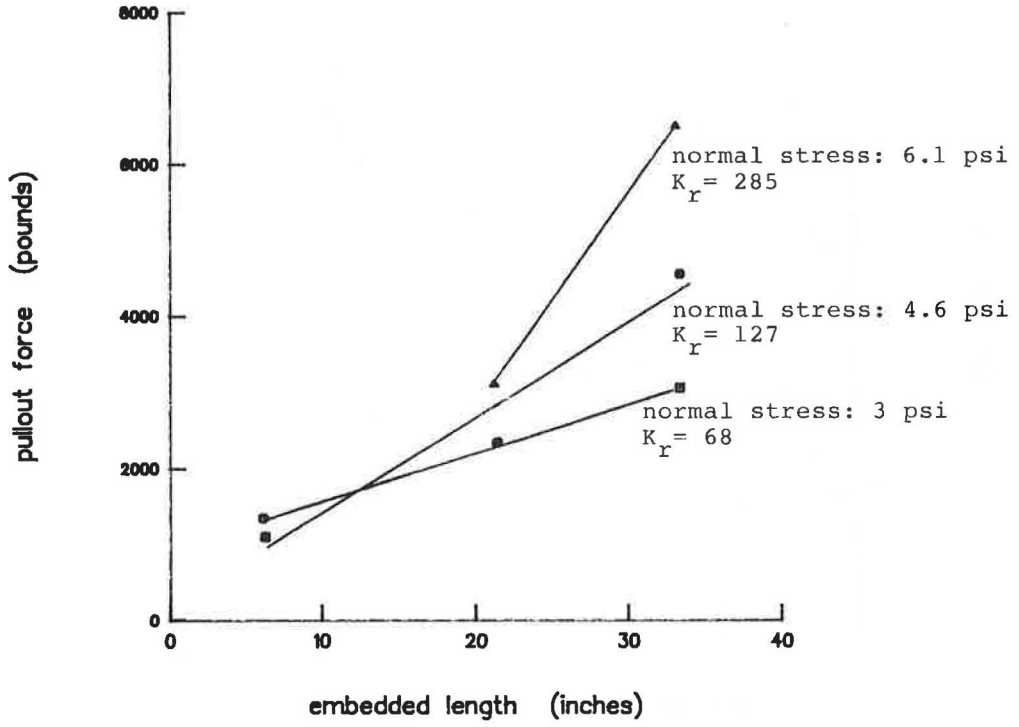

FIGURE 18 K_r **plots—3 × 3 geogrid.**

allowed pull-out resistance values for many types of reinforcement, soil media, and methods of analysis to be compared.

A formal discussion of some of the findings awaits further study and perhaps more testing. Nevertheless, several observations are apparent from the results presented.

- Uniform test procedures for all types of reinforcement facilitate comparisons, and standard procedures should be developed.
- Maximum pull-out resistance values varied from 26 to 352 lb/in. It is understood that much of this variability is due to the wide range of strengths of the materials tested.

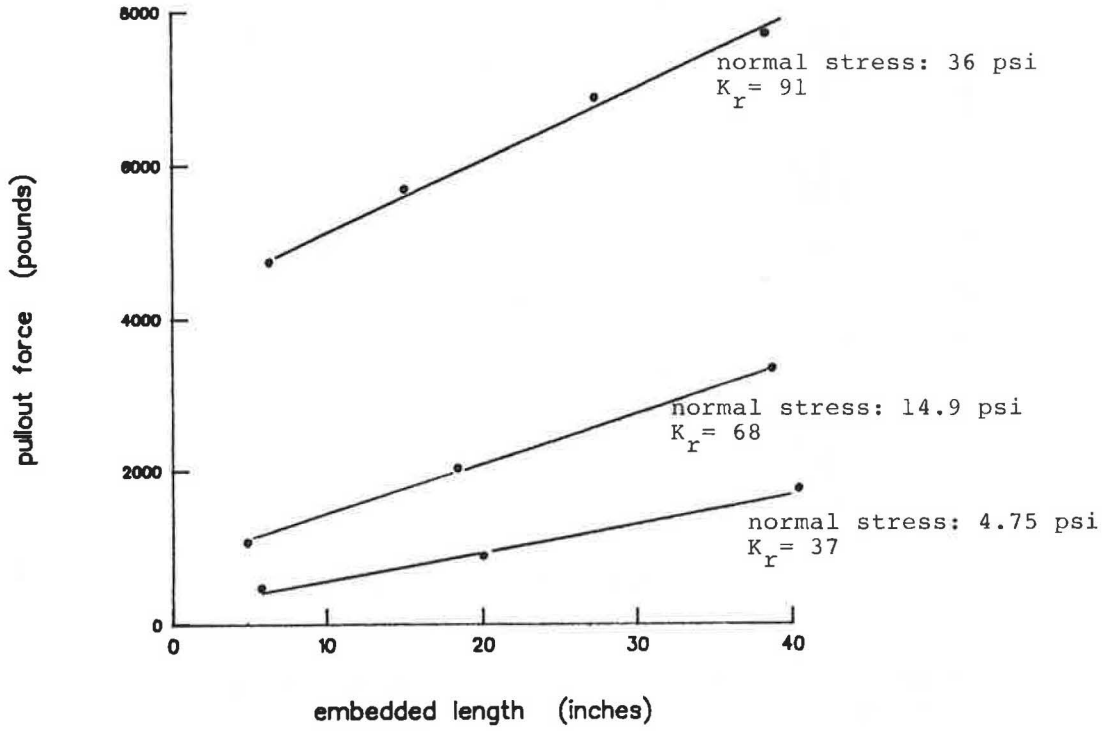

FIGURE 19 K_r **plots—fiber strip reinforcement.**

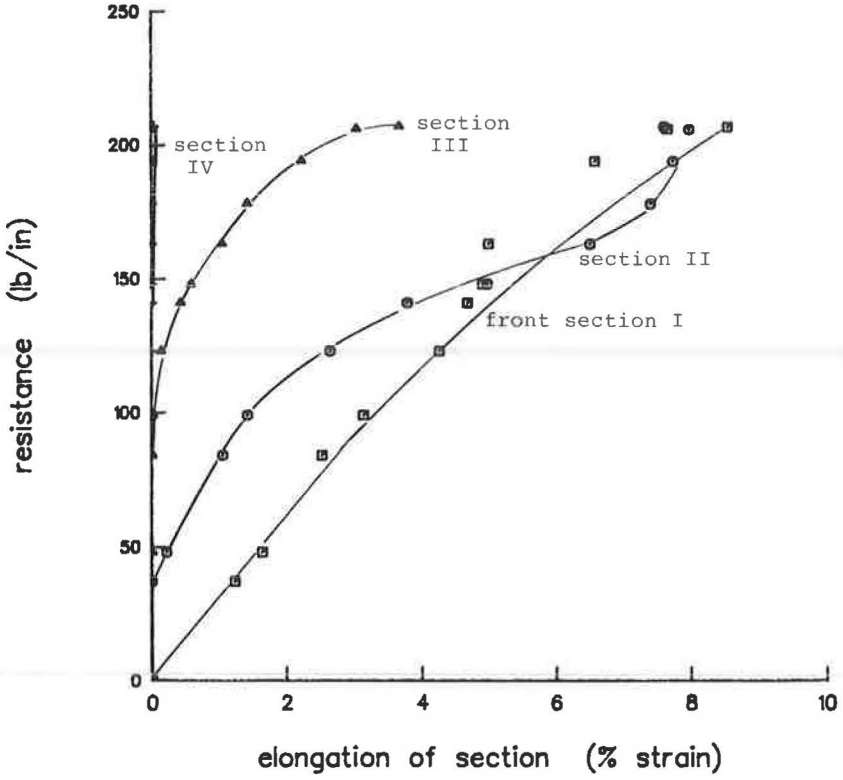

FIGURE 20 Resistance versus elongation from pull-out test—coarse woven geotextile.

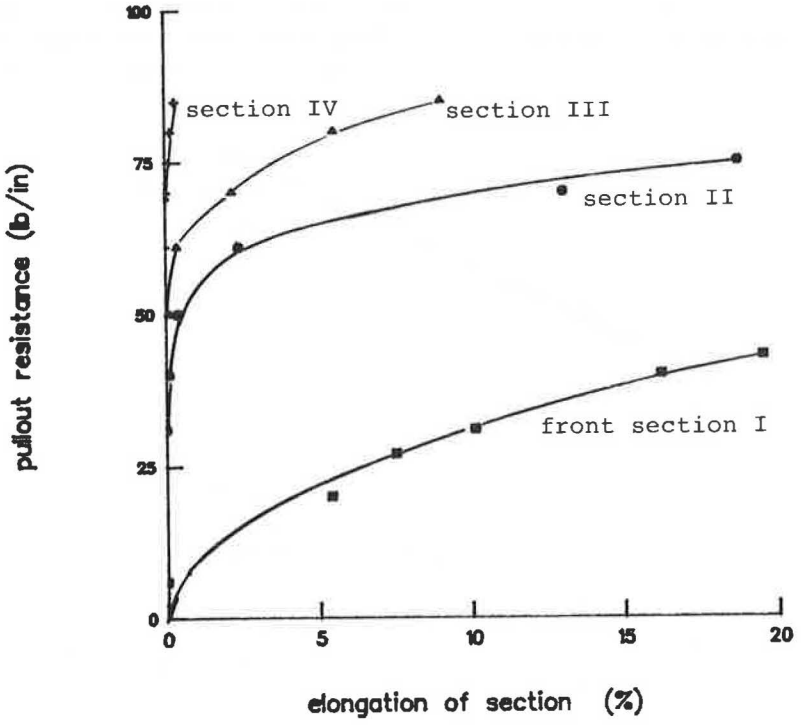

FIGURE 21 Resistance versus elongation from pull-out test—needled nonwoven geotextile.

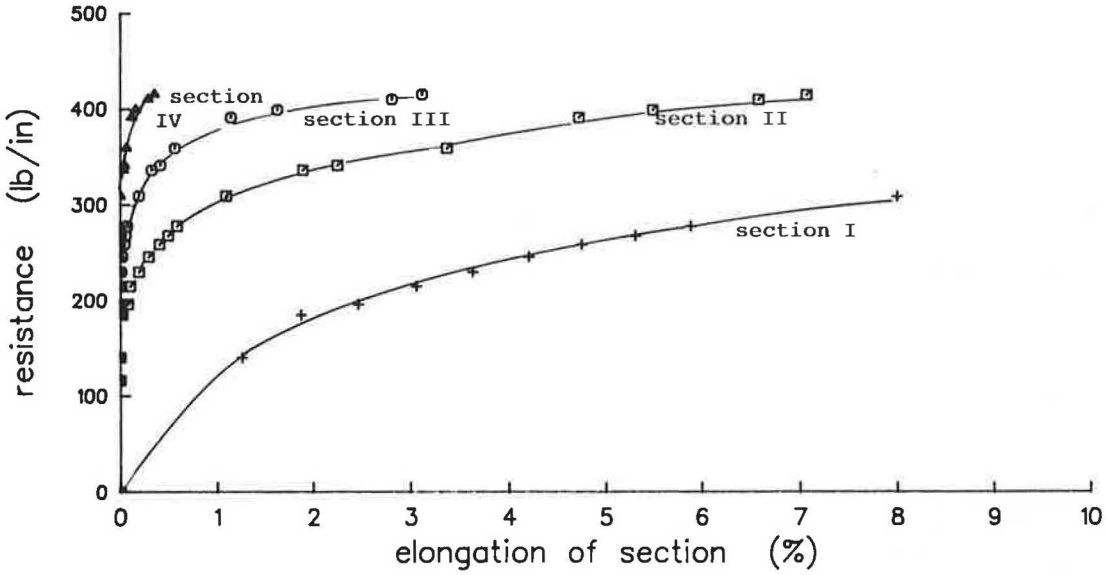

FIGURE 22 Resistance versus elongation from pull-out test—extruded 1 × 4 geogrid.

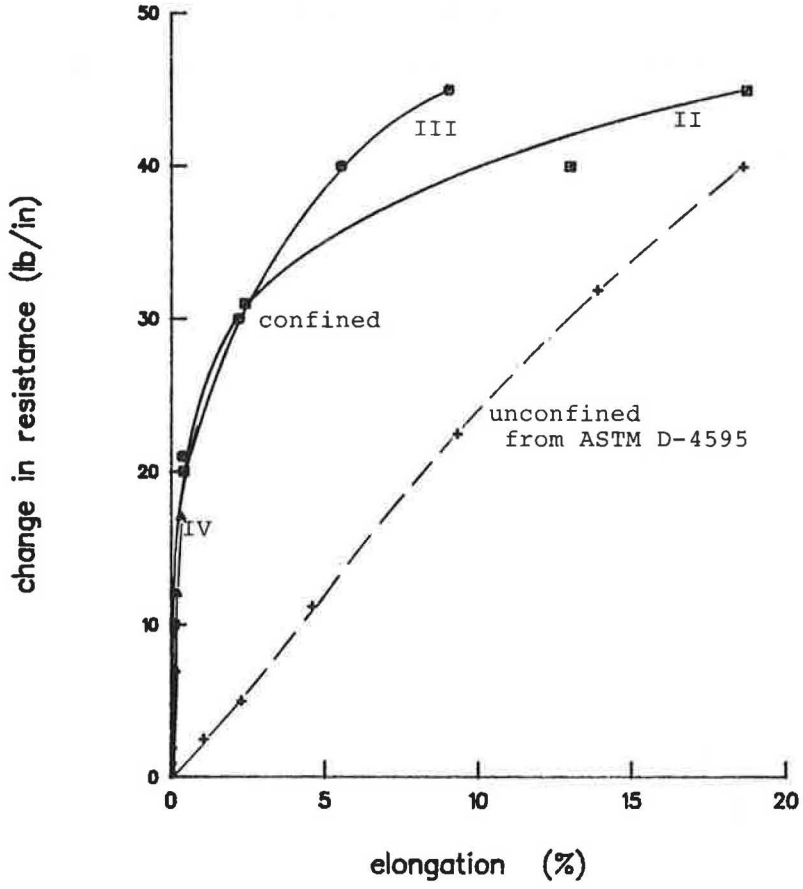

FIGURE 23 Adjusted pull-out data with tensile test data— needled nonwoven geotextile.

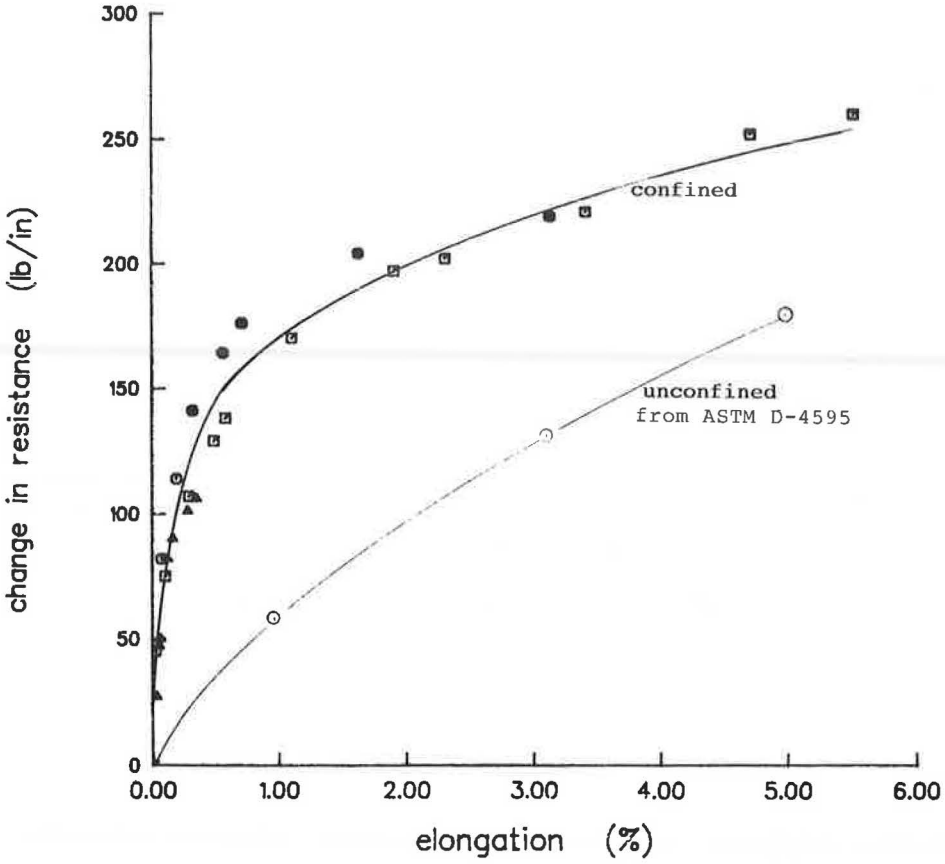

FIGURE 24 Adjusted pull-out data with tensile test data— extruded 1 × 4 geogrid.

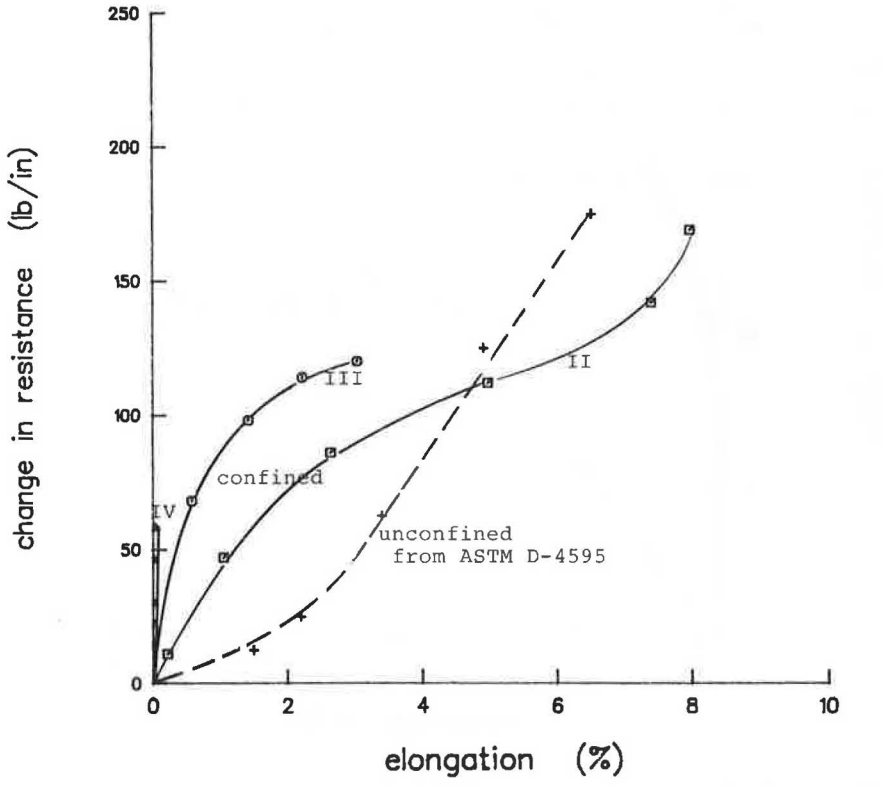

FIGURE 25 Adjusted pull-out data with tensile test data— coarse woven geotextile.

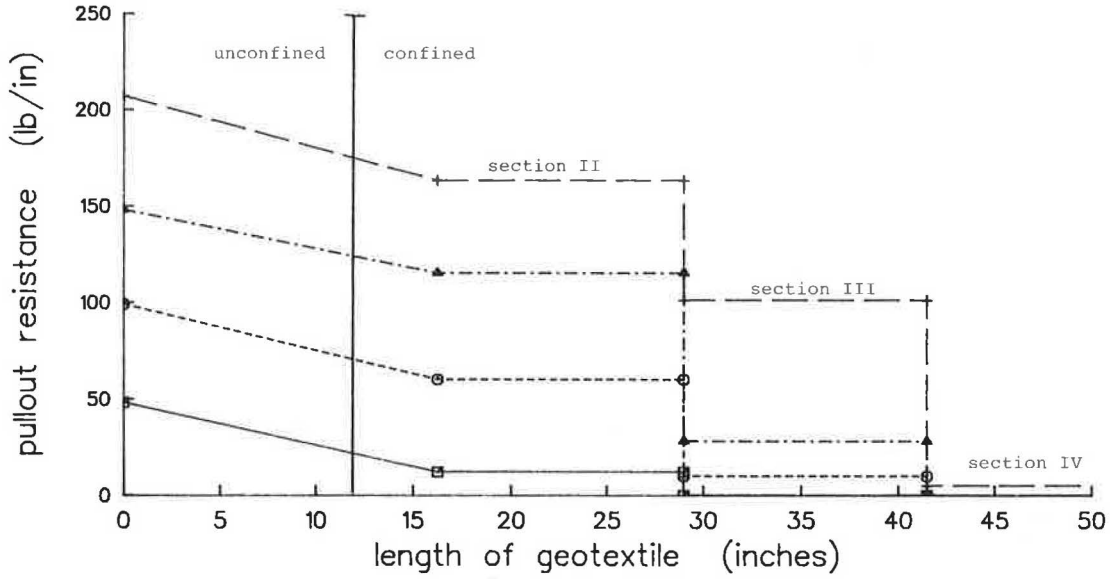

FIGURE 26 Distribution of resistance along coarse geotextile during test.

However, normalizing the results indicates that maximum pull-out resistance values range from 15 to 106 percent of respective unconfined strengths.

- Comparison of results in different soil types showed the highest resistances in compacted gravel but minimal difference in finer-grained soils.
- A resistance factor can be found by using the corrected area and K_r methods, which appear to give a realistic adjustment to the more traditional determinations of δ.
- Finally, the results indicate that the pull-out test may be used to evaluate the confined behavior of reinforcement.

ACKNOWLEDGMENTS

The authors would like to thank Charles Leucht and Jack Joerger for their laboratory work; Reinforced Earth Co., Tensar Corp., Soil Structures Ltd., ITW, Amoco, Nicolon, Chemie Linz, and DuPont for supplying materials for this

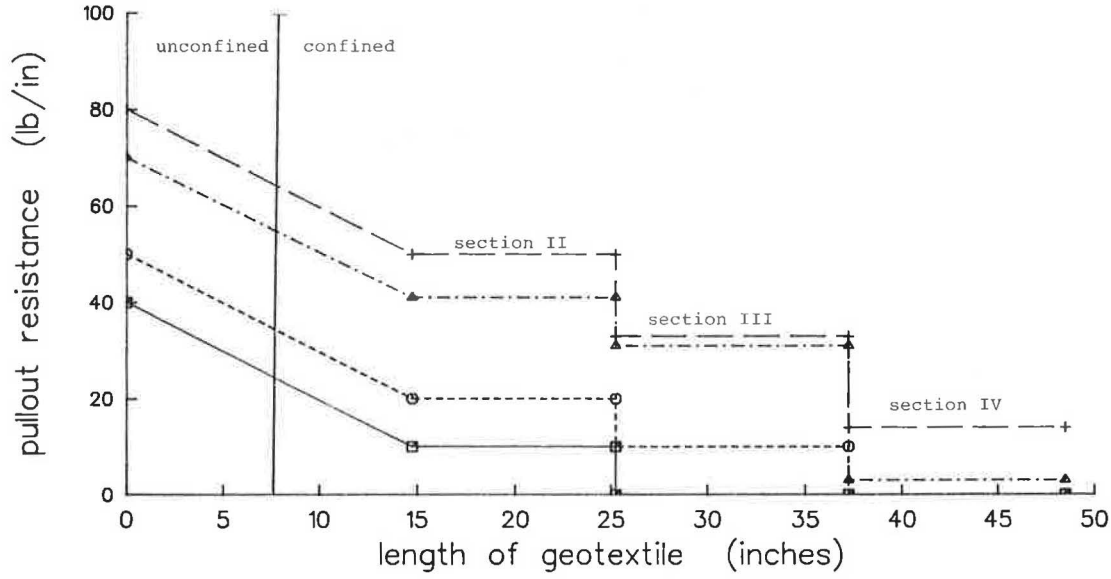

FIGURE 27 Distribution of resistance along needled nonwoven geotextile during test.

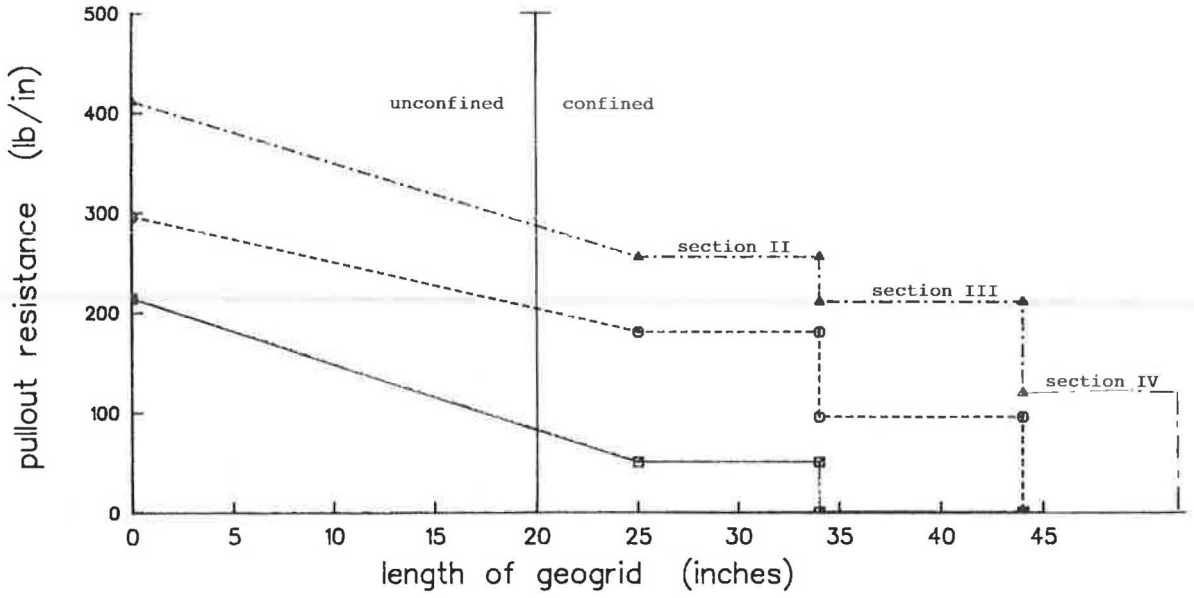

FIGURE 28 Distribution of resistance along 1 × 4 geogrid during test.

study; and, especially, the Federal Highway Administration for their support.

REFERENCES

1. J. R. Steward, Williamson, and J. Mohney. *Guidelines for Use of Fabrics in Construction and Maintenance of Low-Volume Roads*. USDA Forest Service, Portland, Oreg., 1977.
2. W. G. Solomone, E. Boutrup, R. D. Holtz, W. D. Kovacs, and C. D. Sulton. Fabric Reinforcement Designed Against Pull-Out. *The Use of Geotextiles for Soil Improvement*, ASCE, Portland, Oreg., 1980, pp. 80–177.
3. D. Leshchinsky and D. A. Field. In-Soil Load Elongation, Tensile Strength and Interface of Nonwoven Geotextiles. *Proc.*, Geosynthetic '87 Conference, New Orleans, La., April 1987, pp. 238–249.
4. W. H. Tzong and S. Cheng-Kuang. Soil-Geotextile Interaction Mechanism in Pull-Out Test. *Proc.*, Geosynthetic '87 Conference, New Orleans, La., April 1987, pp. 250–259.
5. M. Al-Hussaini and E. B. Perry. Field Experiment of Reinforced Earth Wall. *Symposium on Earth Reinforcement*, Pittsburgh, Pa., April 1978, pp. 127–156.
6. A. McGown, K. Z. Andrews, and M. H. Kabir. Load-Extension Testing of Geotextiles Confined in Soil. *Proc.*, Second International Conference on Geotextiles, Las Vegas, Nev., 1982, pp. 793–798.
7. B. R. Christopher, R. D. Holtz, and W. D. Bell. New Tests for Determining the In-Soil Stress-Strain Properties of Geotextiles. *Third International Conference on Geotextiles*, Vienna, Austria, 1986, pp. 683–688.
8. A. El-Fermaoui and E. Nowatzski. Effect of Confining Pressure on Performance of Geotextiles in Soils. *Proc.*, Geosynthetic '87 Conference, New Orleans, La., April 1987, pp. 799–804.
9. R. Johnston. *Pull-Out Testing of Tensar Geogrids*. Master's thesis. University of California–Davis, June 1985.
10. T. S. Ingold. Laboratory Pull-Out Testing of Grid Reinforcement in Sand. *Geotechnical Testing Journal*, Vol. 6., No. 3, Sept. 1983, pp. 112–119.

Publication of this paper sponsored by Committee on Soil and Rock Properties.

Geogrid Reinforcement of Granular Bases in Flexible Pavements

RALPH HAAS, JAMIE WALLS, AND R. G. CARROLL

A comprehensive laboratory research program to investigate geogrid reinforcement of granular base layers of flexible pavements was carried out at the University of Waterloo and involved repeated load tests on varying thicknesses of reinforced and unreinforced granular bases. Other controlled variables included reinforcement location and subgrade strength. The purpose of this paper is to explain geogrid reinforcement mechanisms in granular base applications through analysis of stress, strain, and deflection measurements. The results of that research are first compared with fabric reinforcement and failure criteria. For high-deformation systems both fabric and grid can be effective in tension membrane action, but for low-deformation systems the interlock and confining action of a grid is required to provide effective reinforcement. The Waterloo work showed that permanent deformation of both types of systems can be significantly reduced by using geogrid reinforcement in the granular base. The reinforcement mechanisms involved with geogrid reinforcement of granular bases, and how the stress-strain-deflection response of the structure varies, are discussed. It is concluded that, for optimum effect, geogrid reinforcement should be placed at the base-subgrade interface of thin base sections and near the midpoint of thicker bases. Moreover, the zone of such placement should not involve elastic tensile strains in the grid that are greater than 0.2 percent. Under these conditions, geogrid reinforcement can be highly effective in reinforcing the granular base material and thereby extend the life of a structure.

The function of reinforcement is to strengthen by additional assistance, material, or support. For the same reason that steel reinforcement is embedded in concrete, reinforcing materials can be incorporated into the base layer of flexible pavements so that the two materials act together to resist forces. Interlock or positive bond between the reinforcement and the aggregate particles is required to truly reinforce the granular base of flexible pavements. Because an unbound base cannot take tension, the function of the interlock or bond is to mobilize the strength of the reinforcement and impart this resisting force to the base. In addition to possessing the appropriate physical properties to interlock with the base layer, a pavement reinforcing material should possess the following mechanical properties:

1. High tensile modulus to resist stretching under load;
2. Dimensional stability to resist radial stresses without deforming, warping, or stretching;
3. Elastic response under dynamic loading;
4. Resistance to plastic strain with repeated load applications; and
5. Inertness and durability.

For more than a decade geotextile fabrics have been used for subgrade stabilization of soft foundation soils. In subgrade stabilization, the separation function of the fabric is the key to performance. It prevents granular base material from punching into soft foundation soils under the wheel or track loads of construction vehicles. Because base punching or localized shear failure is prevented, the subgrade can develop its full bearing capacity. This separation function provides an increase in subgrade load capacity when the soil shear strength is quite low ($<$ 1,000 psf) and the subgrade is prone to deep rutting. As subgrade shear strength increases ($>$ 1,000 psf), however, these benefits diminish.

Fabric applications have been limited for the most part to high-deformation systems in which surface deflections of 3 in. or greater are allowable—for example, haul and access roads over soft ground. But there is little if any evidence to support improvements via fabric separation or reinforcement in low-deformation systems.

Recent developments in geogrid technology, however, suggest that the interlock and tensile modulus characteristics of certain grid products might be beneficial as reinforcement within the granular base of low-deformation systems, such as flexible pavements, as well as high-deformation systems. This was clearly demonstrated in the University of Waterloo research program (*1–3*), which is subsequently discussed.

In addition to possessing the previously mentioned properties, grids can be manufactured with opening sizes compatible with typical base course maximum particle sizes (i.e., 1 to 1½ in.). The grids provide a most efficient means for carrying tensile stresses transmitted through the base course. The result is confinement of the aggregate particles and a reduction in strain due to wheel loads.

R. Haas, Department of Civil Engineering, University of Waterloo, Waterloo, Ontario N2L 3G1, Canada; J. Walls and R. G. Carroll, The Tensar Corporation, 1210 Citizens Parkway, Morrow, Ga. 30260.

The purpose of this paper is to provide some general background, summarize the results of the research program carried out at the University of Waterloo, examine the mechanisms that govern the performance of grid reinforcement, and define the optimum conditions for effective reinforcement of the base layer of flexible pavements.

BACKGROUND

In recent years, several laboratory and full-scale trials have been carried out to study the reinforcement potential of geotextiles and geogrids in both unpaved (high-deformation) and paved (low-deformation) roads. Through these programs, several reliable design methods have been developed. In addition, hundreds of installations have been observed by practicing civil and geotechnical engineers. Despite the vast amount of information available and increased experience with geotextiles and geogrids, many failures still occur because of a lack of understanding of how these materials affect the properties of the basic engineering materials (e.g., subgrades, engineering fills, and pavement materials) or how reinforcement affects the load response of the structure.

Even a review of the literature can be confusing because various studies indicate everything from inferior to superior performance of reinforced paved and unpaved roads compared with unreinforced structures. Several studies report conflicting observations about the optimum location for reinforcement, which ranges from the base-subgrade interface to a location near the top of the base. For example, studies by Halliday and Potter (*4*) and Ruddock et al. (*5*) concluded that the presence of a woven polyester geotextile had no effect on the structural performance of asphalt pavements. In both test programs the geotextile was placed at the bottom of the base course. A field test program by Barker (*6*) showed that grid reinforcement at the midpoint of a 6-in. base course of a flexible pavement had only a minor effect on reducing rutting beneath heavy aircraft loads. On the other hand, large-scale laboratory tests by Bathurst et al. (*7*) indicated that geogrid reinforcement placed in the upper section of railway ballast had a significant impact on reducing tie-ballast settlements over flexible subgrades. Similarly, plate loading tests on Reinforced Earth slabs at the Cooper Union School of Engineering showed decreasing settlement and higher bearing capacities with reinforcement layers placed close to the footing (*8*). In contrast, the Waterloo study showed that maximum rutting reduction benefits of grid reinforcement were evident when grid was placed within the lower half of the base course of flexible pavements.

To explain these apparent discrepancies, it is necessary to look more closely at the variables tested in each of the test programs and to examine the effects reinforcement has on the load response of a system. Variables that might result in apparent discrepancies in test results include type of structure; subgrade type and strength; failure criteria; static versus dynamic load; shape, size, and magnitude of load; and type and location of reinforcement.

Perhaps the most significant of these variables are the failure criteria used for drawing conclusions from a particular study. For example, a test program that considers failure at deformations of 2 in. or more would not be applicable to flexible pavement structures. Furthermore, cyclic load tests that cause initial deflections of more than 0.1 in. would also not be applicable to flexible pavements. In essence the structure being tested would be underdesigned as a flexible pavement but might be appropriate for a temporary haul road. The importance of the failure criteria is that they can dictate design parameters such as type and location of reinforcement and number of reinforcement layers.

For example, it has been shown by several investigators that deformations can be significantly reduced by the inclusion of reinforcement near the surface of an unbound base course. This is true for high-deformation systems because the initial deformations tension the reinforcement and allow it to carry tensile load through tension membrane action. Before it is tensioned, however, the reinforcement is actually in a zone of compression, and the initial deformation that is required to mobilize the reinforcement is typically greater than tolerable rut depths for flexible pavements.

Thus, for reinforcement to be effective in flexible pavement structures, it is apparent that the optimum location must be in a zone of tensile stress during the first load application and remain in a tensile zone throughout the design life. This location will be dictated by the shape, size, and magnitude of the design wheel loads as well as the strength characteristics of the pavement layers, including the subgrade.

WATERLOO TEST PROGRAM

The experimental program involved full-scale cyclic load tests on both reinforced and nonreinforced model pavement sections. These sections consisted of asphalt concrete 3 to 4 in. thick and aggregate base constructed over a sand subgrade. Variables in the test program included subgrade bearing capacity, base layer thickness, asphalt concrete layer thickness, and grid location within the base layer. The principal objectives of the experimental investigation were to

1. Develop equivalency factors for geogrid-reinforced granular base sections;
2. Develop structural design procedures for geogrid-reinforced flexible pavements using the equivalency factors developed in Objective 1; and
3. Analyze geogrid reinforcement mechanisms in flexible pavements through the use of stress, strain, and deflection measurements.

The experimental program was divided into six test series or "loops," each of which contained four separate tests. Each loop was carefully designed to control the key variables in order to isolate and examine the effects of geogrid

reinforcement. A summary of the test arrangements is given in Table 1.

Test Facility

The test facility at the University of Waterloo consisted of a large rectangular box, 15 ft × 6 ft × 3 ft, constructed of plywood reinforced by a steel frame and lined with galvanized steel sheeting.

Loads were applied by a steel plate 12 in. in diameter driven by a servohydraulic actuator rated at 13 kips. Each test section was subjected to an identical loading sequence that consisted of a series of dynamic loads followed by a single static load at predetermined cycle counts. The load applied to the pavement surface for both types of loading was 9,000 lb, which applied a pressure of 80 psi through the load plate. The configuration and magnitude of the applied load were selected to simulate a set of dual wheels under an equivalent 18-kip single axle load. Dynamic loads were applied at a frequency of 8 cycles per second.

Instrumentation

Each test set up was instrumented as shown in Figure 1. Five dial gauges were placed on the asphalt surface and load plate along with an actuator linear velocity displacement transformer (LVDT) to measure surface deflections and permanent deformations of the asphalt surface. In addition, foil-type strain gauges were placed on the mesh at several locations at increasing radial distances from the load center.

In selected tests, pressure cells were placed 1.5 in. below the top of the subgrade to compare differences in stress distribution in reinforced and unreinforced sections.

Subgrade

The prepared subgrade consisted of a very fine-grained beach sand (SP) (99 percent passing the No. 40 sieve, 32 percent passing the No. 100 sieve, 4 percent passing the No. 200 sieve). Because it had an almost uniform grain

TABLE 1 TESTS LOOPS, CONTROLLED VARIABLES, AND OBJECTIVES

Test No.	Asphalt Thickness (in.)	Base Thickness (in.)	Reinforcement Location Within Granular Base	Subgrade CBR	Objectives
Loop No. 1					
1	4	8	None	8	Location effect
2	4	8	Bottom	8	
3	4	8	Mid	8	
4	4	8	Top	8	
Loop No. 2					
1	3	8	None	3.5	Granular base thickness effect and softer subgrade effect
2	3	8	Bottom	3.5	
3	3	6	Bottom	3.5	
4	3	4	Bottom	3.5	
Loop No. 3					
1	3	10	Bottom	–[a]	Thicker granular effect; very weak, saturated subgrade effect; and grid location effect
2	3	8	Mid	–[a]	
3	3	10	None	–[a]	
4	3	12	None	–[a]	
Loop No. 4					
1	3	6	Bottom	1	Very weak subgrade and thickness effect
2	3	8	Bottom	1	
3	3	8	None	1	
4	3	12	Mid	1	
Loop No. 5					
1	2	6	Mid	1	Very weak subgrade and effect of pretensioning geogrid
2	3	6	Mid, tensioned	1	
3	3	12	Mid, tensioned	1	
4	3	12	None		
Loop No. 6					
1	3	12	Subgrade	<1	Very weak subgrade effect, reinforced subgrade effect, and 2 layers of reinforcement effect
2	3	12	Bottom	<1	
3	3	12	None	<1	
4	3	12	Mid and Base	<1	

[a]The subgrade started out at a CBR of 4 but due to loss of moisture became very strong toward the end of this loop.

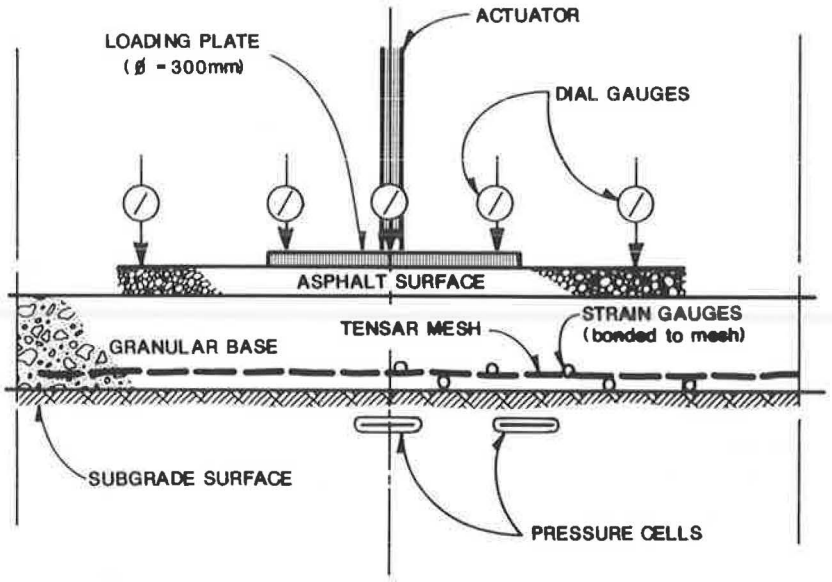

FIGURE 1 General arrangement of instrumentation.

size, it was ideal for varying support strength by changing the moisture content.

Aggregate Base

The base material for all tests was a well-graded crushed stone aggregate (GW) (100 percent passing the 1-in. sieve, 49 percent passing the No. 4 sieve, 4 percent passing the No. 100 sieve, 2.3 percent passing the No. 200 sieve). The optimum moisture content and maximum dry density were determined to be 6 percent and 146 lb/ft^2, respectively.

Asphalt Concrete

The asphalt surface layer for all tests was a dense-graded material with a maximum aggregate particle size of 0.6 in. and an 85/100 penetration grade asphalt cement.

Geogrid Reinforcement

The geogrid used for all tests was Tensar SS1 Geogrid. The key performance properties of this grid are given in Table 2.

TEST RESULTS

In addition to the first two objectives of evaluating the potential of geogrids for effective reinforcement of flexible pavements and developing design relationships, the third objective of the test program was to analyze the reinforcement mechanisms by using stress, strain, and deflection measurements. By gaining an understanding of how geogrids affect the load response of a pavement structure, it is possible to identify conditions for optimum reinforcement benefit as well as conditions for which grid reinforcement may not be as effective.

The major conclusions of the test program, which have been reported elsewhere (*2, 3*), follow:

1. Grid reinforcement can increase the number of load cycles carried by a factor of 3 (for a "failure" criterion of 0.8-in. permanent deformation, which is generally considered appropriate for high-type pavement facilities);
2. Base thickness reductions of 25 to 50 percent are made possible by inclusion of geogrids; and
3. The optimum location of grid reinforcement within the granular layer was found to be dependent on granular thickness and subgrade strength.

These conclusions suggest that the potential benefits of incorporating grid into a base layer are dependent on choosing the appropriate grid location because grid location can dramatically affect the load response of the pavement. Examination of stress, strain, and deflection data clearly indicates how geogrid reinforcement at the optimum location can effectively interlock with and confine an aggregate base, resulting in increased resistance to lateral and vertical deformation.

Stress Measurements

Pressure cells were placed 1½ in. below the top of the subgrade in selected test sections. In Loops 2 to 5, one pressure cell was placed directly beneath the load center and another at 12 in. radial distance from the load center. In Loop 6, one pressure cell was placed beneath the load center only in three of the four tests.

Pressures were monitored at predetermined cycle counts when dynamic loading was temporarily stopped. Readings

TABLE 2 TENSAR SS1 GEOGRID (BX1100)

Geogrid Property	Test Method	Unit	Value
Aperture size	I.D. calipered[a]		
MD (roll direction)[b]		in.	1 (nom.)[c]
CMD (across roll width)[d]		in.	1.3 (nom.)
Open area	COE method[e]	%	70 (min.)
Thickness	ASTM D 1777-64		
Rib		in.	0.03 (nom.)
Junction		in.	0.11 (nom.)
Flexural Rigidity	ASTM D 1388-64		
MD		mg·cm	250,000
CMD		mg·cm	325,000
Tensile modulus	ASTM D 638-82[f] (modified)		
MD		lb/ft	14,000 (min.)
CMD		lb/ft	20,000 (min.)
Junction strength	ASTM D 638-82[g]	%	90 (min.)

[a]Maximum inside dimension in each principal direction measured by calipers.
[b]MD = machine direction, which is along roll length.
[c]Nominal values that shall not vary by more than ± 15 percent.
[d]CMD = cross machine direction, which is across roll width.
[e]Percentage of open area measured without magnification by Corps of Engineers method as specified in CW 02215 Civil Works Construction Guide, November 1977.
[f]Secant modulus at 2 percent elongation measured by tensile loading test (ASTM D 638) modified to clamp single ribs of the grid structure at junctions and apply a constant rate of extension of the rib of 2 in./min at 68°F. No offset allowances are made in calculating secant modulus.
[g]ASTM D 638 modified to accommodate clamping of T-shaped junction and strained at 2 in./min (see TNN:PT2).

were taken using both 0- and 9,000-lb loads after a period of 3 min.

In Loop 2, it was observed that reinforcement at the base of the granular layer reduced the stress on the subgrade by approximately 22 to 23 percent from the first load application up to 10,000 cycles. Permanent deformations at the surface after 10,000 cycles were 0.8 and 0.46 in. for the control and reinforced sections, respectively. After 150,000 cycles the reduction in stress due to grid reinforcement was just 12 percent with deformations of 2.7 and 1.9 in., respectively. Although these deformations considerably surpassed the failure point (i.e., 0.8-in. permanent deformation) of both sections, the greater percentage reduction in stress in the control section can be attributed to shear failure of the asphalt concrete, base layer, and subgrade. Figure 2 shows the changes in subgrade stress with increasing load cycles.

In Loops 4 to 6, the subgrade strength was lowered to values of California bearing ratio (CBR) less than or equal to 1.0 by the addition of peat moss and moisture. However, given the physical constraints of the test facility, it was not possible to build pavement sections thick enough to be considered adequately designed for loads that would typically be carried by a highway pavement. Thus the final pavement sections tested, both with and without reinforcement, were underdesigned.

In contrast to the stress reductions that were observed in Loop 2 over a relatively weak subgrade, comparison of pressure cell readings in Loops 4 and 6 over very weak subgrades showed higher initial stresses (3 to 25 percent) in the subgrade beneath reinforced pavement sections changing to approximately equal stress values at the end of testing. Deformations at the end of testing were 1.9 in. (reinforced) and 2.4 in. (unreinforced) in Loop 4 and 1.8 in. (reinforced) and 2.3 in. (unreinforced) in Loop 6 after 10,000 cycles.

In summary, it was shown in Loop 2 that the grid contributed to a significant reduction in vertical stress on the subgrade, which suggests that the interaction of grid with the base course aggregate affects the distribution of stresses through the base layer of a low-deformation pavement and reduces the maximum vertical stress transmitted to the subgrade. On the other hand, the pavement sections of Loops 4 and 6 were so underdesigned that the grid was significantly stressed beyond its range of totally recoverable elastic response, and reductions in maximum stress were not initially apparent. In high-deformation structures, such as temporary haul roads, relatively large deformation occurred rapidly in both reinforced and control sections, and stresses on the subgrade were not reduced until tensioned membrane forces were taken up by the reinforcement. Thus, for grid reinforcement to be most effective, it is reasoned that the optimum location will be dictated by acceptable levels of stresses and strains within the grid itself.

Strain Measurements in Grid

Strain gauges were attached to the bottom side of the geogrid at various radial distances from the load center. As was the case with pressure cell measurements, strain readings were taken at predetermined cycle counts when dynamic loading was stopped. Comparison of strain data with performance criteria such as permanent deformations indicated that grids provided reinforcement benefit for low-

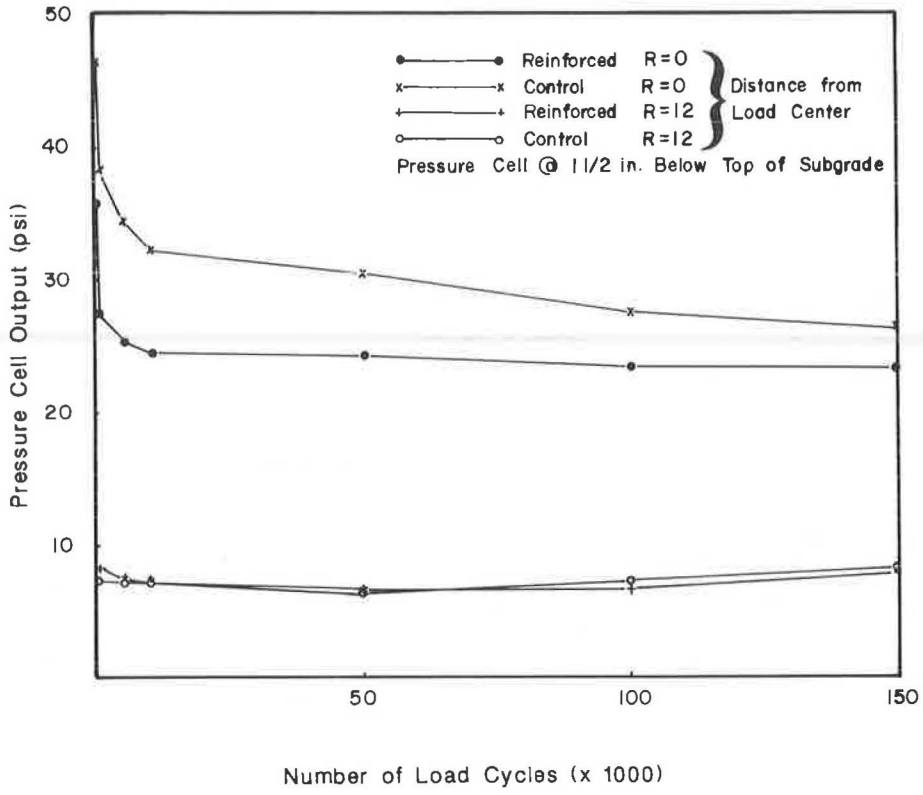

FIGURE 2 Pressure cell output versus load cycles, Loop 2.

deformation sections when initial elastic strain beneath the load center was less than or equal to 0.2 percent, provided that the grid was placed within the lower portion of the base layer. Under these ideal conditions, it was observed that elastic strain in the grid would decrease with increasing radial distance from the load center (Figure 3). At distances of 10 to 15 in. from the load center (approximately twice the radius of the load plate), small compressive values of strain were observed.

These results clearly illustrate the confinement effect of geogrids in the vicinity of the load. The grid is immediately mobilized to carry tensile stresses; long anchorage lengths

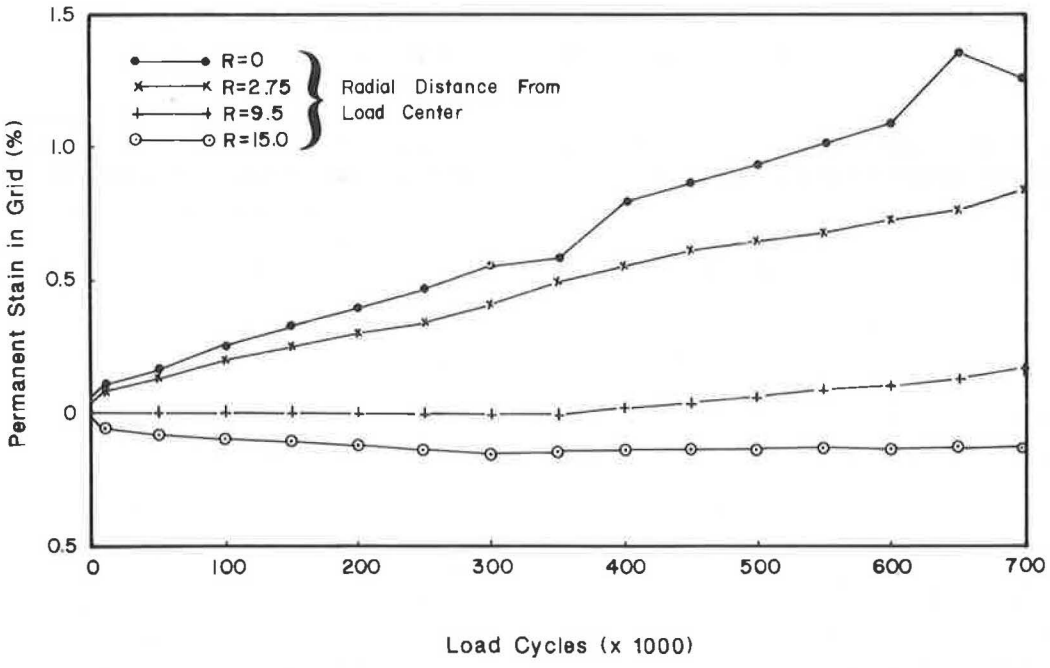

FIGURE 3 Permanent strains in grid versus load cycles: Loop 1, Test 2.

are not required, and large deformations do not have to occur.

As was the case with permanent deformations, plastic strain in the grid increased gradually with an increasing number of load cycles. Although the grid behaves elastically under moderate stress, these immeasurable plastic strains appeared to increase linearly with the number of load cycles, as shown in Figure 3. It was found that, at the failure level of 0.8-in. total deformation, plastic strains in the grid ranged from 1.0 to 1.8 percent in tests in which grid provided the most benefit (i.e., in the lower half of the base of structurally adequate pavements).

On the other hand, when grid was placed near the top of the base layer, no performance benefit was observed. Observation of both elastic and plastic strains revealed that both were initially very low. As the number of load cycles increased beyond 500, the grid went into compression beneath the load center until relatively large surface deformations occurred. These were in the order of 0.6 in. after 100,000 cycles. Thus the pavement section was approaching failure (i.e., 0.8 in.) before the grid began to take up tensile load. It was further noted that the grid was in tension 15 in. from the load center, suggesting that it was acting more independently to support load than when it was placed in the lower portion of the base.

As stated previously, Loops 4 to 6 were underdesigned for the soft subgrade conditions. This was also evidenced by the considerably higher elastic strains that were observed in the grid (i.e., 0.2 to 1.0 percent strain under the load center). Furthermore, high tensile strains were also noted at 9 and 14 in. from the load center in some cases. The higher strains away from the load center indicate that the grid was overstressed for its confinement function in a flexible pavement (i.e., it was being stretched more like a membrane). Thus the cumulative strain along the tensioned member resulted in the rapid occurrence of a permanent deformation of 0.8 in., which is similar to the deformation of the pavement section without reinforcement. However, it was found that the rate of deformation was less for the grid-reinforced test sections after the initial 0.8-in. deformation had occurred and that if a high value were chosen for the failure criterion (e.g., 1.5 in., which is used for lower-type paved roads) grid-reinforced sections again carried two to three times as many load cycles to failure.

The important finding here is that stress or strain levels for which grid reinforcement is most effective in flexible pavements can be quantified by stress-strain analysis and taken into consideration during design. Thus layered elastic theory can be used to design a pavement with geogrid reinforcement such that radial strains under the load center at the proposed grid location will fall within some limiting range, for example, 0.05 to 0.2 percent.

Deflection Measurements

In all tests five dial gauges were used in conjunction with the actuator LVDT to measure elastic deflection and permanent deformations at various locations along the asphalt surface. Two of the dial gauges were placed on the loading plate ½ in. in from the outside edge. Again, static readings were taken on all five gauges at predetermined cycle counts. In addition, dynamic deflections of the load plate itself were recorded by the actuator LVDT at the beginning and end of each series of dynamic loading.

Although it has been reported previously that geogrid reinforcement shows no appreciable reductions in static or dynamic deflections directly beneath the load, an examination of average static deflection readings in Loops 1 and 2 did indicate that the shape of the deflection basin was somewhat flatter for reinforced pavements than for control sections of equal thickness.

In Figure 4, average deflection values for the four tests of Loop 1 have been plotted at various distances from the load center. As can be seen, the two sections reinforced with grid in the lower half of the base layer show consistently lower values for elastic deflection, particularly at the critical location near the edge of the load plate. This implies that the base course of the reinforced section is stiffer (i.e., has a higher elastic modulus) and is indeed yielding less than the control section at the edges of the plate. In other words, the cantilevered portion of the 1-in.-thick plate bends more in the reinforced tests.

The vertical scale of Figure 4 is, of course, considerably exaggerated compared with the horizontal scale. This is normal practice in the pavement engineering field, particularly for field measurements during which deflection bowls measured by such devices as the Dynaflect or Falling Weight Deflectometer are plotted to a much exaggerated vertical scale. The purpose is to more clearly illustrate differences that may be small in absolute magnitude but highly significant with regard to behavior of the pavement structure.

Figure 4 also shows that elastic deflections in the section with grid near the surface of the base were considerably greater than those in the control section, although the shapes of the two deflection bowls are fairly similar. This indicates that placing the grid near the surface of the base does not provide much confining or stiffening effect.

Because of the soft subgrade conditions of Loops 4 to 6, static deflections were excessive for higher-type flexible pavements, ranging from approximately 0.2 to 0.6 in. under the load center. Nevertheless, the data still provided useful information about optimum location and limitations of grid reinforcement in high-deformation structures. For example, in Loop 4, the plate deflections were reduced by approximately 17 percent at cycles 1 and 20,000 when grid was placed at the bottom of an 8-in. base layer, as shown in Figure 5. Again, it was observed that the angle of curvature of the deflection basin was reduced in the grid section. The resultant permanent deformations at the surface after 20,000 load cycles were 1.794 and 2.371 in. for the reinforced and control sections, respectively, or a 25 percent reduction in rut depth.

On the other hand, when grid was placed at the midpoint of a 12-in. base layer over the weakest subgrade of all, Loop 6, it was found that deflections of the load plate were significantly less in the control section although the shape

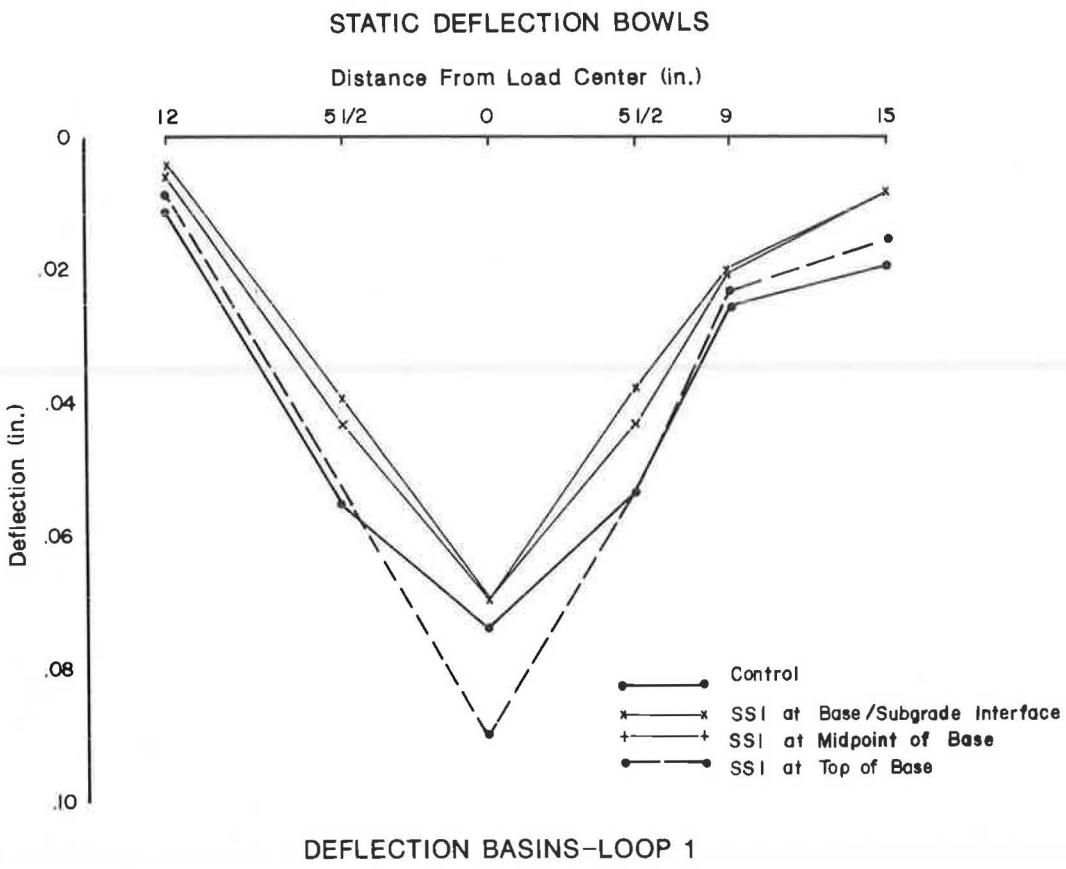

FIGURE 4 Deflection basins, Loop 1.

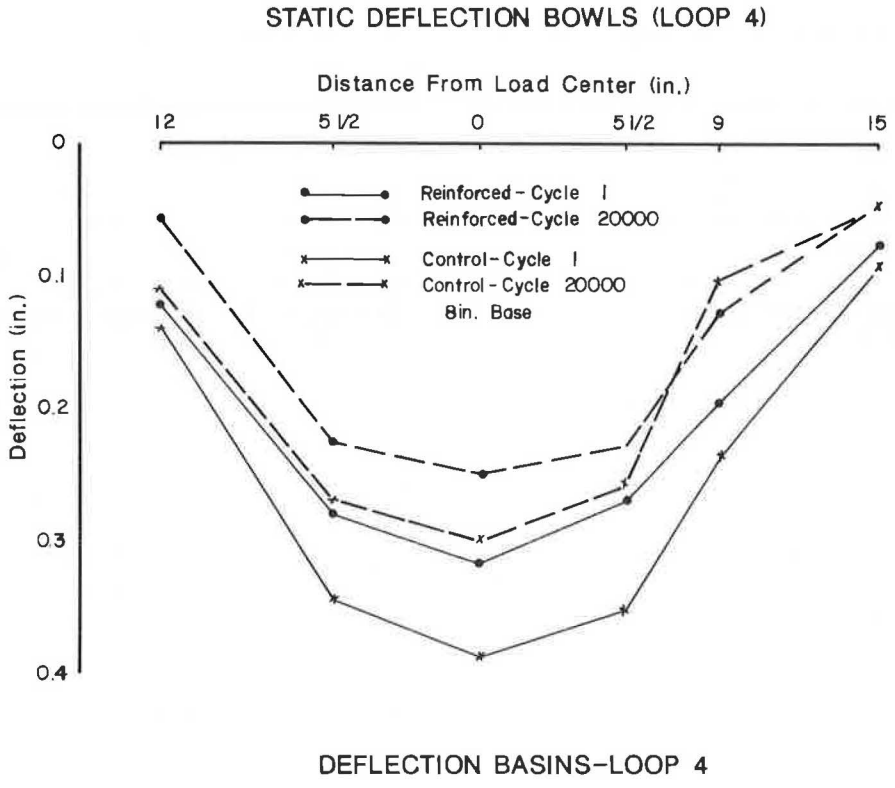

FIGURE 5 Deflection basins, Loop 4.

of the deflection basins was approximately the same. Permanent deformations at the surface after 40,000 cycles were 1.67 and 1.68 in. for the reinforced and control sections, respectively, indicating no benefit from grid under the conditions of the test. This finding is consistent with the results of another test program on grid reinforcement of granular base over peat carried out at the Royal Military College (RMC) of Canada. It was found in the RMC study that grid reinforcement at the midpoint of a 12-in. granular base did not provide any improved rutting resistance under load until permanent deformations were quite large (i.e., on the order of 6 to 8 in.). In addition, there was no appreciable decrease in static deflections. When the granular base was removed, it was found that aggregate had punched into the peat in a manner similar to that observed on the unreinforced section. However, when placed at the bottom of the base layer, geogrid reinforcement significantly reduced rutting, subgrade deformation was more gradual and widespread, and little or no punching of aggregate into the peat occurred. This last observation suggests that the grid can be an effective separator, if placed at the interface.

CONCLUSIONS

Through analysis of stress, strain, and deflection data, it has been shown that grid reinforcement does alter distribution of load-induced stresses in flexible pavements. The result is that the rate of permanent deformation (rutting) can be decreased and pavement life can be extended. However, it has also been shown that conditions exist for which grid reinforcement does not offer performance benefits. The key to optimizing geogrid potential is proper design. Proper design requires appropriate layer thicknesses and selection of optimum geogrid location.

For thin bases, the optimum grid location is usually considered to be at the base-subgrade interface. However, for thicker bases, there is sufficient evidence to suggest that the optimum location is in the middle portion. No benefits are expected when a single layer of grid is placed within a zone of compression, such as

- Near the top of the base layer under an asphalt concrete surface or
- Within the base layer (e.g., midpoint or higher) of thick bases over very soft flexible subgrades.

In the second case, it has also been found through field experience that geogrid reinforcement at the base-subgrade interface over soft, flexible subgrades segregates the layers and facilitates construction of a stiffer base using less material. If the base is very thick, a second layer of geogrid may be placed at some middle location to retard the rate of permanent deformation within the base itself.

In summary, for optimum grid reinforcement of flexible pavements, the grid must be placed in a zone of moderate elastic tensile strain (i.e., 0.05 to 0.2 percent) beneath the load center, and maximum permanent strain in the grid over the design life should not exceed 1 to 2 percent, depending on the rut depth failure criteria. Under these ideal conditions, grid reinforcement behaves elastically and effectively confines aggregate base, thus prolonging the life of the pavement structure.

REFERENCES

1. G. Kennepohl, N. Kamel, J. Walls, and R. Haas. Geogrid Reinforcement of Flexible Pavements: Design Basis and Field Trials. *Proceedings of the Association of Asphalt Paving Technologists*, Vol. 54, 1985, pp. 45–70.
2. R. Penner, R. Haas, J. Walls, and G. Kennepohl. Geogrid Reinforcement of Granular Bases. Presented at the Roads and Transportation Association of Canada Annual Conference, Vancouver, Canada, 1985.
3. R. Penner. *Geogrid Reinforcement of the Granular Base Layer in Conventional Three-Layer Pavement Sections*. MASc thesis. University of Waterloo, Waterloo, Ontario, Canada, Aug. 1985.
4. A. R. Halliday and J. F. Potter. *The Performance of a Flexible Pavement Constructed on a Strong Fabric*. Report LR1123. Transport and Road Research Laboratory, Crowthorne, Berkshire, England, 1984.
5. E. C. Ruddock, J. F. Potter, and A. R. McAvoy. *Report on the Construction and Performance of a Full Scale Experimental Road at Sandleheath*. Project Record 245. Construction Industry Research and Information Association, London, England, 1982.
6. W. R. Barker. *Open-Graded Bases for Airfield Pavements*. Miscellaneous Paper GL-86. U.S. Army Corps of Engineers Waterways Experiment Station, Vicksburg, Miss., July 1987.
7. R. J. Bathurst and G. P. Raymond. Geogrid Reinforcement of Ballasted Track. In *Transportation Research Record 1153*, TRB, National Research Council, Washington, D.C., 1987, pp. 8–14.
8. V. A. Guido, J. V. Knueppel, and M. A. Sweeny. Plate Loading Tests on Geogrid-Reinforced Earth Slabs. *Proc.*, Geosynthetic '87 Conference, New Orleans, La., 1987, Vol. 1, pp. 216–225.

Publication of this paper sponsored by Committee on Soil and Rock Properties.

Large-Scale Model Tests of Geocomposite Mattresses over Peat Subgrades

RICHARD J. BATHURST AND PETER M. JARRETT

Prefabricated flexible polymeric soil confinement systems (called geoweb or geocell mattresses in this paper) hold great promise for increasing the trafficability and load-bearing capacity of thin granular bases placed over very compressible subgrades such as peat. A large-scale model test program was undertaken to compare the load-deformation performance of gravel-infilled geoweb/geocell mattresses and unreinforced gravel bases over peat under plane-strain static loading. In this investigation the geoweb mattress reinforcement was nonperforated plastic strips ultrasonically welded together (geoweb). The geocell reinforcement was constructed from strips of polymeric mesh (geogrid) attached by metal bodkins. Tests showed that the geocomposite mattresses significantly improved the load-bearing capacity of the gravel base layer in comparison with equivalent depths of unreinforced gravel bases. The stiffer geoweb construction gave a greater load-bearing capacity at a given rut depth than did the less stiff geocell construction. In addition, tests showed that the reinforcing effect due to the geocomposite construction of the geoweb was initiated at a lower rut depth than was that due to the geocell structure. Comparisons between geoweb-reinforced gravel bases and unreinforced bases showed that the geoweb composites were equivalent to about twice the thickness of unreinforced gravel bases. For comparison purposes, the study also presents the results of reinforced tests using single layers of geotextile and geogrid polymeric reinforcement placed at the gravel base–peat interface.

Prefabricated flexible polymeric soil confinement systems (called geoweb or geocell mattresses in this paper) hold great promise for increasing the trafficability and load-bearing capacity of thin granular bases over weak subgrades.

The potential of near-surface confinement systems to enhance granular bases was first demonstrated in tests carried out by the U.S. Army Corps of Engineers at the Waterways Experiment Station (WES) in the late 1970s (*1*). Prototype tests were carried out using plastic tubes 300 mm deep arranged to form a three-dimensional mattress over soft clay subgrades that had a California bearing ratio (CBR) of 1. The cellular mattress was infilled with sand and subjected to repeated passes of truck wheel loads. This reinforcement scheme was seen to generate wheel ruts under cumulative axle loads equivalent to the performance of unreinforced sand bases 500 mm thick (i.e., 40 percent saving in granular fill). Significant savings were also reported in a similar study at WES that used a cellular grid fabricated from slotted aluminum sheeting (*2*). Variables such as cell dimensions, cell material, and sand infill density were subsequently investigated at WES to optimize these systems for beach stabilization under vehicle loadings (*3, 4*). These studies also concluded that polymeric material may be effective in reinforcing near-surface soil confinement systems for expedient roadway construction over subgrades other than sand. The soil confinement concept was realized commercially with the introduction of a product called "Geoweb" constructed from 200- or 100-mm-wide nonperforated high-density polyethylene strips ultrasonically welded together to give a durable cellular mattress (*5*).

More recently, researchers at Sunderland Polytechnic U.K. have reported the results of model tests carried out with geoweb mattresses constructed over subgrades of two different stiffnesses (*6, 7*). The mattresses were constructed from 200-mm-thick geoweb infilled with a granular material. Reinforced and unreinforced test configurations were subjected to repeated static loading and plate bearing tests with a plate 300 mm in diameter. The tests showed that the reinforced sections significantly outperformed the unreinforced sections. For example, unpaved reinforced sections with poorly graded granular infill and a firm subgrade recorded a cumulative vertical deformation after about 104 load applications that was 50 percent of that recorded for the comparable unreinforced test. For a similar pair of test configurations with a soft subgrade, the data indicate that after 104 load applications the reinforced system recorded only 40 percent of the deformation recorded by the corresponding unreinforced configuration. These researchers also measured the vertical bearing pressures at the geocomposite-subgrade interface. They found that vertical stresses at these locations were significantly reduced for the reinforced sections, indicating that the reinforced base layers were more effective in distributing surface loads over a wider subgrade area. Finally, the test data showed that permanent deformations and vertical interface stresses for reinforced sections over soft subgrades were further reduced by using a well-graded granular fill.

Geoweb mattress composites have been used in practice to provide cost-effective road bases over compressible terrain, including soft organic clays (*8*, p. 81) and landfills (*9*), and to stabilize ballasted track (*10*).

Civil Engineering Department, Royal Military College of Canada, Kingston, Ontario K7k 5L0, Canada.

GEOWEB AND GEOCELL REINFORCEMENT MECHANISMS

The mechanisms that are responsible for the improved capacity of geocomposite mattresses are complex, and at present no analytical models exist to predict load-deformation behavior of these systems where they are constructed over very compressible terrain. Nevertheless, qualitative features of reinforcement mechanisms have been identified (*11, 12*). In simple terms, the cellular reinforcement in these systems improves the load-deformation behavior of the infilled soil through lateral confinement. Lateral spreading of reinforced base materials is resisted by hoop stresses in the cell walls and passive resistance developed in adjacent cells. Penetration of base materials in soft subgrades is reduced by the combined effect of high lateral confining stresses and soil–cell wall friction. Granular bases that have insufficient bearing capacity can develop adequate shear capacity under static or repeated load when confined in this manner. In pavement systems, the geocomposite mattresses increase the flexural stiffness of the structure and distribute surface loadings over a wider area at the pavement structure–subgrade interface.

OBJECTIVES

The principal objective of the current study was to investigate the static load-deformation behavior of geoweb and geocell mattress composites constructed over peat subgrades. A second objective was to evaluate the performance of these geocomposites by comparing the test results with those recorded for unreinforced sections and gravel bases reinforced with a single layer of geogrid or geotextile at the gravel-peat interface.

GENERAL

The general test arrangement is shown in Figure 1. Reinforced and unreinforced test sections were constructed in

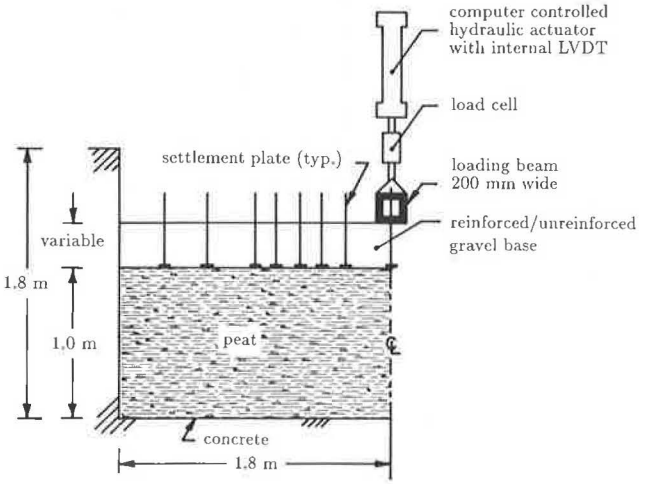

FIGURE 1 General test arrangement.

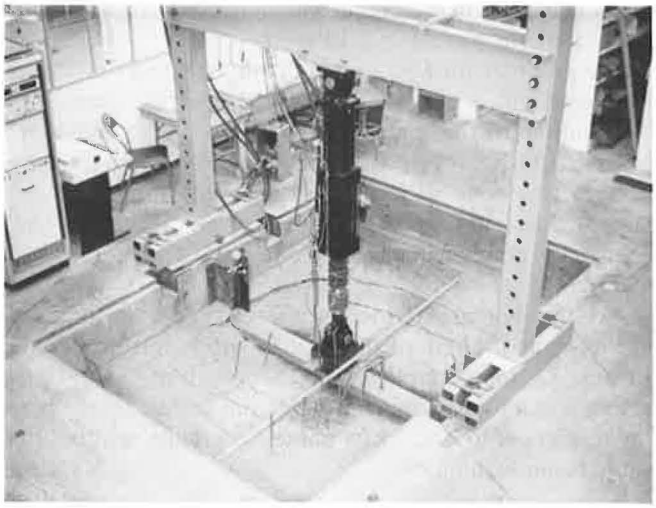

FIGURE 2 Overview of RMC test facility.

a concrete pit measuring 2.4 m wide by 3.6 m long by 1.8 m deep. An overview of the test facility is given in Figure 2. Reinforced and unreinforced gravel base layers varying from 150 to 600 mm in depth were constructed over a reproducible artificial peat subgrade nominally 1 m thick. A hydraulic actuator was used to apply a series of static load increments to a 200-mm-wide beam spanning the width of the test pit.

The current study is focused on the load-deformation behavior of two types of near-surface soil confinement schemes that include polymeric materials:

- Geoweb-gravel mattresses and
- Geocell-gravel mattresses.

The performance benefit due to these geocomposite constructions was determined by comparing these systems with unreinforced systems constructed from the same soil materials. In addition, the performance of the geocomposite mattresses was compared with that observed in a number of similar tests of single-layer polymeric sheet reinforcement. A number of these tests have been previously reported by the second author (*13, 14*).

CONSTRUCTION

Soil Materials

For the tests on reinforced and unreinforced systems reported in this paper, a very compressible subgrade comprised of a finely fibrous horticultural sphagnum peat with a low degree of decomposition was used. For each test the peat was reconstituted by adding water and then dispersing the peat-water mixture with compressed air through a system of perforated pipes at the bottom of the test facility. Preconsolidation of the peat subgrade before fill placement was achieved by downward drainage through the same system of perforated pipes. Typical moisture content of

the peat before fill placement was 750 ± 50 percent. Shear vane strengths were 3 ± 1 kPa.

The granular fill was a good quality crushed limestone aggregate with a top size of about 20 mm. The grain size distribution for this material is shown in Figure 3. Where possible, the aggregate was placed in 150-mm lifts. Compaction was done with a gasoline-driven vibrating plate tamper that had a mass per unit area of 150 kg/m^2. The compacted gravel had an average density of 1950 ± 50 kg/m^3.

As a result of fill placement, some settlement and increase in the shear strength of the peat subgrade was observed. In Test 12, for example, a 300-mm depth of gravel base resulted in a total settlement of 60 mm and an increase in shear strength to 6 ± 1 kPa in the underlying peat before static beam loading.

Geoweb-Gravel Mattress Tests

Three tests were carried out using a geoweb-gravel composite construction. The geoweb reinforcement was nonperforated polyethylene strips, 100 and 200 mm wide, ultrasonically welded together to give an open-cell construction that had a cell area of 265 cm^2. An example of the 200-mm-deep geoweb reinforcement is shown in Figure 4. The tensile capacity of the reinforcement strips in isolation is controlled by the welds, which have a seam tensile peel strength of about 7 kN/m (*5*). One test was carried out using a geoweb reinforcement 100 mm deep infilled with gravel and covered with a 50-mm layer of the same compacted fill. A second test used the same fill in a cell mattress 200 mm deep and included a compacted gravel fill cover 100 mm deep. The second test was repeated to confirm load-deformation behavior. The depth of cover in each test was selected to bring the composite gravel base course thickness up to 150 or 300 mm, which represent standard base thicknesses for a large number of reinforced and unreinforced tests that have been carried out at the Royal Military College (RMC) of Canada. In actual expedient road construction it would be reasonable to place a similar depth of unbound gravel to protect the confinement system from direct traffic loading. For brevity in the following text, these tests are referred to as 150- and 300-mm geoweb mattress tests. Finally, the reinforced sections included a layer of lightweight woven polypropylene filter fabric at the gravel-peat interface to act as a separator during construction (geotextile weight = 244 g/m^2).

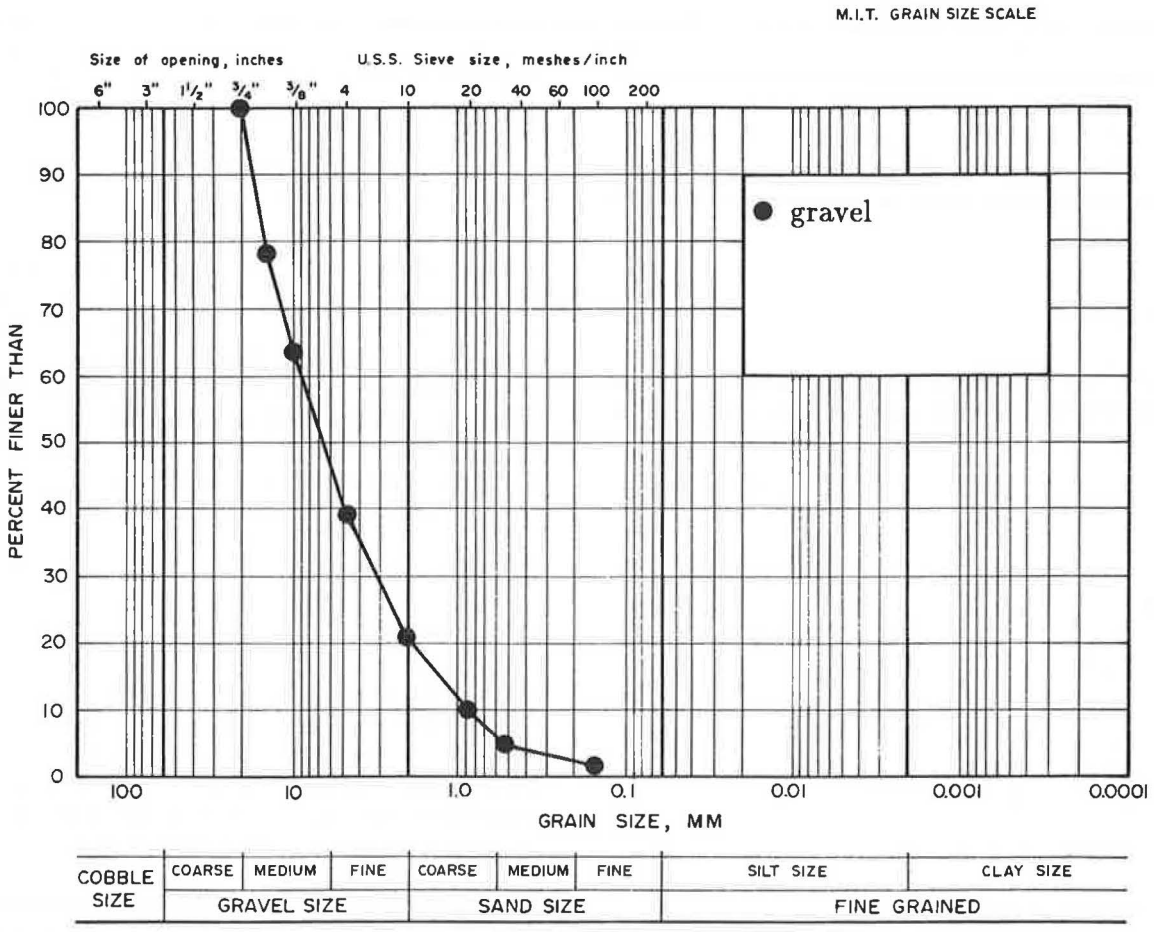

FIGURE 3 Grain size distribution of gravel fill.

Geocell-Gravel Mattress Test

A single test was carried out using a geocell-gravel mattress configuration manufactured in-house. The soil confinement material in this instance was 150-mm-wide strips of relatively high-strength open-grid reinforcement constructed from oriented high-density polyethylene (Tensar SR2 geogrid). The in-isolation load-strain-time properties of this material are well documented (*15*), and it has an index tensile test capacity of about 65 kN/m (*16*). Reinforcement strips were laced together using vertical steel bodkins to give cell areas of approximately 260 cm^2. The expanded geocell mattress was placed over a Tensar SS2 geogrid oriented with its strong direction in the plane-strain direction of the test. The original intention was to have this layer act as a gravel-peat separator during construction. The mattress was infilled and covered with 150 mm of compacted gravel fill to give a total composite thickness of 300 mm.

Single-Layer Reinforcement Tests

For comparison purposes, the results for gravel bases 300 mm thick reinforced with a single layer of geosynthetic material are also presented. Two tests employed a single layer of Tensar SS2 geogrid at the gravel-peat interface and the third a lightweight woven polyamide geotextile at the same location (geotextile weight = 229 g/m^2).

Unreinforced Tests

A total of five unreinforced tests were carried out to evaluate the load-deformation performance improvement due to geosynthetic composite construction. The unreinforced tests included 0, 150, 300, 460, and 600 mm of gravel base material.

TESTING PROGRAM

In each test a series of monotonically increasing static loads was applied to the beam seated directly on the gravel base layer (or directly on the peat for the unreinforced test with no gravel base material). The beam was loaded using a MTS computer-controlled closed-loop electrohydraulic actuator. Each load was sustained until the vertical deformation rate became less than 0.02 mm/min. This initial loading sequence was discontinued after a total vertical beam displacement (rut depth) of 200 mm had been achieved. The initial loading procedure represents a standard method that the authors have adopted over a period of several years; it has been employed in numerous similar tests to investigate a variety of geosynthetic composite structures at RMC (*13, 14*). The 200-mm rut depth criterion was selected simply because it represents a tire rut depth that may impede vehicular traffic in a comparable field case. Depending on the test, one of several different loading strategies was adopted after this initial loading

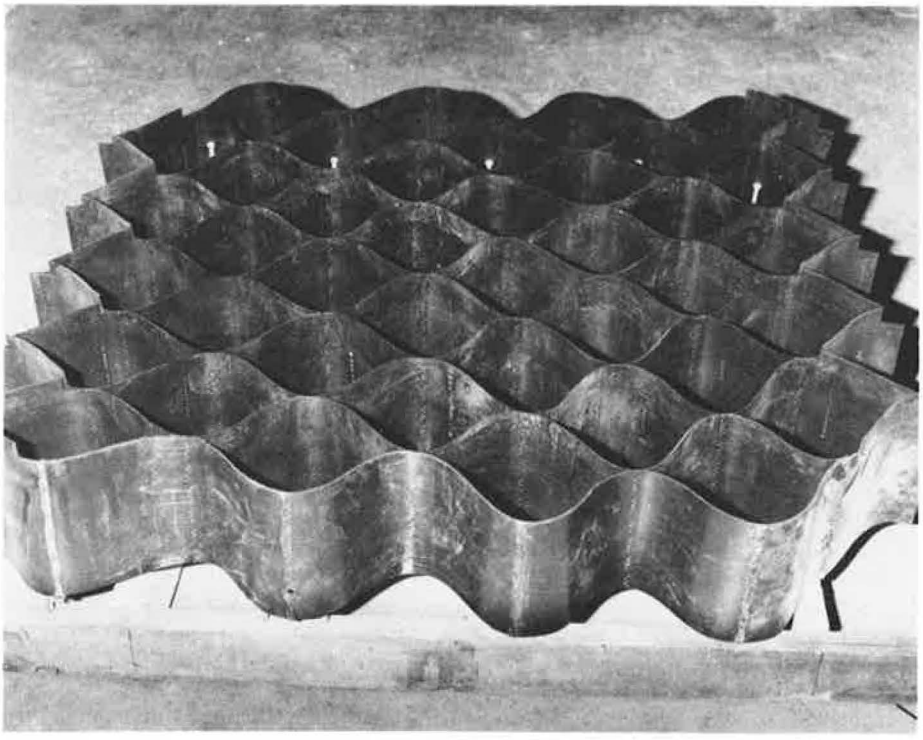

FIGURE 4 Expanded 200-mm-deep geoweb reinforcement material.

sequence. For instance, some tests were subjected to five cycles of the (previous) maximum load and then the rut was backfilled. After backfilling, the beam was again cycled at the same load level for five cycles and then subjected to a series of greater static loads. In some thin-layer unreinforced tests, the sections failed by punching before the displacement rate criterion or 200-mm rut depth had been achieved. For this reason, backfilling had to be carried out before further loading could be undertaken. Because of the different backfilling and load histories after the initial loading program, it is not possible to compare test results beyond the initial loading sequence. The second-stage loading programs of two selected tests are given later in the paper to illustrate the influence of rut backfilling and repeated static loading on the performance of geocomposite mattress constructions. A summary of the test configurations repeated in the current study is given in Table 1.

TEST RESULTS

Load Deformation

The results of (initial) load-deformation measurements taken for all tests are shown in Figures 5–7. Figure 5 shows the results of the geoweb mattress tests along with the results of the five unreinforced (control) tests. As expected, the unreinforced tests show a systematic increase in load capacity at a given rut depth with increasing gravel base thickness. It should be noted that the unreinforced tests with 0, 150, and 300 mm of gravel base were at or very near punching failure during the last applied load increment. For example, the 0.02-mm/min deformation rate criterion for the 300-mm unreinforced section could not be achieved after 200 mm of deformation. All other tests reported in this study were able to support sustained load increments after 200 mm of deformation and in many instances indicated system strain hardening.

The 150-mm geoweb mattress test (Test 1) gave a load-deformation response comparable to the response of the 300-mm unreinforced test (Test 9). Similarly, the 300-mm geoweb mattress tests (Tests 2 and 12) gave load-deformation behavior that falls between that of unreinforced base courses 460 mm thick and that of unreinforced base courses 600 mm thick (Tests 10 and 11).

Figure 6 is a plot of the results of reinforced tests of a 300-mm geocell mattress (Test 3) and a 300-mm gravel

TABLE 1 SUMMARY OF TESTS

Test No.	Composite Base Thickness (mm)	Description
1	150	geoweb mattress
2	300	geoweb mattress
3	300	geocell mattress
4	300	SS2 Geogrid at gravel/peat interface*
5	300	(repeat of 4)
6	300	geotextile at gravel/peat interface
7	0	unreinforced*
8	150	unreinforced*
9	300	unreinforced*
10	460	unreinforced*
11	600	unreinforced
12	300	geoweb mattress (repeat of 2)

*Taken from Jarrett (*13, 14*).

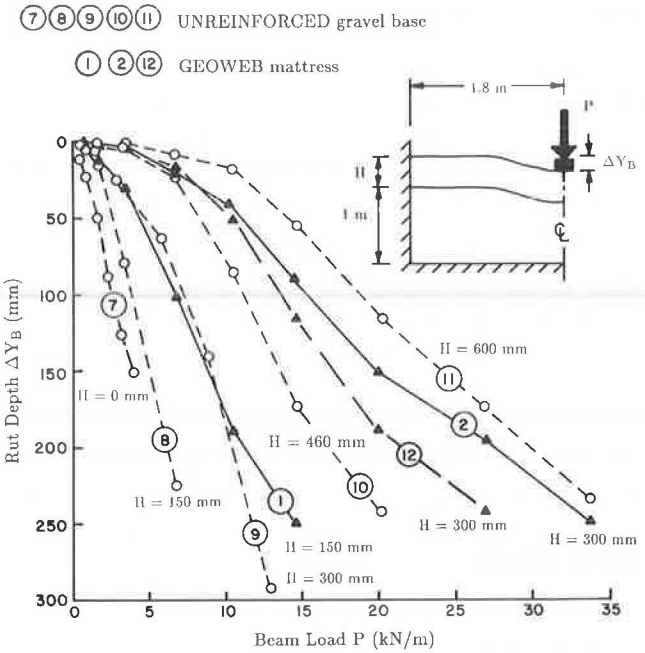

FIGURE 5 Load-deformation results for tests on geoweb mattress and unreinforced gravel base.

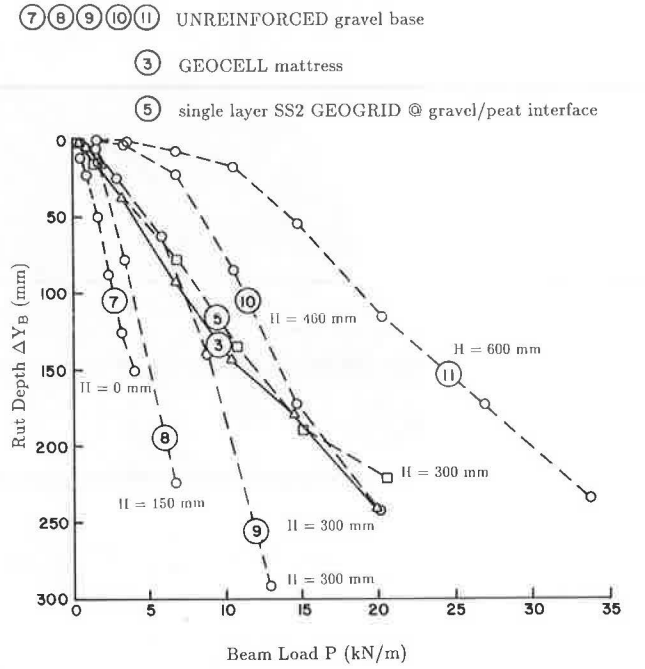

FIGURE 6 Load-deformation results for test on geocell mattress, gravel base with a single layer of geogrid reinforcement, and unreinforced gravel base.

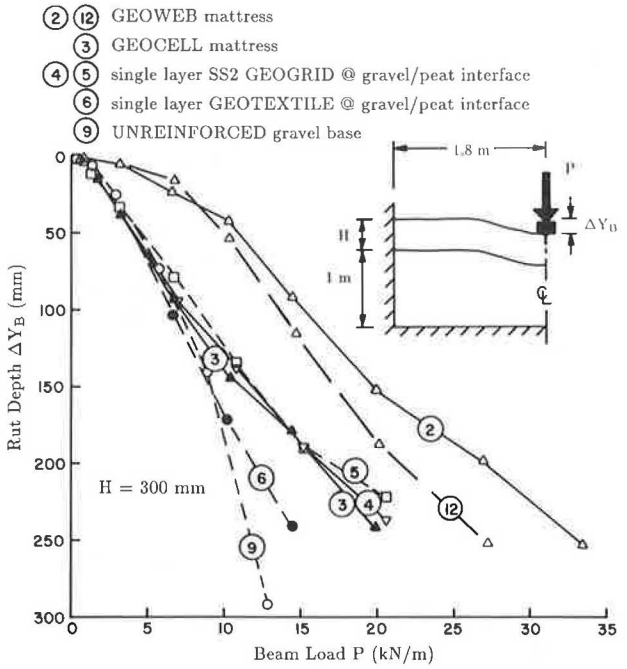

FIGURE 7 Comparison of reinforced and unreinforced tests with 300 mm of gravel base.

base reinforced with a single layer of SS2 geogrid at the gravel-peat interface (Test 5). The horizontal reinforcement in both of these tests was Tensar SS2, oriented in the same direction for both configurations. Surprisingly, both reinforced tests show similar load-deformation behavior indicating that, in this study, the geocell soil confinement system in conjunction with a single layer of SS2 geogrid offered no additional system capacity over that offered by the single layer of geogrid alone. Both tests gave load-deformation responses that were between the 300- and 460-mm unreinforced test results. At a 200-mm rut depth both reinforcement schemes gave load capacities comparable to unreinforced tests with 1.5 times the depth of compacted gravel.

The results of tests with 300 mm of gravel base are plotted in Figure 7. A variety of reinforcing systems, including single layers of polymeric reinforcement and geocomposite mattresses, is shown in this figure. All reinforced sections were stable at 200 mm of vertical deformation in contrast with the unreinforced test (Test 9), which was terminated early because of punching failure. The relative performance benefit of the reinforcing schemes is illustrated in the figure. The least improvement was indicated by the test with a geotextile reinforcement (Test 6) and the best by the 300-mm geoweb mattress tests (Tests 2 and 12). A repeat of the 300-mm reinforced test with SS2 geogrid is also plotted in the figure. The two nominally identical constructions gave sensibly equivalent load-deformation behavior indicating that test procedures were reproducible for the single-sheet reinforcement schemes.

Tests 2 and 12 indicated a similar load-deformation response up to 50 mm displacement but diverged somewhat with further application of load. This discrepancy is thought to be due to the relative difficulty of controlling uniform compaction of the gravel within the 200-mm-high cells of the geoweb composite. Figures 5–7 also illustrate that, unlike the single-layer and geocell mattress reinforcement methods of construction, the geoweb mattresses showed improved load capacity over similar thicknesses of unreinforced gravel at low rut depths. For example, Tests 3–5 indicated load capacity improvement with respect to the same depth of unreinforced gravel base after about 100 mm of vertical displacement had occurred. In contrast, the stiffer geoweb mattress configurations showed improvement after 10 to 20 mm of vertical displacement. The relative improvement due to geocomposite mattress construction is illustrated in Figure 8, which shows "equivalent" depths of unreinforced gravel base course for the same beam load and rut depth under first-time loading. For example, Curve 1 indicates that a 150-mm geoweb composite is equivalent to about 300 mm of unreinforced gravel base (a factor of 2 improvement). Similarly, the 300-mm geoweb composites over a range of rut depths are equivalent to between 500 and 600 mm of unreinforced gravel base. The relative improvement associated with the 300-mm geoweb composites is somewhat less than that inferred for the 150-mm geoweb composite as a result of the better compaction that was achieved in the shallower construction where the geoweb cells were only 100 mm high.

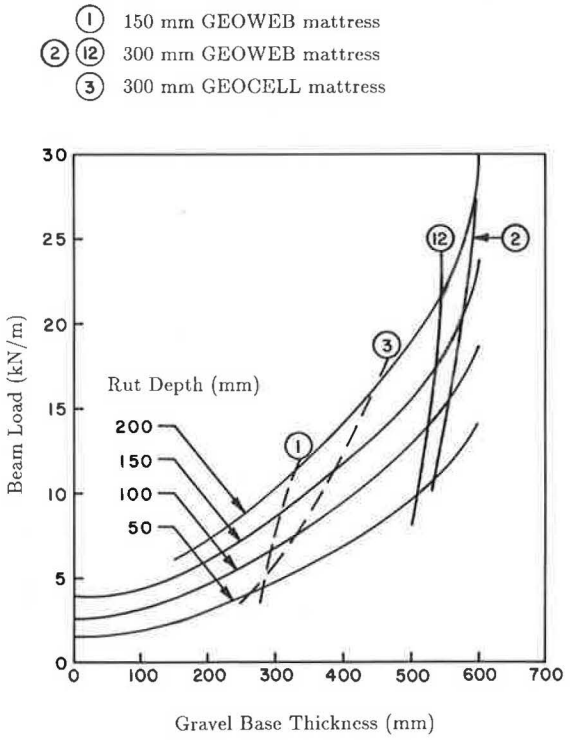

FIGURE 8 Equivalency chart for geocomposite mattress tests and unreinforced gravel bases (initial loading only).

ADDITIONAL OBSERVATIONS

At the end of each reinforced test reported in the current study, the geosynthetic reinforcements were excavated to determine any evidence of rupture. No rupture of geosynthetic reinforcements was observed in any test, nor was there any indication of tearing at the welded seams in the geoweb mattress tests or at the bodkin connections in the geocell mattress test.

DISCUSSION OF RESULTS

The relatively better performance of the geocomposite mattresses compared with that of single-sheet reinforcement schemes is consistent with the concept of greater soil confinement in geocomposite mattress construction. The performance difference of the relatively stiffer 300-mm geoweb mattress and the comparable 300-mm geocell mattress indicates that soil confinement is further enhanced through stiffer cell walls in geocomposite mattresses of similar cell dimensions. The welded geoweb strip construction was intrinsically more effective in reducing lateral spreading of the gravel fill under load than was the more flexible geogrid-and-bodkin construction. For example, in all reinforced tests, including the single-layer reinforcement tests, the gravel base course was observed to pull away from the sides of the test facility located 1.8 m from the beam. However, the geoweb mattresses showed this effect relatively early in the initial loading program, indicating that soil confinement was more effective in these configurations. The greater stiffness of the expanded 300-mm geoweb mattress compared with that of the comparable 300-mm geocell mattress before installation was visually apparent to the authors. The inherent greater flexural stiffness of the geoweb/mattresses in isolation may account for the improved load-deformation behavior of these geocomposites at low load levels. In addition, it was noticed that the gravel infill and cover were more easily compacted when geoweb mattresses were used. Nevertheless, it may be difficult to achieve uniform levels of compaction through the entire depth of a geoweb composite when aggregate with a 20-mm top size is used as infill for the 200-mm-deep geoweb material. The relative flexural stiffness of gravel base layers in the current investigation can be seen in Figure 9, which shows normalized vertical deformations recorded at the gravel-peat interface at the end of the initial loading program. The data indicate that the footing loads are distributed over a wider area for the geocomposite mattresses than for the unreinforced test and that this trend is more pronounced for the geoweb mattress construction.

On roads with gravel bases, vehicular traffic will cause any new base to rut. Conventional practice with these structures is to allow the rutting to occur during construction in order to mobilize the reinforcement capacity of the geosynthetic. Subsequently, the ruts are backfilled; this procedure is repeated until an acceptable level of surface deformation under traffic is achieved. The benefit of backfilling to system stiffness is shown in Figures 10 and 11. In Figure 11 the combined effect of backfilling followed by cyclic and static loading is seen as a further 100 mm of rutting at a beam load of 35 kN/m compared with an initial response of 240 mm at a beam load of 20 kN/m.

The current investigation has been restricted to the investigation of load-deformation of geocomposites and unreinforced gravel bases over very compressible subgrades (i.e., peat). At the time of writing, no comprehensive study of the influence of subgrade stiffness on the behavior of geocomposite mattress systems had been undertaken. A limited number of tests with relatively stiff subgrades have been reported in the literature, but they indicate only that bearing capacity of a geocomposite mattress increases with greater subgrade stiffness (*11, 12*). Recent work reported by the authors on single-layer reinforcement of coarse granular bases indicates that the relative performance ben-

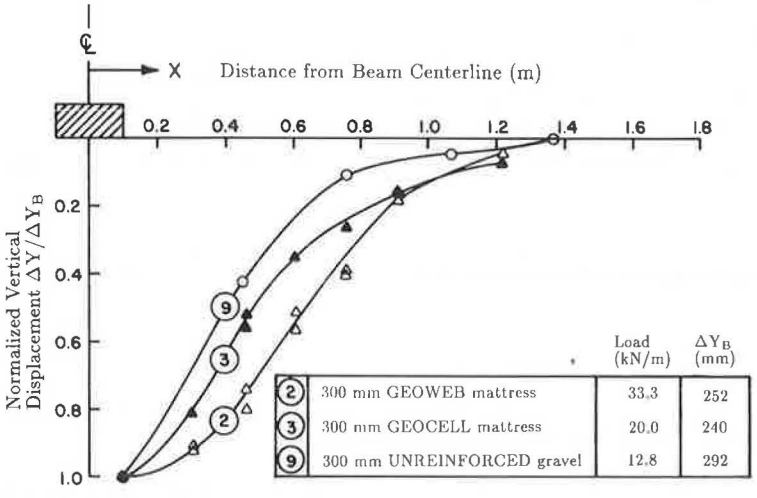

FIGURE 9 Deformation profiles at gravel base–peat interface for selected tests.

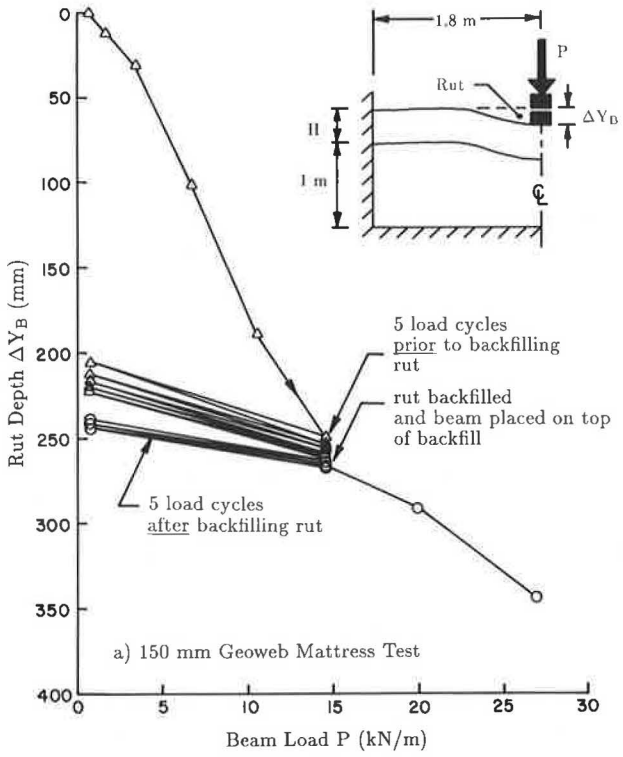

FIGURE 10 Load deformation for geocomposite mattress tests including backfilling and repeated static loading—150-mm geoweb mattress test.

efit of reinforced systems over that of comparable unreinforced systems diminishes with increased subgrade stiffness (*17, 18*). It is possible that the high-deformation models employed in the current test program show both geocomposite mattresses and single-sheet geotextile geogrid reinforcement schemes at their best. More work remains to be done to investigate the performance benefit of geocomposite mattresses constructed over subgrades that are more competent than the ones reported here.

CONCLUSIONS

A series of large-scale static tests was undertaken to investigate the load-deformation behavior of geocomposite mattresses constructed over a compressible peat subgrade and to compare this behavior with that of comparable unreinforced gravel bases and gravel bases reinforced with a single layer of geotextile or geogrid at the gravel-peat interface. The major conclusions from this study are summarized as follows:

1. All reinforced gravel bases showed significant load capacity improvement at large rut depths compared with similar thicknesses of unreinforced gravel bases.
2. The geocomposite mattresses constructed from still nonperforated polyethylene geoweb showed the greatest performance improvement of all geocomposite reinforce-

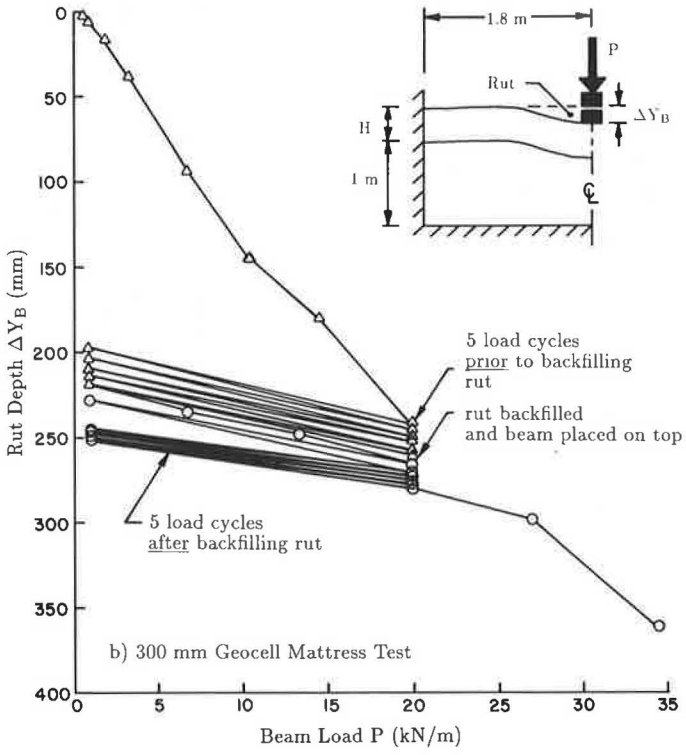

FIGURE 11 Load deformation for geocomposite mattress tests including backfilling and repeated static loading—300-mm geocell mattress test.

ment schemes investigated. The enhanced soil confinement due to the stiff geoweb cellular construction is thought to be responsible for this.

3. A test of a relatively flexible geocell construction and and an SS2 geogrid as a gravel-peat separator gave essentially the same load-deformation behavior as reinforced tests using only the SS2 layer.

4. Over a range of rut depths (up to 200 mm) the 150-mm-thick geoweb mattress gave a load-deformation response equivalent to that of unreinforced configurations with about 300 mm of gravel base material. Similarly, 300-mm-thick geoweb composites are considered equivalent to unreinforced gravel bases 500 to 600 mm thick.

5. The performance benefit due to the geoweb mattress construction was observed to occur at relatively low rut depths of 10 to 22 mm, which were significantly lower than the 100 to 150 mm of beam displacement required to mobilize the reinforcing effect of the other geocomposite configurations investigated.

6. The influence of subgrade stiffness on the relative performance benefit of geocomposite mattresses over similar unreinforced configurations requires investigation.

ACKNOWLEDGMENTS

The authors would like to thank J. Bell (research assistant) who carried out the experiments reported in this paper and J. DiPietrantonio who drafted the figures. Funding for this project was provided by the Department of National Defence (Canada).

REFERENCES

1. S. L. Webster and J. E. Watkins. *Investigation of Construction Techniques for Tactical Bridge Approach Roads Across Soft Ground*. Report S-77-1. Soils and Pavements Laboratory, U.S. Army Engineer Waterways Experiment Station, Vicksburg, Miss., Feb. 1977.
2. S. L. Webster and S. J. Alford. *Investigation of Construction Concepts for Pavements Across Soft Ground*. Report S-78-6. Geotechnical Laboratory, U.S. Army Engineer Waterways Experiment Station, Vicksburg, Miss., July 1978.
3. S. L. Webster. *Investigation of Beach Sand Trafficability Enhancement Using Sand-Grid Confinement and Membrane Reinforcement Concepts*. Report GL-79-20 (1). Geotechnical Laboratory, U.S. Army Engineer Waterways Experiment Station, Vicksburg, Miss., Nov. 1979.
4. S. L. Webster. *Investigation of Beach Sand Trafficability Enhancement Using Sand-Grid Confinement and Membrane Reinforcement Concepts*. Report GL-79-20 (2). Geotechnical Laboratory, U.S. Army Engineer Waterways Experiment Station, Vicksburg, Miss., Feb. 1981.
5. *GEOWEB Grid Confinement Systems: Technical Data*. Presto Products, Inc., Appleton, Wis., 1985.
6. G. Jamnejad, G. Kazerani, R. C. Harvey, and J. D. Clarke. Polymer Grid Cell Reinforcement in Pavement Construction. *Proc.*, 2nd International Conference on Bearing Capacity of Roads and Airfields, Plymouth, U.K., Sept. 1986, pp. 537–546.
7. B. Kazerani and G. H. Jamnejad. Polymer Grid Cell Reinforcement in Construction of Pavement Structures. *Proc.*, Geosynthetics '87 Conference, New Orleans, La., Feb. 1987.
8. G. Kimel. Grid Confinement System Used to Upgrade Streets. *Public Works*, May 1987.
9. M. O'Grady. Three-Dimensional Geogrid Soil Stabilization. Presented at Symposium on the Reclamation, Treatment and Utilization of Coal Mining Wastes, Durham, U.K., Sept. 1984.
10. ATSF Tests Grid System for Track Stabilization. *Progressive Railroading*, March 1987, p. 54.
11. C. Rea and K. Mitchell. Sand Reinforcement Using Paper Grid Cells. *Proc.*, Symposium on Earth Reinforcement, ASCE Annual Convention, Pittsburgh, Pa., April 27, 1978, pp. 644–663.
12. J. K. Mitchell, T.-C. Kao, and E. Kavazanjian. *Analysis of Grid Cell Reinforced Pavement Bases*. Report GL-79-8. Geotechnical Laboratory, U.S. Army Engineer Waterways Experiment Station, Vicksburg, Miss., July 1979.
13. P. M. Jarrett. Evaluation of Geogrids for Construction of Roadways over Muskeg. Paper 4.5. *Proc.*, Symposium on Polymer Grid Reinforcement in Civil Engineering, London, U.K., 1984.
14. P. M. Jarrett. Load Tests on Geogrid Reinforced Gravel Fills on Peat Subgrades. *Third International Conference on Geotextiles*, Vienna, Austria, 1986.
15. A. McGown, K. Andrawes, K. Yoe, and D. Dubois. The Load-Strain-Time Behavior of Tensar Geogrids. Paper 1.2. *Proc.*, Symposium on Polymer Grid Reinforcement in Civil Engineering, London, U.K., 1984.
16. *Test Methods & Physical Properties of "Tensar" Geogrids*. Tensar Corp., Morrow, Ga., 1986.
17. R. J. Bathurst, G. P. Raymond, and P. M. Jarrett. Performance of Geogrid-Reinforced Ballast Railroad Track Support. *Third International Conference on Geotextiles*, Vienna, Austria, April 1986, Vol. 1, pp. 43–48.
18. R. J. Bathurst and G. P. Raymond. Geogrid Reinforcement of Ballasted Track. In *Transportation Research Record 1153*, TRB, National Research Council, Washington, D.C. 1988, pp. 8–14.

Publication of this paper sponsored by Committee on Soil and Rock Properties.

Soil-Geotextile Pull-Out Interaction Properties: Testing and Interpretation

ILAN JURAN AND CHAO L. CHEN

In this paper are presented a soil-reinforcement load transfer model and a procedure for interpreting pull-out tests on extensible reinforcements. The model combines the constitutive equation of the reinforcement with interaction laws relating the shear stress mobilized at any point of the interface to the soil-reinforcement shear displacement. The main conclusions are (a) extensibility has a major effect on soil-reinforcement interaction; (b) for extensible reinforcement, extrapolation of pull-out test results to reinforcement of different dimensions requires a careful evaluation of the scale effect; and (c) a meaningful interpretation of pull-out test results on geotextiles and geogrids requires an adequate estimation of the in-soil confined properties of the reinforcement and an appropriate soil-geotextile interaction law.

Pull-out interaction properties are fundamental design parameters for reinforced soil systems. The friction interaction between granular soils and quasi-inextensible metallic reinforcing strips has already been extensively investigated by Alimi et al. (*1*), Schlosser and Elias (*2*), Elias (*3*), Guilloux et al. (*4*), Schlosser and Guilloux (*5*), and others. Interpretation of pull-out tests on quasi-inextensible reinforcements provides an apparent friction coefficient that is conventionally defined by the ratio of the interface limit lateral shear stress to the nominal overburden pressure (i.e., the weight of the soil mass above the reinforcement). Compilation of available data from both laboratory and in situ pull-out tests has provided an empirical basis for the development of guidelines for the design of Reinforced Earth structures (*6*).

More recently, the rapid development of a large variety of reinforcing materials and elements has stimulated research on the interaction mechanisms that develop between soil and different types of inclusions such as metallic or plastic geogrids and geotextiles. Pull-out tests have been conducted by McGown (*7*), Gourc et al. (*8*), Ingold (*9*), Jewell (*10*), Rowe et al. (*11*), Johnston (*12*), Shen (*13*), B. Koerner (unpublished internal report No. 1 on Direct Shear/Pull-Out Tests on Geogrids, Drexel University, Philadelphia, Pa., 1986), and others to obtain relevant interaction design parameters (apparent friction coefficient or interface limit lateral shear stress) for different types of geotextiles and geogrids.

Depending on the constitutive material (metal, plastic, woven or nonwoven geotextiles), the geometry and structural aspect of the inclusion (linear strip, ribbed strip, plane reinforcement, geogrid with in-plane or out-of-plane transverse elements, woven or nonwoven geotextiles), the internal grid (or geotextile fiber) spacings, the type of soil and more specifically its grain size and dilatancy properties, different types of load transfer mechanisms can be generated. These mechanisms fundamentally involve four interaction phenomena: (a) lateral friction, plane (membranes) or three dimensional (linear strips, longitudinal elements of geogrids); (b) interlocking (geogrids, geotextiles); (c) passive soil pressure on transverse elements (geogrids, ribbed strips); and (d) the effect of restrained dilatancy on normal stress at the interface (linear inclusions in dilatant granular soils). The relative movement of soil and reinforcement required to bring these phenomena into play can be substantially different. With metallic strip reinforcements, the soil displacement necessary to generate lateral friction at the interfaces is small [millimetric (*1, 2*)]. However, with more extensible reinforcements, or with systems that rely on passive soil pressure on transverse elements, the soil displacement required to generate pull-out resistance can be substantially greater. Therefore, in order to rationally design these systems, it becomes essential to develop a load transfer model that is capable of predicting the pull-out response of the inclusion and specifically its displacements under the applied tension force.

The extensibility of the reinforcement significantly affects the load transfer mechanism. Pull-out tests on geotextiles (*7*) have demonstrated that the interaction between soil and extensible inclusions results in a nonuniform shear displacement distribution that is associated with a shear stress concentration at the front part of the inclusion. Consequently, the concept of a uniformly mobilized interface limit lateral shear stress (or apparent friction coefficient), which is generally used in the design of Reinforced Earth structures with metallic reinforcements, is not adequate for the interpretation of pull-out tests on geogrids and geotextiles. Moreover, as indicated by McGown (*7*), Gourc (*8*), Jewell et al. (*14*), and Koerner, the limit lateral shear stress obtained from the pull-out tests can be significantly different from that determined by direct shear tests with a soil-inclusion interface.

Modeling the load transfer mechanism generated in a pull-out test on extensible inclusions requires appropriate constitutive equations for the soil and the inclusions as well as a rational interaction law to relate the shear stress mobilized at any point of the interface to the soil-rein-

Department of Civil Engineering, Louisiana State University, Baton Rouge, La. 70803.

forcement shear displacement. This interaction law can be obtained from direct shear tests with soil-geotextile interface (*11, 15–17*, and Koerner). The load transfer model should allow for an estimate of the shear stress distribution along the reinforcement and of the front edge displacement caused by the applied pull-out force.

In this paper the authors present an interpretation procedure for pull-out tests on extensible inclusions. This procedure is derived from the "t-z" method, which is commonly used in design of friction piles (*18*). Two interface models are considered in which it is assumed that the interface layer is (a) elastic–perfectly plastic and (b) elasto-plastic with strain hardening and softening during shearing. This interface soil model can be obtained from the results of direct shear tests with a soil-geotextile interface and integrated numerically in the analysis.

To evaluate the proposed test interpretation procedure and the two interface soil models, the results of pull-out tests performed by Juran (*19*) on extensible inclusions (woven polyester and nonwoven geotextile strips) and by Jewell (*10*) on metallic grids were analyzed and compared with numerical test simulations. A parametric study was conducted to assess the effect of the extensibility of the inclusion on its displacement response to the applied pull-out load.

FORMULATION OF SOIL-INCLUSION LOAD TRANSFER MODEL AND PULL-OUT TEST INTERPRETATION PROCEDURE

The principles of discretizing and modeling the load transfer along the reinforcement are illustrated in Figure 1. As indicated previously, the interaction law, which relates the interface shear stress to the soil-reinforcement shear displacement, can be obtained from direct shear tests on a soil sample in which the reinforcement is placed at the level of the failure surface. However, to simplify this analysis, two interface models are considered. These models and their use in test interpretation to obtain the relevant interaction design parameters are presented.

Elastic–Perfectly Plastic Interface Soil Model

The following assumptions are made:

1. The reinforcement is elastic, that is,

$$\varepsilon(x) = \frac{\delta y}{\delta x} = \frac{T(x)}{ES} \tag{1}$$

where

$\varepsilon(x)$ = the elongation of the inclusion at point (x);
$T(x)$ = the tension force at this point;
$y(x)$ = the displacement of the inclusion at point (x);
S = the section area; and
E = the elastic modulus; nonlinear behavior can be considered by introducing an elastic modulus that is a function of the actual strain.

2. The interface layer is elastic–perfectly plastic. The soil-inclusion interaction law can be written as

$$\tau(x) = k \cdot y(x) \quad \text{if } y < \tau_{max}/k \tag{2a}$$

$$\tau(x) = \tau_{max} \quad \text{if } y \geq \tau_{max}/k \tag{2b}$$

where

τ_{max} = $\tan \psi \cdot \gamma h$,
$\tau(x)$ = the shear stress mobilized at point (x),
k = the shear modulus of the interface,
ψ = the soil-inclusion friction angle,
γh = the overburden pressure, and
τ_{max} = the ultimate lateral shear stress at the interface.

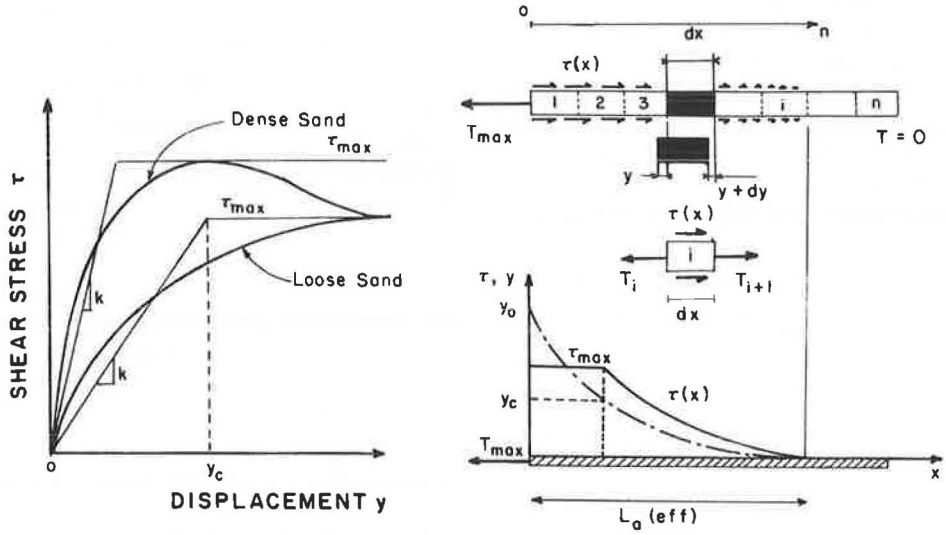

FIGURE 1 Modeling load transfer between soil and extensible inclusion.

The local equilibrium of each segment of the inclusion (Figure 1) implies that

$$\tau(x) = \frac{1}{p}\frac{\delta T}{\delta x} \tag{3}$$

where p is the perimeter ($p = 2b$; b is the width of the inclusion).

By combining Equations 1 and 3, the following differential equation is obtained:

$$\frac{\delta^2 y}{\delta x^2} = \frac{p}{ES}\tau(x) \tag{4}$$

where $\tau(x)$ is given by the interaction law (Equation 2).

The solution of this differential equation for infinitely long inclusion provides the distribution of displacement and tensile forces along the inclusion:

- For $y < y_c = \tau_{max}/k$, the interface is in an elastic range:

$$y = -\frac{\lambda T_0}{ES}e^{-x/\lambda};\ y_0 = -\frac{\lambda T_0}{ES} \tag{5a}$$

$$T(x) = ES\frac{dy}{dx} = T_0 e^{-x/\lambda} \tag{5b}$$

where $\lambda = (ES/KP)^{1/2}$ is a reference "transfer length."

- For $y \geq \tau_{max}/k$, the interface is in a plastic range:

$$y = -\frac{pT_{max}}{ES}\cdot\frac{x^2}{2} + \frac{T_0}{ES}\cdot x + y_0 \tag{5c}$$

$$T(x) = T_0 - p\,\tau_{max}\cdot x \tag{5d}$$

For this case, the front edge displacement of the inclusion (y_0) is calculated by using the compatibility condition at the limit of the elastic and plastic zones, which yields

$y = y_c = -\tau_{max}/k$ and $y_c' = \tau_{max}/(k\lambda)$

Hence, for $y_0 > y_c$,

$$y_0 = \frac{1}{2}y_c\left[1 + \left(\frac{\lambda}{y_c}\right)^2\cdot\left(\frac{T_0}{ES}\right)^2\right] \tag{6}$$

Although the solution is developed for infinitely long inclusions, for the reinforcements commonly used (length l greater than 3λ), the error is negligible.

Figure 2 shows a graphic procedure that can be used for the interpretation of pull-out tests on extensible inclusions to obtain the interaction parameters k and $\tan\psi$. In the plane of $(T/ES)^2$ versus y_0, a linear regression will provide an experimental straight line with

- An initial coordinate at the origin equal to $y_c/2$ and
- A slope equal to $\lambda^2/(2y_c)$.

The soil-reinforcement interface friction angle can then be calculated from

$$\tan\psi = \left(\frac{ES}{p\cdot\gamma h}\right)\cdot\left(\frac{y_c}{\lambda^2}\right) \tag{7}$$

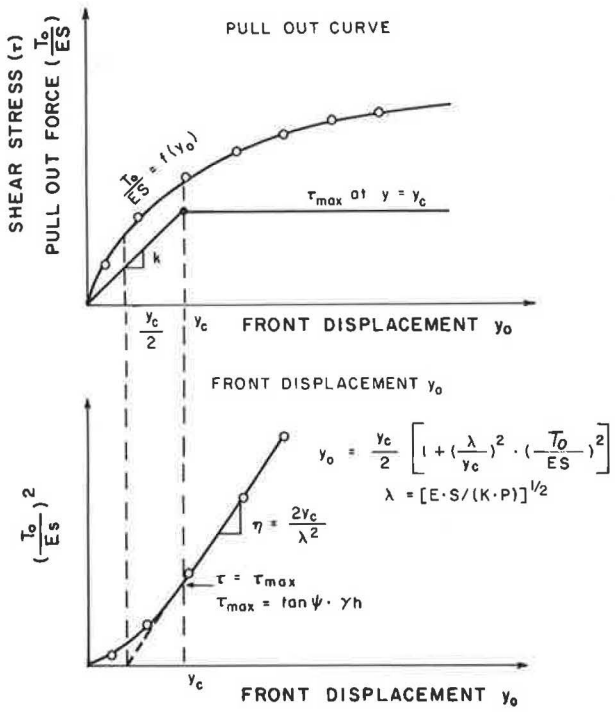

FIGURE 2 Interpretation procedure for pull-out tests on extensible inclusions.

Elastoplastic Strain Hardening Interface Soil Model

To develop a more realistic load transfer model, an elastoplastic constitutive equation is used to simulate the behavior of the interface layer during shearing. This model (*20*), which is implemented by using the finite difference method, allows for the integration of both strain hardening and strain softening in the shear stress–displacement relationship of the soil-inclusion interface. This relation can be written as

$$\frac{\tau(y)}{\sigma_y} = cy\frac{y - a}{(y + b)^2} \tag{8}$$

The constants a, b, and c are determined from the following conditions:

1. The initial shear modulus of the interface layer is equal to

$$\left[\frac{\partial(\tau/\sigma)}{\partial y}\right]_{y\to 0} = \frac{G}{\sigma_y\cdot d}$$

where d is the thickness of the interface layer.

Results of direct shear tests performed by Jewell (*10*) using an x-ray radiographic technique to measure the dis-

placement field in the soil suggest that, in dense unreinforced sand, the thickness of the sheared layer (d) is about 10 to 20 mm.

2. At the peak of the shear displacement–shear stress curve,

$$\frac{\tau}{\sigma_y} = \tan \psi_p$$

where ψ_p is the peak soil-inclusion friction angle.

3. At the residual critical state,

$$\frac{\tau}{\sigma_y} = \tan \psi_r$$

where ψ_r is the residual critical state soil-inclusion friction angle. Hence,

$$a = -4 \frac{\sigma_y d}{G} [\tan^2 \psi_p \cdot J^2]/\tan \psi_r \quad (9a)$$

$$b = 2 \frac{\sigma_y d}{G} [\tan \psi_p \cdot J] \quad (9b)$$

$$c = \tan \psi_r \quad (9c)$$

and

$$J = 1 + [1 - \tan \psi_r/\tan \psi_p]^2 \quad (9d)$$

Coupling the equilibrium equation with the constitutive equations of the inclusion and the interface layer (Equations 4 and 8), the numerical solution for the given boundary conditions of $T_0 = T_p$ (applied pull-out force) and $T_n = 0$ provides the distributions of the displacements and tensile forces along the inclusion. The interaction parameters [$G/(\sigma_y d)$, $\tan \psi_p$, $\tan \psi_r$] are determined using a curve-fitting procedure.

EXPERIMENTAL RESULTS AND NUMERICAL TEST SIMULATIONS

Pull-out tests have been performed on both woven polyester and nonwoven geotextile strips. Figure 3 shows the pull-out box and the instrumentation of the reinforcements. The front edge displacement of the inclusion was measured using both an externally placed graduated scale and potentiometers (change of electrical voltage was calibrated in terms of point displacement). Potentiometers were also placed at different points along the inclusion to provide the displacement distribution under each pull-out load.

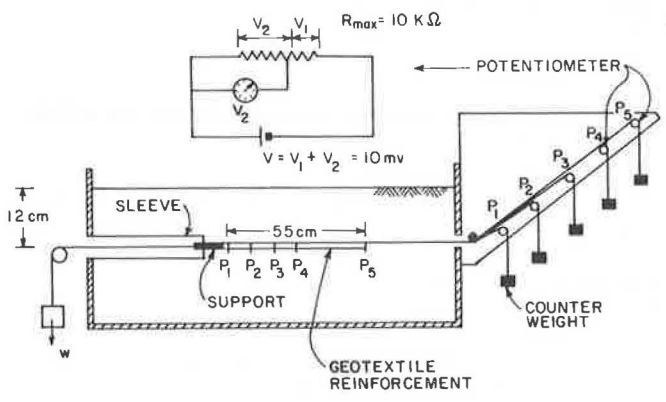

FIGURE 3 Pull-out box and instrumentation.

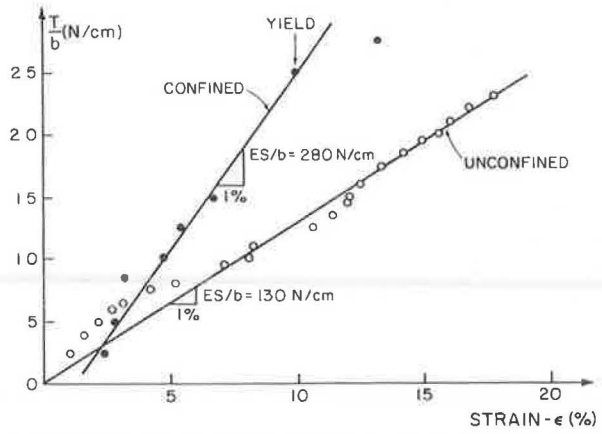

FIGURE 4 Confined and unconfined stress-strain relationship of woven polyester.

Before the pull-out tests, "confined" and "unconfined" extension tests were performed on the reinforcements to determine their in-air and in-soil constitutive equations.

The confined extension tests were performed in the pull-out box under a confining pressure of $\sigma_y = 2$ kPa. The testing procedure consists of applying successive load increments at the front edge of the reinforcement while the rear edge is fixed or simultaneously subjected to the same load increments. A similar load-controlled testing procedure was also used in the pull-out tests with the rear edge of the reinforcement unattached. To avoid any unconfined extension of the front part of the reinforcement during the test, this part was placed between two metal plates. A sleeve was used to minimize the boundary effect, and during the test the inclusion was entirely confined by the surrounding sand.

Figures 4 and 5 show the confined and unconfined stress-

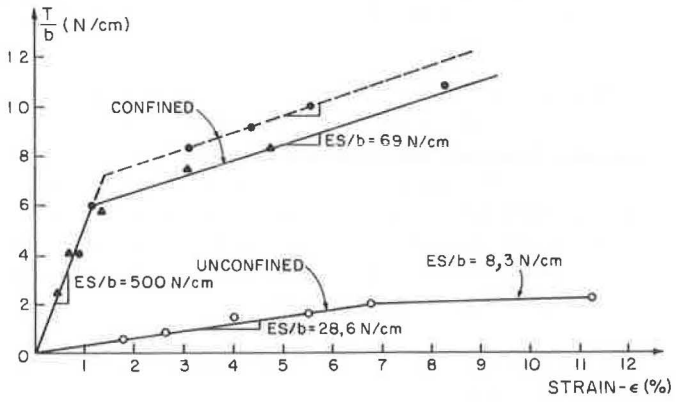

FIGURE 5 Confined and unconfined stress-strain relationship of nonwoven geotextile.

TABLE 1 CONFINED AND UNCONFINED MATERIAL PROPERTIES OF THE REINFORCEMENTS

Reinforcing Material	Unconfined		Confined (σ_y = 2 kPa)		Specimen Length (cm)
	ES/b (N/cm)	T_{cr}/b (N/cm)	*ES/b* (N/cm)	T_{cr}/b (N/cm)	
Woven polyester	130	24	280	28	55
Nonwoven geotextiles	28.6	2.5	500	10	30

NOTE: T_{cr} is the ultimate tensile force at breakage of the sample during a tensile test.

strain relationships of the woven polyester and nonwoven geotextile reinforcements. The related material properties are given in Table 1. These results demonstrate that, for the nonwoven geotextile reinforcement, the confined elastic modulus is about 20 times the unconfined one, and the confined tensile strength is about 4 times the unconfined one.

Figure 6 shows the results of pull-out tests on a woven polyester strip. The distance lag between the front edge displacements measured with the graduated scale and with the potentiometer is most probably due to a local deformation of the metallic wire connecting the measurement point with the potentiometer (such displacement could occur during placement in the soil). It should also be noted that the available instrumentation does not provide accurate displacement readings under relatively low loading levels. However, as shown in Figure 7, the displacement increments measured with the potentiometer correspond fairly well with those measured with the graduated scale. The experimental straight line $y_0 = f([T/ES]^2)$ yields the following interaction parameters:

$\lambda^2/(2y_c) = 3302.88$ mm,
$y_c = 0.7$ mm,
$\lambda = 58$ mm,
$k/\sigma_y = 1.5$, and
$\tan \psi = 1.1$.

Figure 8 shows the variations of the displacements along the inclusion measured under different pull-out loading

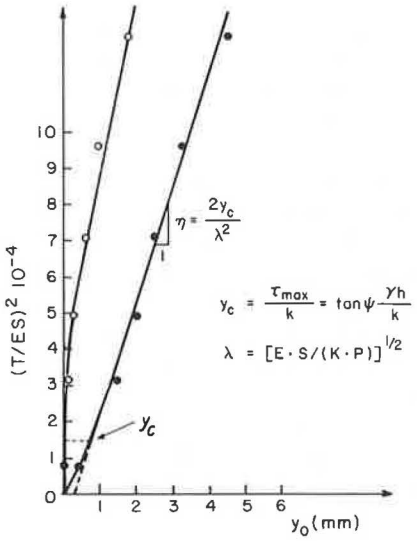

FIGURE 7 Pull-out test on woven polyester: interpretation.

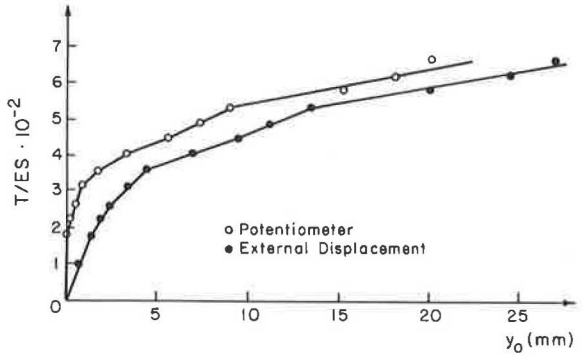

FIGURE 6 Pull-out test on woven polyester: force displacement curve.

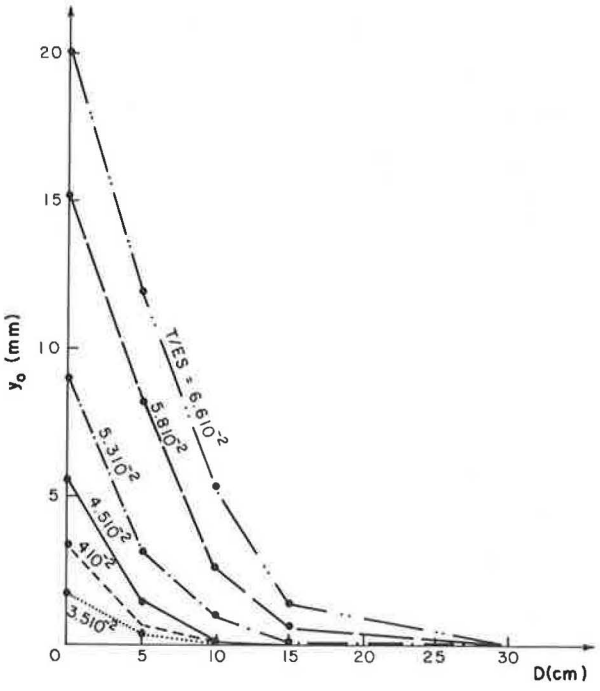

FIGURE 8 Variation of displacements along a woven polyester strip during pull-out test.

levels. Figures 9 and 10 show the results of two pull-out tests on nonwoven geotextile reinforcements. Using the interpretation procedure outlined previously, the following interaction properties are obtained:

$\lambda^2/(2y_c) = 1.5 \times 10^5$ mm,
$y_c = 1$ mm, and
$\lambda = 550$ mm.

The calculated transfer length is greater than the specimen length and therefore the solution derived for infinitely long reinforcement is not applicable.

To evaluate the proposed elastoplastic interface soil model, the experimental results of the pull-out tests performed on the woven polyester and nonwoven geotextile strips as well as those performed by Jewell (*10*) on metallic geogrids were compared with numerical test simulations. Figures 11 and 12 show the experimental and theoretical pull-out curves obtained from tests performed on woven polyester and nonwoven geotextile strips.

For the woven polyester strips, the curve-fitting procedure yields $G/(\sigma_y \cdot d) = 6$ (1/mm) (or $G/\sigma_y = 60$), $\psi_p = 42$ degrees, and $\psi_r = 32$ degrees. Confined elastic modulus is considered in this analysis. These interaction parameters correspond fairly well with the material properties of the Fountainebleau sand used in this study: $G/\sigma_0 = 60$, (σ_0 is the isotropic consolidation pressure), $\phi_p = 38$ to 42 degrees, and $\phi_{cv} = 32$ degrees. It is also of interest to note that the peak soil-reinforcement friction angle obtained using this curve-fitting procedure corresponds to that obtained using the "t-z" method with an elastic–perfectly plastic interface soil model. However, the elastic–perfectly plastic model provides a secant shear modulus (k), which is significantly smaller than the initial shear modulus obtained using the proposed elastoplastic load transfer model.

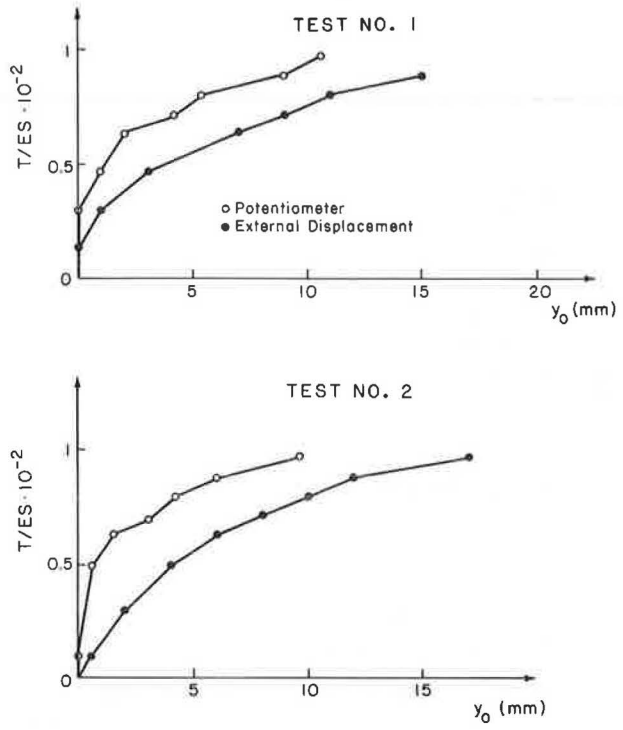

FIGURE 9 Pull-out tests on nonwoven geotextile strips: force-displacement curves.

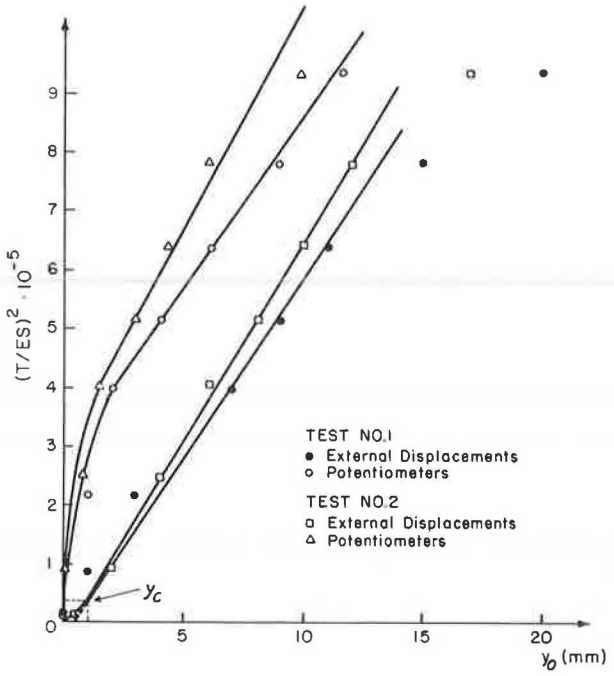

FIGURE 10 Pull-out tests on nonwoven geotextile strips: interpretation.

For the nonwoven geotextile strip, comparison of the theoretical and experimental pull-out curves indicates that using the confined elastic model for test interpretation leads to significantly underestimated displacements. If the unconfined elastic modulus of the reinforcement is used, and assuming that the interface soil properties correspond to the mechanical properties of the Fountainebleau sand, the calculated pull-out curve agrees fairly well with the experimental one.

Figure 13 shows the results of a pull-out test performed

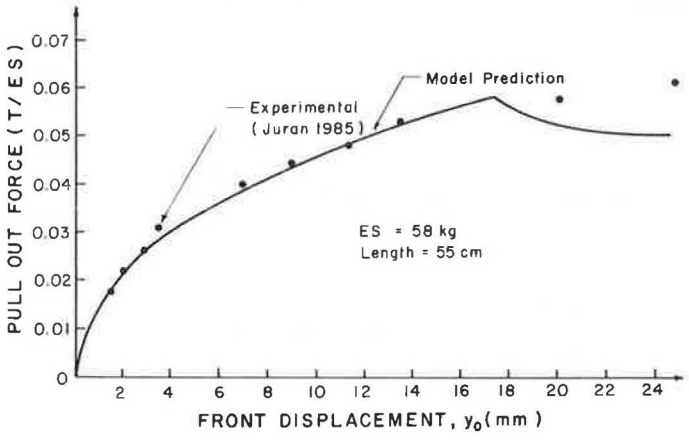

FIGURE 11 Numerical simulation of pull-out test on woven polyester strips.

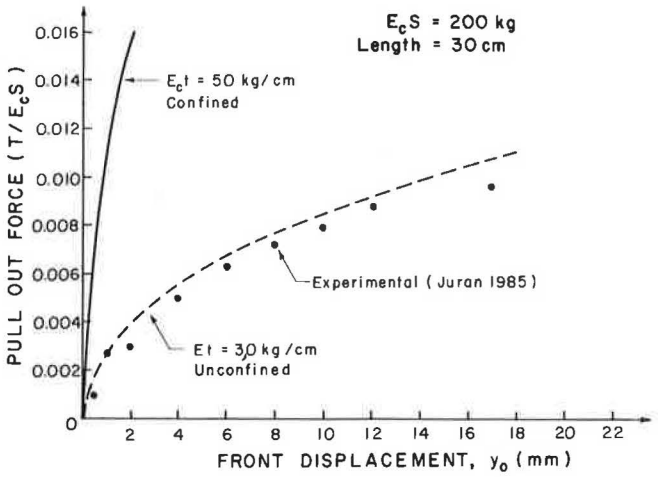

FIGURE 12 Numerical simulation of pull-out test on nonwoven geotextile strips.

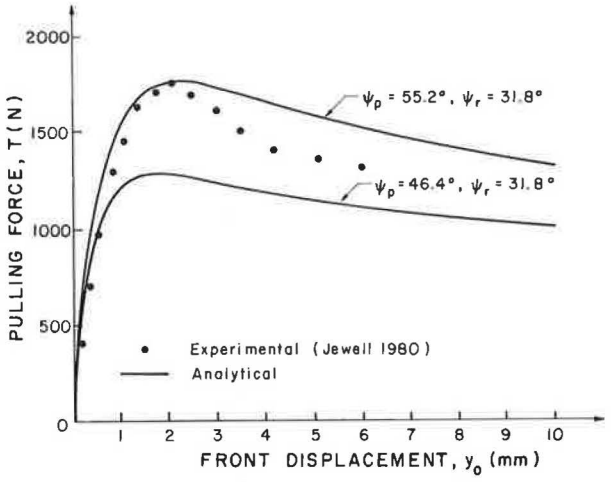

FIGURE 13 Numerical simulation of pull-out test on metallic grid (*10*).

by Jewell (*10*) on metallic grids in Leighton Buzzard sand. The mechanical characteristics of this sand are $G/(\sigma_y d)$ = 4 (1/mm), ϕ_p = 46.4 degrees, and ϕ_{cv} = 31.8 degrees; the applied normal stress is σ_y = 75 kPa. The curve-fitting procedure yields, for interaction parameters, $G/(\sigma_y d)$ = 3 (1/mm), ψ_p = 55.2 degrees, and ψ_r = 31.8 degrees. It can be observed that the peak interface friction angle obtained under the relatively low confining pressure of this test is greater than the peak friction angle of the soil. These results are consistent with those reported by several authors (*9, 12, 14–15*, and Koerner), which indicates that, under low normal stresses, the apparent soil-inclusion interface friction angle obtained from pull-out tests on grids can be significantly greater than the friction angle of the unreinforced soil. The results also indicate that, for this quasi-inextensible reinforcement, the calculated transfer length is significantly greater than the specimen length and therefore the elastic–perfectly plastic solution for an infinitely long reinforcement is not applicable.

Table 2 gives a summary of the interface properties calculated according to the two interaction models and how they compare with soil properties.

EFFECT OF EXTENSIBILITY OF REINFORCEMENT ON PULL-OUT INTERACTION MECHANISM

The proposed soil-inclusion load transfer model can be used to evaluate the effect of the extensibility (or the elastic modulus) of the inclusion on the pull-out curve. Figure 14 shows that pull-out resistance increases with the elastic modulus and that post-peak-strain softening has a significant effect on the soil-inclusion interaction. Figure 15 shows the effect of extensibility on the distribution of displacements along the inclusion, calculated for a loading level approaching the limit pull-out load. Figure 16 shows the effect of extensibility on both the front and the rear edge displacements of the inclusions. The quasi-inextensible inclusion undergoes a quasi-rigid movement, and the shear stress mobilized at the interface is rather uniform. With extensible inclusions (E = 100 MPa), the front edge displacement integrates both the shear displacement of the inclusion and its elongation. The shear stress mobilized at the interface is a function of the soil-inclusion shear displacement and therefore varies along the inclusion. For a loading level approaching the limit pull-out load, the shear

TABLE 2 SOIL AND SOIL-REINFORCEMENT INTERACTION PROPERTIES

	Soil				Interface Model					
					Elastic–Perfectly Plastic			Elastoplastic Strain Hardening		
Reinforcement	G/σ_0 Triaxial	$G/\sigma_y d$ Direct Shear (1/mm)	ϕ_p (degrees)	ϕ_r (degrees)	K/σ_y (1/mm)	y_c (mm)	ψ (degrees)	$G/(\sigma_y d)$ (1/mm)	ψ_p (degrees)	ψ_r (degrees)
Woven polyester geotextile (Juran (*19*))	60	6.0	40–45	32	1.5	0.7	47	6.0	42 (confined *ES*)	32
Nonwoven geotextile (Juran (*19*))	60	6.0	40–45	32	NA	NA	NA	6.0	42 (unconfined *ES*)	32
Metallic grids (Jewell (*10*))	–	4.0	46.4	32	NA	NA	NA	3.0	55	32

NOTE: NA = Not applicable because transfer length exceeds a third of the specimen length ($3\lambda > l$).

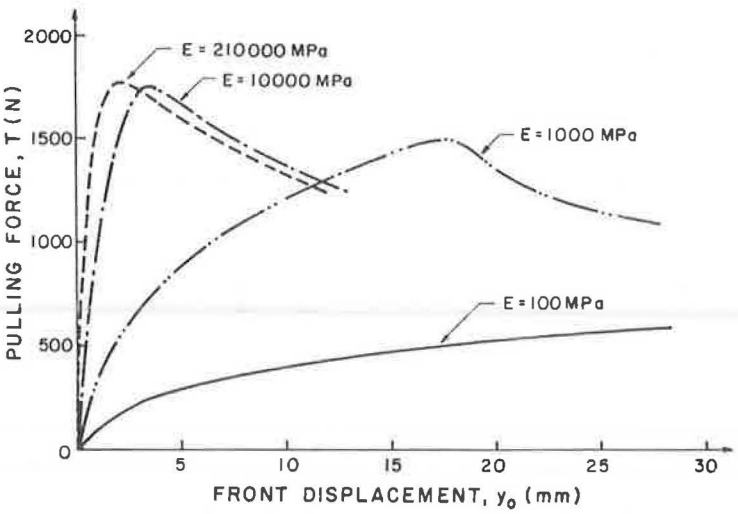

FIGURE 14 Effect of extensibility on pull-out curves.

stress at the front point of the inclusion has attained the residual shear resistance, whereas, at the rear part of the inclusion, the mobilized shear stress is still negligible. At a certain point along the reinforcement, the interface shear stress attains the peak shear resistance.

This nonuniform shear stress distribution demonstrates that the concept of a limit interface shear stress uniformly mobilized along the inclusion (or the apparent friction angle concept), which is currently used in designing with metallic reinforcements, is not adequate for the interpretation of pull-out tests on extensible inclusions to provide relevant interaction design parameters. It also indicates that, in a dense dilating sand, particularly under relatively low normal stresses, the limit interface shear stress obtained from direct shear tests should be superior to that obtained from the pull-out tests. Figure 17 shows the effect of soil density and hence of post-peak-strain softening on the pull-out curve.

EFFECT OF LENGTH OF INCLUSION ON PULL-OUT INTERACTION DESIGN PARAMETERS

The major concern in the engineering interpretation of a pull-out test is scale effect on the relevance of the pull-out

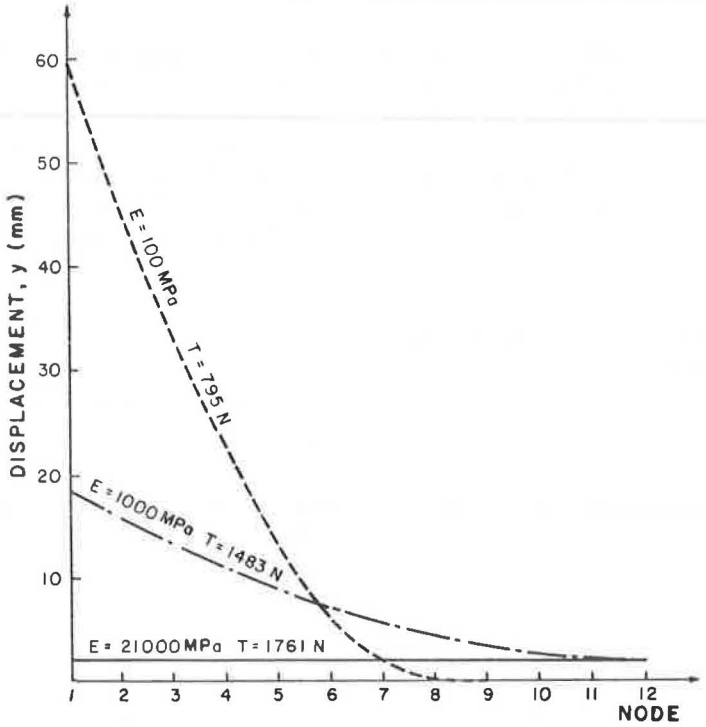

FIGURE 15 Effect of extensibility on distribution of displacements along inclusion.

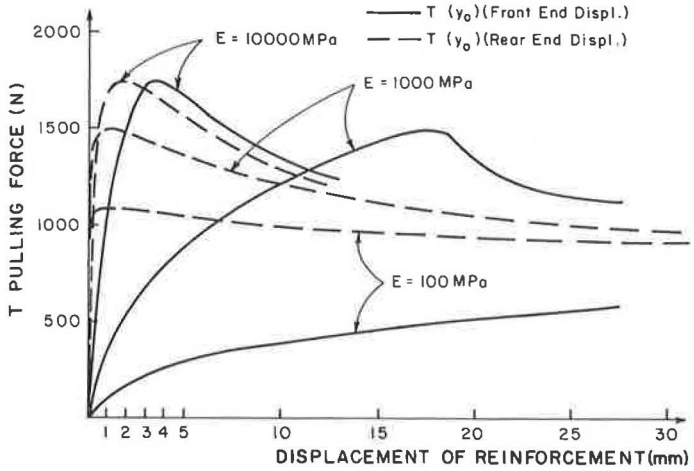

FIGURE 16 Effect of extensibility on front edge and rear edge displacements.

interaction design parameters. Parameters to be used in the design of soil structures with reinforcements of different lengths have to be independent of the dimensions of the sample subjected to a pull-out test.

Figure 18 shows the effect of the length of the reinforcement on the average limit shear stress mobilized at the interfaces at the peak of the pull-out curve. Figure 19 shows the effect of length on peak pull-out displacement. The results of these numerical simulations illustrate that, with quasi-inextensible inclusions, the concept of an apparent friction coefficient, or a uniformly mobilized limit lateral interface shear stress, can be adequately used. The design limit shear stress (or apparent friction coefficient) is independent of the sample dimension, and the results of pull-out tests can therefore be used in the design of actual structures.

With more extensible inclusions, because of nonuniform shear stress distribution, the average limit shear stress mobilized at the peak of the pull-out curve is a function of the sample dimension. Therefore extrapolation of pull-out test results to reinforcements of different lengths requires a careful evaluation of the scale effect.

The numerical simulations also show that as the length of an extensible inclusion increases, the average limit shear stress decreases and approaches a limit value corresponding to the residual interface friction angle. Peak pull-out displacement increases significantly with sample dimension, and consequently a design criterion for allowable pull-out displacement should be considered.

CONCLUSIONS

The main conclusions that can be drawn from this study follow.

1. Soil-inclusion friction interaction depends significantly on the extensibility of the inclusion and the mechanical properties of the interface soil layer.

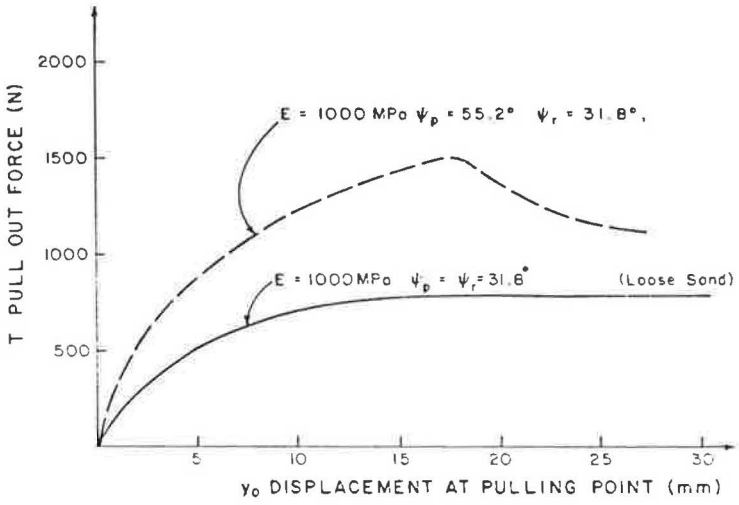

FIGURE 17 Effect of soil density on pull-out curve.

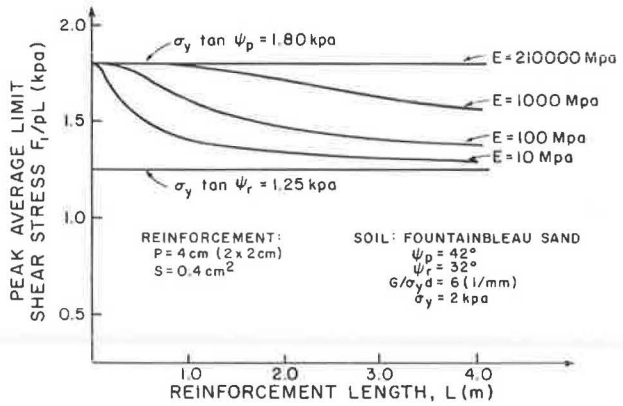

FIGURE 18 Effect of reinforcement length on average limit shear stress.

2. With quasi-inextensible metallic inclusions, the concept of a limit shear stress uniformly mobilized at the interfaces can be adequately used to determine the pull-out resistance of the inclusion. Because the three-dimensional friction interaction between the soil and the inclusion is rather complex, in situ pull-out tests should be performed to provide relevant design parameters.

3. With more extensible inclusions, the elongation of the inclusion during pull-out loading results in a nonuniform shear stress distribution along the reinforcement. The effect of extensibility on the shear stress distribution and the front edge displacements raises major difficulties with regard to the current use of pull-out tests on extensible reinforcements to obtain relevant interaction design parameters. Specifically, because the pull-out resistance is not proportional to the length of the reinforcement, a careful evaluation of the scale effect is required in an extrapolation of pull-out test results to reinforcements of different lengths.

4. A meaningful interpretation of the results of pull-out tests on geotextiles and geogrids requires an appropriate load transfer model. A reliable procedure for the determination of interaction design parameters and the estimation of the pull-out resistance of inclusions therefore necessitates (a) an adequate constitutive equation for the in-soil confined inclusion that is capable of integrating the effect of soil confinement on the mechanical properties of the geofabric and (b) an appropriate interaction law relating the mobilized interface shear stress to the actual soil-reinforcement shear displacement. For geotextiles, this interaction law can be obtained from direct shear tests on a soil-inclusion interface. The pull-out tests, however, allow for an experimental evaluation of the proposed interaction law. They can be efficiently used in situ to determine through a curve-fitting procedure the model-related interaction design parameters.

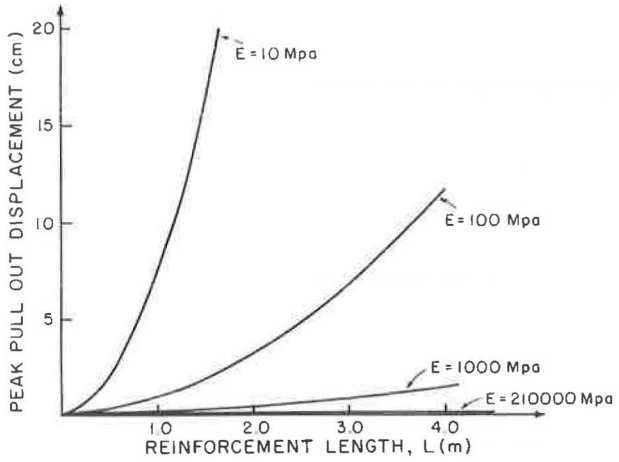

FIGURE 19 Effect of reinforcement length on peak pull-out displacement.

REFERENCES

1. I. Alimi, J. Bacot, P. Lareal, N. T. Long, and F. Schlosser. Etude de l'adherence sol-armatures. *Proc.*, 9th International Conference on Soil Mechanics and Foundation Engineering, Tokyo, Japan, 1977, Vol. 1, pp. 11–14.
2. F. Schlosser and V. Elias. Friction in Reinforced Earth. *Proc.*, Symposium on Earth Reinforcement, ASCE Annual Convention, Pittsburgh, Pa., 1978.
3. V. Elias. Friction in Reinforced Earth Utilizing Fine Grained Backfills. *Proc.*, International Conference on Soil Reinforcement, Paris, France, 1979, pp. 435–438.
4. A. Guilloux, F. Schlosser, and N. T. Long. Etude du frottement sable-armature en laboratoire. *International Conference on Soil Reinforcement*, Paris, France, 1979, Vol. 1, pp. 35–40.
5. F. Schlosser and A. Guilloux. Le frottement dans le renforcement des sols. *Revue Française de Géotechnique*, No. 16, 1981, pp. 65–77.
6. F. Schlosser and P. Segrestin. Dimensionnement des ouvrages en terre armée par la méthode de l'éqilibre local. International Conference on Soil Reinforcement, Paris, France, 1979.
7. A. McGown. The Properties of Nonwoven Fabrics Presently Identified as Being Important in Public Works Applications. *Proc.*, INDEX 78 Congress, European Disposables and Nonwovens Association, 1978, pp. 1.1.1–1.3.1.
8. J. P. Gourc, P. Delmas, and J. P. Giroud. Experiments on Soil Reinforcement with Geotextiles. Presented at ASCE National Convention, Portland, Oreg., 1980.
9. T. S. Ingold. Laboratory Pull-Out Testing of Grid Reinforcements in Sand. *Geotechnical Testing Journal*, Vol. 6, No. 3, 1983, pp. 101–111.
10. R. A. Jewell. *Some Effects of Reinforcement on the Mechanical Behavior of Soil*. Ph.D. dissertation. Cambridge University, Cambridge, England, 1980.
11. R. K. Rowe, S. K. Ho, and D. G. Fisher. Determination of Soil-Geotextile Interface Strength Properties. *Proc.*, 2nd Canadian Symposium on Geotextiles, 1984, pp. 25–34.
12. R. S. Johnston. *Pull-Out Testing of Tensar Geogrids*. M.S. thesis. University of California, Davis, 1985.
13. C. K. Shen. *Final Report on Pull-Out Testing of Tensar SR-2 Geogrids*. Tensar Corporation, Morrow, Ga., 1985.
14. R. A. Jewell, G. W. F. Milligan, R. W. Sarsby, and D. Dubois. Interaction Between Soil and Geogrids. *Symposium on Polymer Grid Reinforcement*, London, England, 1984, pp. 18–30.
15. A. McGown. Reinforced Earth, Discussion to Session 8. *Proc.*, 7th European Conference on Soil Mechanics and Foundation Engineering, Brighton, England, 1979, Vol. 4, pp. 284–287.
16. B. Myles. Assessment of Soil Fabric Friction by Means of

Shear. *Proc.*, 2nd International Conference on Geotextiles, Las Vegas, Nev., 1982, pp. 787–791.
17. S. K. Saxena and J. S. Budiman. Interface Response of Geotextiles. *Proc.*, 11th International Conference on Soil Mechanics and Foundation Engineering, 1985, pp. 1801–1804.
18. H. M. Coyle and L. C. Reese. Load Transfer for Axially Loaded Piles in Clay. *Journal of the Soil Mechanics and Foundation Division*, ASCE, Vol. 92, No. 2, 1966, pp. 1–26.
19. I. Juran. *Internal Research Report on Behavior of Reinforced Soils*. FHWA Project No. DTFH-61-84-C-00073. FHWA, U.S. Department of Transportation, 1985.
20. I. Juran, M. H. Ider, C. L. Chen, and A. Guermazi. Numerical Analysis of the Response of Reinforced Soils to Direct Shearing, Part 2. *International Journal for Numerical and Analytical Methods in Geomechanics*, Vol. 12, No. 2, 1988, pp. 157–171.

Publication of this paper sponsored by Committee on Soil and Rock Properties.

Pull-Out Resistance of Geogrids in Sand

RODNEY W. LENTZ AND JAMES N. PYATT

To further knowledge of the pull-out resistance of grids, a series of pull-out tests was performed in the laboratory. The test regimen included the effects of overburden pressure, grid specimen length and width, and relative density of the sand on the pull-out resistance of the reinforcement. Tests were also performed to find the effect of soil particle size on the pull-out resistance of grids. It was found that the pull-out resistance of grids is a function of the relative density of the soil, the particle size, the length and width of the grid specimen, and the mechanical properties of the grid material. A mechanism of soil-geogrid interaction is described and used to explain the results of the pull-out tests. A significant finding is that the selection of geogrid specimen dimensions for laboratory pull-out tests must take into account the strain to failure of the soil and the stiffness of the geogrid in order to properly represent the maximum pull-out stress that will be available in field applications.

Reinforced soil is a composite construction material that consists of alternating layers of compacted backfill and tensile reinforcing material. The theory behind reinforced soil is that the vertical normal stresses that the backfill exerts on the embedded reinforcement are a source of frictional resistance that results in tensile stresses being carried by the reinforcement.

Long galvanized steel strips were almost exclusively used as reinforcement in early applications in reinforced soil structures. It has been found that ribbing the metal strips greatly improves the frictional resistance developed between the reinforcement and the soil. Newer materials such as geotextiles and geogrids are now being used in some reinforced soil structures. Geotextiles appear to be useful when large deformations are allowable and when stresses are relatively low. Geogrids, made of strong plastics, are not as extensible as textiles and develop higher resistance to pulling out of soil.

Two requirements common to the design of all reinforced soil structures are that (a) the reinforcement must not fail in tension, and (b) the reinforcement must not pull out of the soil. Designing against a tension failure requires that the stresses in the reinforcement be less than the ultimate strength of the reinforcing material. This is done by adjusting the cross-sectional area of each reinforcing member or varying the number of reinforcing elements per unit area of the structure.

In designing against pull-out failure of metal strip reinforcement, a coefficient of friction between the soil and the reinforcement is used. It is assumed that the pull-out resistance is supplied by friction along both surfaces of the reinforcement and is given by the relation

$$T = 2LW\,\sigma_n \tan \delta \quad (1)$$

where

T = maximum pull-out force developed,
L = length of reinforcement,
W = width of reinforcement,
σ_n = overburden pressure, and
δ = friction angle between the soil and reinforcement.

An assumption associated with the use of this equation is that the frictional resistance is uniform along the length of the reinforcement. It is known, however, that the friction developed along the reinforcement is not uniform but varies along the length. In a reinforced soil retaining wall, for example (*1–4*), it has been found through careful instrumentation that the tensile stress reaches a maximum near the point of crossing the theoretical Rankine failure wedge boundary. The stress decreases to zero at the free end of the reinforcement. It does appear, however, that the use of this equation for the design of metal strip reinforcement is adequate if care is taken. The required length of embedment of the reinforcing strips must be selected to provide an adequate factor of safety against pulling out of the soil.

For design of geotextile-reinforced retaining walls the same approach is sometimes used. Barrett (*5*) recommends using $\delta = \frac{2}{3}\,\phi_{soil}$ in the design. Murray (*6*) attempts to make allowances in the design for the large strains that develop in the fabric.

Material published by a geogrid manufacturer (Tensar Corporation, 1210 Citizens Parkway, Box 986, Morrow, Georgia 30260) also recommends using a two-dimensional approach in designing against pull-out for their grids.

Three test methods are commonly used to determine the pull-out characteristics of a reinforcing material. The first is a modified direct shear test in which the reinforcing material is firmly attached to a solid block and placed in the upper ring of a direct shear device. Soil is prepared in the lower ring. The test is then performed exactly like a conventional direct shear test to find the friction angle between the soil and the reinforcement.

The second test is called a "free shear" test. It is similar to the first test except that the reinforcement is placed at midheight of a soil sample. The reinforcement is attached to the top ring of the device on the side toward the direction of movement. As the soil and reinforcement are sheared,

R. W. Lentz, Department of Civil Engineering, University of Missouri–Rolla, Rolla, Mo. 65401. J. N. Pyatt, Soil Consultants, Inc., 333 Mid Rivers Mall Drive, St. Peters, Mo. 63376.

the reinforcement is allowed to strain freely between the soil layers.

The third method is a reduced-scale pull-out test. A reinforcing member is placed horizontally at midheight of a prepared soil sample, an appropriate overburden pressure is applied to the soil, and the reinforcing member is pulled out. Data from a pull-out test may be interpreted to give a soil/reinforcement friction coefficient (δ). The test is a systems test that most closely approximates the condition of the reinforcement in an actual structure.

Schlosser and Elias (*4*) presented results of pull-out tests performed on smooth bronze strips in sand. They drew several conclusions from their tests:

- The pull-out resistance offered by dense sand is much greater than that offered by soils of lower densities.
- At low densities (of soil) the friction is uniformly distributed across the length of the reinforcement.
- At higher densities deformation of the reinforcement predominates, and, as a result, the mobilized friction is maximum at the end that is pulled out and decreases to zero at the free end.
- At low densities the δ angle observed during pull-out testing is less than δ obtained from direct shear methods, probably because of collapse of the sand structure under strain during the pull-out test.
- At higher densities the δ angle from the pull-out testing is more than δ obtained from direct shear testing, probably because of dilatancy effects of dense sand.
- More pull-out resistance is developed from ribbed reinforcement than from smooth reinforcement.
- The peak pull-out resistance occurs at larger displacements for the ribbed strips than for the smooth. Also, smooth strips have a much more pronounced peak in the force-displacement curve than do ribbed strips. (The authors suggested that the more pronounced peak with the smooth strips is probably due to an effective collapse of the structure of the sand surrounding the strips during pull-out. The zone of affected sand is larger for the ribbed strips; therefore the displacement to peak is larger and the strength is less affected by the displacement.)
- δ increases as the length of the strip increases.
- δ increases as the overburden stress increases.

Bacot et al. (*7*) found that in compacted samples of sandy gravel the pull-out resistance was less than in uncompacted samples. (They said that this might be because the compaction process used smoothed out the surface of the sand. The undulations in the uncompacted sand probably caused the increased pull-out resistance.) They also found that, as the length of reinforcement increases, the friction angle (δ) between the soil and the reinforcement increases.

Ingold (*8*) reported on a comparison of the modified direct shear, free shear, and the pull-out tests for evaluating the pull-out resistance of grids. The pull-out resistance of textiles (woven and nonwoven) was also compared with that of grids. Ingold concluded that, for reinforcements that are extensible (such as textiles) or have a three-dimensional structure (such as geogrids), the pull-out test is the only reasonable method for determining pull-out characteristics. From the pull-out tests, it was determined that, for very low normal stresses, the friction angle between the reinforcement and the soil can be a very large value (from 55 to 85 degrees for the materials tested). For the textile materials, the δ angle decreased to a value that was less than the friction angle for the soil alone at normal stresses of about 15 psi and appeared to reach a constant value at some fraction of the soil friction angle at normal stresses of about 20 to 25 psi. The grid material, at normal stresses of about 15 psi, reached a constant value of δ at a value of about 10 degrees above the friction angle of the soil alone.

In a later study, Ingold (*9*) concluded that the pull-out resistance of grids is a function of the cumulative embedded area of grid members normal to the direction of pull-out and not the embedded plan area of the reinforcement. An analytical model was presented that shows that pull-out resistance is dependent on the normal stress level and some exponential function of the friction angle of the sand and the geometry of the grid member.

Jones (*10*) stated that the pull-out resistance of grid reinforcement in sand is a combination of the frictional resistance presented by the grid plus the anchor resistance of the grid. The frictional resistance was the same as that of methods using the δ angle. The anchor resistance was evaluated through the use of a modified bearing capacity equation.

In the present study, the pull-out resistance of grids in sand was studied. The effects of the following parameters on pull-out resistance were evaluated in the testing:

1. Relative density of the sand,
2. Grid sample length,
3. Grid sample width,
4. Particle size of the soil, and
5. Grid type.

EQUIPMENT

The pull-out test box is 11.5 in. wide by 30 in. long by 4 in. deep (inside dimensions). It is made of aluminum plates ⅜ in. thick. At one end of the box there is a slot, parallel to the bottom, that allows a geogrid to be pulled through. There is a pistonlike lid, made of aluminum plates, that fits into the box. The lid has a reinforced honeycomb structure attached to it to make it very stiff. Attached to the honeycomb structure at the top is a heavy steel plate with a small depression in the center in which a steel ball is placed. The normal load is applied to the steel ball. This ensures that there are no eccentricities of the normal load. The stiffness of the lid plus the great care with which the sand surface is smoothed ensure that the load is applied uniformly over the entire area of the box.

The pull-out box is mounted on a large frame from an old consolidometer modified for this purpose. A weight hangar is used to apply the normal load to the lid of the testing box. There is room for about 900 lb of weights in the weight hangar.

The pull-out force is applied manually by a gearbox from an unconfined compression test device that is attached to the testing box by a bracket. A 1-kip load cell is attached in line with the pull-out force. A grid-holding device connects into the other side of the load cell. This device was designed to fit the type of grid tested and consists of a small piece of angle, approximately 10 in. long, with notches cut in one leg. A grid specimen hooks into the notches and is held in place by two 4-in.-long pieces of iron that are held to the angle by bolts. Attached to the end of the pull-out mechanism is a linear varying differential transformer (LVDT) that is used to measure the displacement of the moving parts of the pull-out mechanism and the geogrid as the pull-out test is performed. With this equipment it was found that pull-out forces of approximately 1,000 lb could be achieved. The equipment is shown in Figure 1.

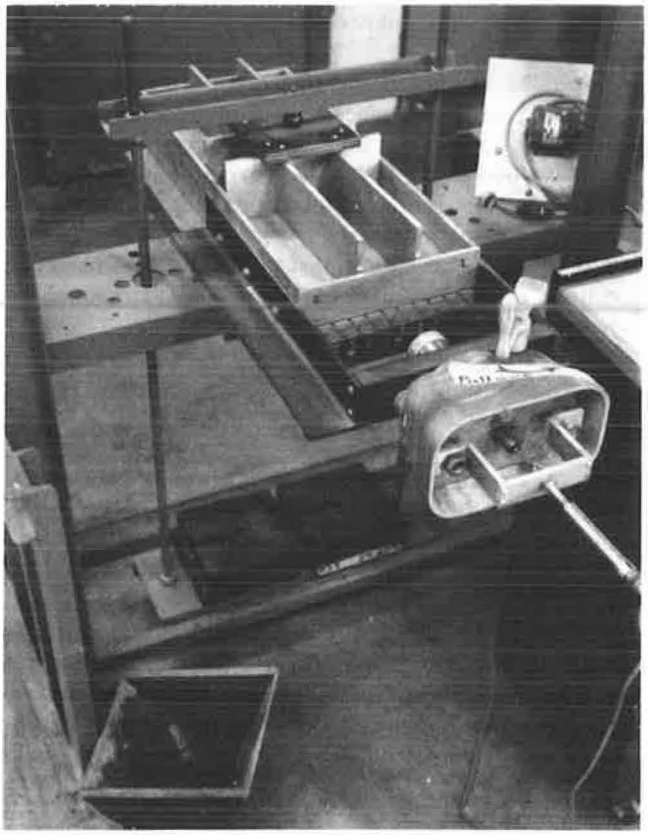

FIGURE 1 Pull-out test apparatus.

SAND

A fine sand and a coarse sand were used in the testing program. The fine sand consisted predominantly of subrounded quartz particles. The coarse sand had subangular particle shapes. A sieve analysis was performed to determine the gradation of each sand.

From these analyses, index properties of effective particle size (D_{10}), average grain size (D_{50}), coefficient of uniformity (C_u), coefficient of skew (C_z), and Unified Soil Classification were determined (Table 1). The minimum and maximum densities of each sand were determined by the methods described in ASTM standards 04254-83 and 04253-83 and are also given in Table 1.

The frictional characteristics of the sand were determined by consolidated-drained triaxial tests. Specimens of sand were prepared by placing a weighed amount of sand in a membrane-lined split mold and vibrating the mold until the height of the specimen indicated that the target relative density had been obtained. The angles of internal friction for the fine sand were 34 and 39 degrees for relative densities of 41 ± 3 percent and 84 ± 3 percent, respectively. The angle of internal friction for the coarse sand at a relative density of 40 ± 4 percent was 41 degrees. The Mohr envelopes from the triaxial tests are shown in Figures 2–4.

GEOGRIDS

Geogrids are made of parallel-oriented long-chain polymers such as polypropylene or high-density polyethylene. The grid structure is attained by heat-stretching a perforated sheet of the polymer. The geogrids used in this study were Tensar SS1 and SS2 made of polypropylene.

Tensar geogrid type SS2 was used in nearly all of the tests performed. The hole size in these grids is slightly smaller than 1.5 by 1.1 in. The grid members are 110 mils wide and 50 mils thick. At the juncture of grid members, the thickness is 160 mils. The tensile strength of grid type SS2 is 2,190 lb/ft width in the primary direction and 1,230 lb/ft width in the secondary direction.

Grid type SS1 is a slightly lighter-weight version of grid type SS2. The hole size is the same, but the grid thickness is only 30 mils and the juncture thickness is 100 mils. The tensile strength of grid type SS1 is 1,430 lb/ft width in the primary direction and 860 lb/ft width in the secondary direction. (The preceding information is from the manufacturer's literature.) All pull-out tests on both types of grid were performed with the grids pulled in the primary direction.

It was necessary to determine the volume per unit area for each type of grid so that the calculated density of sand in the pull-out device could be adjusted for the volume

TABLE 1 INDEX PROPERTIES OF SAND

	D_{10} (mm)	D_{50} (mm)	C_u	C_z	Class	γ_{dmax} (pcf)	γ_{dmin} (pcf)
Fine sand	0.22	0.35	1.86	1.00	SP	108.7	92.6
Coarse sand	3.00	4.50	1.67	1.01	SP	95.2	83.4

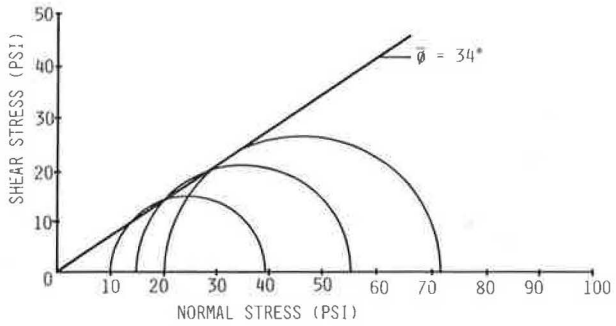

FIGURE 2 Mohr envelope for loose fine sand.

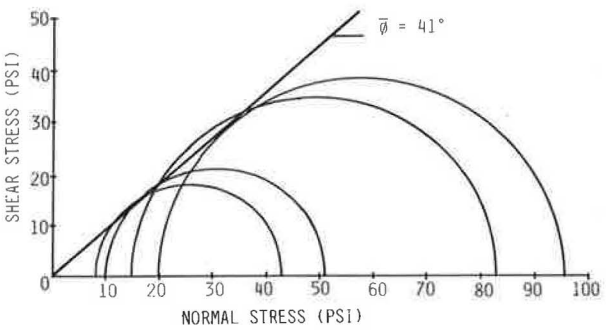

FIGURE 4 Mohr envelope for coarse sand.

occupied by the geogrid. This was done by immersing a known area of the grid in a graduated cylinder of water and determining the volume of water displaced.

TESTING PROCEDURE

The sand was placed in lifts that were roughly ½ in. thick with a sand-spreading device. The sand spreader was a V-shaped hopper that was moved along the sides of the pull-out box to place each lift in multiple passes. The sand particles were dropped from a 1-in. height at the start of the lift. The drop height decreased to ½ in. at the end of the lift. When the sand had been placed, it was screeded smooth. Then the height of sand was measured with a dial gauge device and the density was calculated. The same procedure was used on the second lift of sand.

In the tests with the dense samples, after the second lift had been placed, the sand was densified by using a vibrating motor mounted on a 10.5- by 10.5-in. aluminum plate. After it was vibrated, the sand was screeded smooth, the new height of sand was measured, and the density was calculated.

After the second lift was prepared, the grid was placed on the sand surface and inserted through the slot in the end of the box. The grid was placed with a grid member within the plane of the end of the box. This allows about ¾ in. of grid travel during a pull-out test without appreciable interaction of the grid and sand with the slot of the box. The free end of the grid was attached to a grid-gripping device that was, in turn, attached to a 1-kip load cell. The other end of the load cell was attached to the pull-out mechanism.

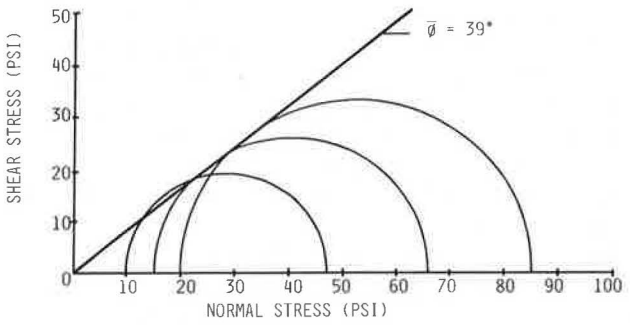

FIGURE 3 Mohr envelope for dense fine sand.

After the grid had been positioned, the second two lifts of sand were placed. The procedure was identical to that used for the first two lifts.

It was found that, by using the procedure discussed previously with the fine sand, an average loose relative density of 41 ± 4 percent and an average dense relative density of 85 ± 3 percent could be consistently achieved. With the coarse sand, an average loose relative density of 38 ± 13 percent was achieved. The relative density for each test is given in Table 2. Note that there is more variation in relative density for the coarse sand because of the small range between maximum and minimum density, which makes the result sensitive to small variations in placement density. Also, the large particle size made it more difficult to screed the surface smooth without disturbing the density.

PULL-OUT

After the sample had been prepared with the grid at mid-height, the following pull-out test procedure was used: First, the lid of the testing box was carefully placed on the sand surface. Then the loading ball and weight hangar were placed on the lid. Next, weights were carefully placed on the shelf of the weight hangar, below the testing box. It was determined through monitoring with four dial gauges that placing the lid, weight hangar, and weights on the sand has a negligible effect on the density and that the lid moves downward uniformly.

The pull-out force was applied by turning the crank on the pull-out mechanism. A constant, slow rate of approximately 0.1 in./min was maintained throughout each test. The test was continued until the displacement of the grid was about 0.6 in. A peak in the pull-out force was reached in all tests at or before this displacement.

Pull-out force, measured by the load cell, and displacement, measured by the LVDT, were recorded directly in the form of a load-deformation curve using an X-Y recorder.

TABLE 2 PULL-OUT TEST RESULTS

Test No.	Soil	q	L	W	D_r	P	δ
1	FS	1.265	29.50	10.38	39	576	36.6
2	FS	1.265	29.50	10.38	39	547	35.2
3	FS	1.841	29.50	10.38	40	777	34.6
4	FS	0.690	29.50	10.38	37	268	32.4
5	FS	2.416	29.50	10.38	40	965	33.1
6	FS	1.265	29.50	10.38	86	750	44.1
7	FS	0.690	29.50	10.38	81	375	41.6
8	FS	1.841	29.50	10.38	84	965	40.6
9	FS	1.265	24.25	10.38	42	394	31.8
10	FS	1.265	18.50	10.38	40	295	31.3
11	FS	1.265	18.50	10.38	84	493	45.4
12	FS	1.265	12.25	10.38	41	236	36.3
13	FS	1.265	29.50	8.13	41	493	39.1
14	FS	1.265	29.50	5.88	43	450	45.7
15	FS	1.265	29.50	5.88	84	563	52.1
16	FS	1.265	29.50	3.63	45	375	54.2
17[a]	FS	1.265	29.38	10.50	45	515	33.4
18[a]	FS	1.265	29.38	10.50	44	523	33.8
19	FS	1.265	29.50	3.63	86	450	59.0
20	FS	1.265	29.50	10.38	41	545	35.1
21	FS	1.265	29.50	10.38	87	680	41.3
22	FS	0.690	29.50	10.38	40	285	34.0
23	FS	1.265	24.25	10.38	41	462	36.0
24	FS	1.265	24.25	10.38	87	540	40.3
25	FS	1.265	18.25	10.38	42	320	33.7
26	FS	1.265	12.25	10.38	43	280	41.1
27	FS	1.265	12.25	10.38	87	415	52.2
28	FS	1.265	29.50	8.13	86	635	46.3
29	CS	1.265	29.50	10.38	51	760	44.5
30	CS	0.259	29.50	10.38	25	240	56.6
31	CS	1.265	29.50	10.38	37	740	43.7
32	CS	1.265	22.75	10.38	36	700	49.5
33	CS	1.265	16.63	10.38	38	660	56.5
34	CS	1.265	10.63	10.38	35	620	65.8
35	CS	0.690	29.50	10.38	43	500	49.8

NOTE: Tests 17 and 18 were performed with Tensar grid type SS1.

TEST RESULTS

The results of the 35 pull-out tests are given in Table 2. All tests but Tests 17 and 18 were performed with Tensar grid type SS2. Tests 17 and 18 were performed using Tensar grid type SS1. In the table, the following terminology is used:

Soil = soil type tested,
CS = coarse sand,
FS = fine sand,
q = normal stress (psi),
L = length of embedment (in.),
W = width of reinforcement (in.),
D_r = relative density of sand before loading (percent),
P = maximum pull-out force (lb), and
δ = average friction angle between soil and grid.

DISCUSSION OF RESULTS

All tests were performed at stresses in the working range of the grids tested. In only 1 of the 35 tests did the grid break, causing a very sudden loss of pull-out force. Test 19, during which the grid broke at a tensile force of 68 percent of the material's ultimate strength (according to the manufacturer), was the test with the highest stressed grid sample. To avoid damage to the equipment, no deliberate attempts to reach the ultimate strength of the grids were made.

Effect of Normal Stress

From the study of the effect of normal stress on pull-out resistance, it was found that, for each soil type tested, pull-out stress is directly proportional to normal stress. Figure 5 is a graph of pull-out stress versus normal stress; the figure shows the results for the loose fine sand, the dense fine sand, and the coarse sand. These results compare well with the results presented by Ingold (*9*), except that the plot presented by Ingold had a concave down curvature at the low-stress end.

The same results presented as friction angle (δ) between the soil and the grid versus normal stress are shown in Figure 6. The coarse sand, because of its large pull-out resistance, was only tested at normal stresses below 1.5

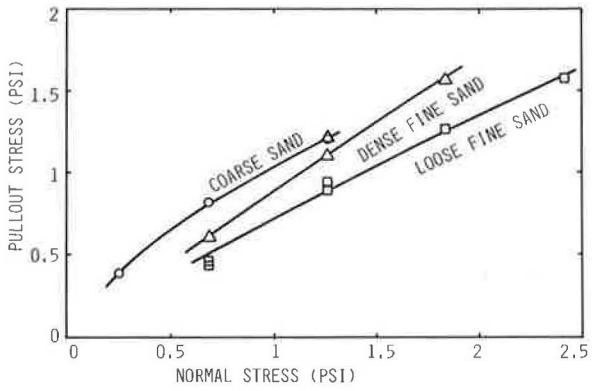

FIGURE 5 Pull-out stress versus normal stress.

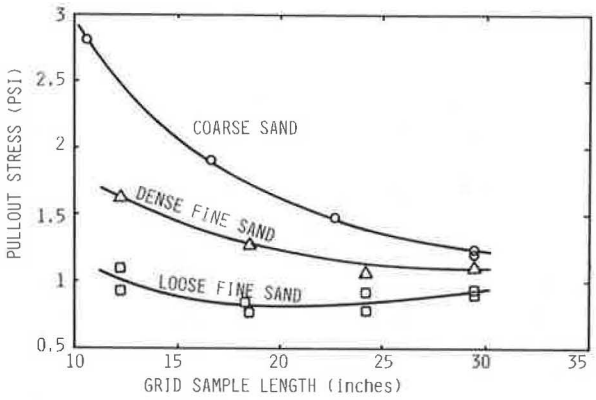

FIGURE 7 Pull-out stress versus grid sample length.

psi. Higher normal stresses would have resulted in pull-out forces approaching the ultimate strength of the geogrid. The results indicate that the friction angle tends to decrease toward the friction angle of the soil as the normal stress increases. This result is also in agreement with the results presented by Ingold. Inspection of Figure 6 shows that for the dense and loose fine sand the normal stress has less effect on the friction angle than for the coarse sand.

An assumption common to all design procedures studied is that pull-out stress is directly proportional to normal stress.

Effect of Grid Specimen Embedment Length

To study the effect of embedded length, several grid specimens, all the same width but of various lengths, were tested. All tests were at the same normal stress. The results are shown in Figures 7 and 8. Tests in loose fine sand showed a nearly constant pull-out stress for all embedded lengths. The friction angle (δ) from the length study on the loose sand showed a slightly decreasing trend, very near the friction angle of the soil alone. The same plots for the dense fine sand and the loose coarse sand show relatively high pull-out stresses (or friction angle) for short lengths that decrease to a constant value as the length increases. The friction angle decreases to a value slightly above that of the friction angle of the soil alone.

The curved, decreasing nature of the curves for the length study on the dense fine sand and the coarse sand is probably due to the extensibility of the grid reinforcement. A curve presented by McGown et al. (*11*) may be used to approximate the deformation of the grid material due to the stress levels present. For example, if a force of 600 lb is transferred by a grid 29 in. long and 10.4 in. wide held only at the ends, the specimen will elongate about ½ in. Given this, it is supposed that as the average pull-out stress in the grid reinforcement reaches higher values, the extensibility of the grid starts to play a more important role. For example, in the length study tests with the loose sand, the stress levels remained in a range slightly less than 1 psi, which indicates that the extensibility of the reinforcement plays only a minor role, if any. For the length study tests with the dense fine sand and the coarse sand, the frictional resistance is high enough at smaller lengths to produce large pull-out stresses. Over the short embedded length, there is not enough accumulated strain to cause the amount of mobilized soil strength to be appreciably different from one end of the grid specimen to the other. Therefore the soil at each grid member reaches its peak resistance at the same time. But, as the length of the grid specimen increases, the extensibility of the material plays a more important role. As the length of the specimen

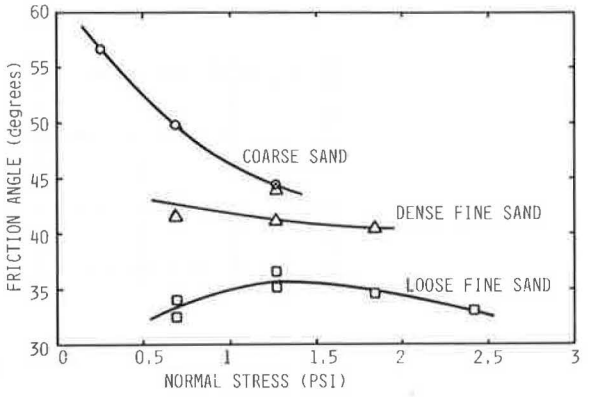

FIGURE 6 Friction angle versus normal stress.

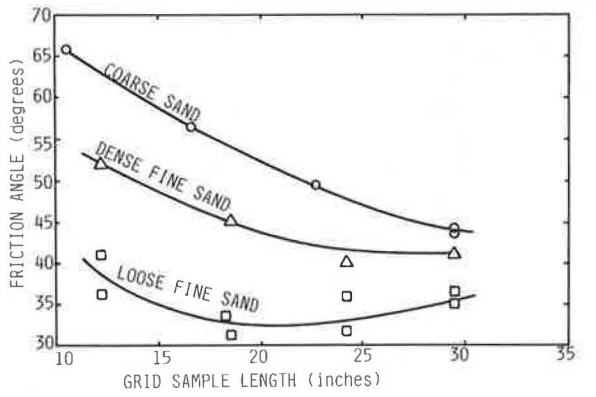

FIGURE 8 Friction angle versus grid sample length.

increases, the average pull-out stress (and also the δ angle) was observed to decrease.

It is hypothesized that, for the longer specimens, the geogrid deforms such that, as the pull-out test is performed, the embedded end does not contribute much to pull-out resistance because it has not been strained enough to mobilize the full strength of the soil surrounding it. The end of the specimen near the clamping device moves far enough to mobilize the full strength of the soil and possibly pass over a peak strength to a lower residual strength value. This will occur if the soil reaches its peak strength at a relatively low strain as does dense sand or angular material that exhibits dilatant behavior on straining. The grid material in the middle of the specimen is in some intermediate condition—the material is being stretched and is mobilizing at least part of the full soil strength. The maximum pull-out stress for the longer grid specimen will be lower than for the shorter specimens because the soil at some members will be past the peak strength.

As the embedded length of geogrid specimen in a dilatant soil increases, the variation in strain over the length of the specimen increases, which means that the soil surrounding a larger percentage of the grid members will have passed its peak strength. Thus the longer the specimen, the lower the average maximum pull-out stress. However, each successive increment of length increase results in a smaller decrease in pull-out stress until an almost constant value is approached.

Assuming that this soil-geogrid interaction mechanism is correct leads to the conclusion that, for a given soil condition, the stiffer the geogrid material, the longer the specimen must be to reach constant pull-out stress.

Effect of Grid Specimen Width

Specimens of geogrid of various widths but the same length were used to study the effect of width of reinforcement on pull-out resistance. The tests were performed on the fine sand in both the loose and dense condition. It was found that as the width increases, the pull-out stress decreases toward a constant value for the given normal stress level. If represented as friction angle versus width of reinforcement, the shape of the curve is the same with the friction angle decreasing, as specimen width increases, to a constant value that is very near the friction angle of the soil alone (Figure 9).

The shape of the curves from the width study can be qualitatively explained if the pull-out resistance of grids is broken down into two components. The first component is the passive resistance offered by the grid members perpendicular to the direction of pull-out. The second type of resistance is the frictional resistance that is offered by the grid members parallel to the direction of pull-out (Figure 10). In the tests performed, all grid specimens were cut such that no partial grid members were at the edges (i.e., sides) of the specimen. Grid members parallel to the direction of pull-out were at the extreme edges of the specimen, and, at the embedded end, grid members perpendicular to the direction of pull-out were at the extreme edge.

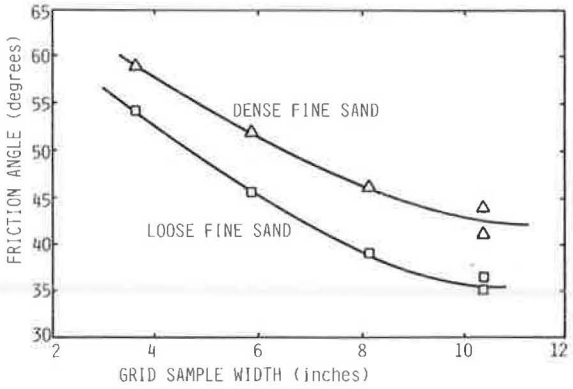

FIGURE 9 Friction angle versus grid sample width.

Suppose that pull-out tests are performed on a grid specimen one grid wide (one row of grid members perpendicular to the direction of grid travel and two rows of grid members parallel to the direction of travel). If the grid specimen width were doubled, the area of the grid members perpendicular to the direction of grid travel would also be doubled. This would cause the passive portion of the pull-out resistance to double. But doubling the specimen width only increases the total area of the grid members parallel to the direction of pull-out by 50 percent (from two rows to three rows). Similarly, if the width of the original one-grid-wide specimen were tripled, the area of the grid members perpendicular to the direction of pull-out would triple (from one to three rows), but the area of the parallel members would only double (from two to four rows). The passive resistance would triple and the frictional resistance would only double.

The data in Figure 9, then, indicate that the effect of the varying proportional contributions of the two components of pull-out resistance on total pull-out resistance is to cause pull-out stress to decrease with increasing width of grid specimen.

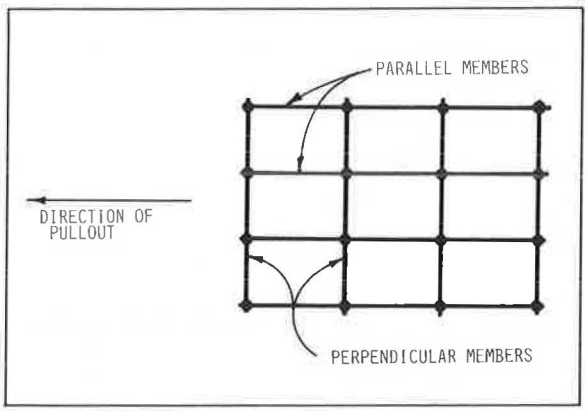

FIGURE 10 Grid sample configuration.

Effect of Soil Density

The effect of soil density on pull-out resistance is shown clearly in Figures 5–9. An increase in average relative density of the fine sand from 41 to 87 percent gave increases in the friction angle between the reinforcement and the soil of anywhere from 5 to 14 degrees. It appears that, for working sizes of reinforcement, the difference in friction angle (δ) is probably near the difference in the friction angle for the soil alone (i.e., 6 degrees). It was interesting to note that the pull-out force versus displacement curves from the pull-out tests on the dense fine sand had pronounced peaks, as did the stress-strain curves of dense fine sand in the triaxial shear tests. After the pull-out force reached a peak, it approached a smaller, residual value. The pull-out test curves from the tests on the loose fine sand exhibited no peaks.

Effect of Grid Type

Two pull-out tests were performed using a slightly lighter-weight Tensar grid. Grid type SS1 is the same size as type SS2, except that the thickness of the cross members is 40 percent less and the thickness of the junctures is 37.5 percent less. The decrease in cross-sectional area of the grid resulted in a decrease of pull-out resistance of about 7 percent. Although the results of the tests compared (Tests 1, 2, and 21 versus Tests 17 and 18) were consistent, a further study was not done because of the modest difference in pull-out resistance. The result does give some support to Ingold's hypothesis (*9*) that pull-out resistance is a function of the grid area normal to the direction of pull-out.

CONCLUSIONS

The results of laboratory pull-out tests using Tensar SS1 and SS2 geogrids in sand show that pull-out stress is a function of normal stress, relative density of the sand, angle of internal friction of the sand, the three-dimensional structure of the geogrid, and the dimensions of the geogrid specimen. A soil-geogrid interaction mechanism has been described and used to explain the results of the pull-out tests.

In the field the embedded area of geogrid is likely to be large enough that stretching will cause the pull-out stress to approach some minimum value, as demonstrated by the pull-out tests reported. Thus, if laboratory tests are performed on specimens too small to include this effect, the pull-out stress will be overpredicted, which will lead to unsafe design. This is most likely to happen with stiff geogrid material in a dilatant soil.

The significance of the results of this study is that when conducting laboratory pull-out tests to obtain friction angles for design of geogrid-reinforced structures the effect of the stress-strain behavior of the soil and the extensibility of the geogrid must be taken into account when choosing the size of geogrid specimen to test. The maximum dimensions of geogrid specimens used in the present study appear to be barely large enough to meet these criteria.

For the Tensar SS2 geogrid, the soil-geogrid friction angle (δ) approaches the angle of internal friction of the soil used in the pull-out tests. It could therefore be concluded that, for field conditions using the same geogrid and the same soil, the design δ could be taken equal to the angle of internal friction of the soil as determined by drained triaxial tests.

In comparison, Ingold (*9*) reported that, for pull-out tests using smaller specimens of a much stiffer geogrid and much higher normal stresses, δ was about 10 degrees greater than the angle of internal friction of the soil. This higher difference between δ and ϕ may be due partly to the different geometry of the geogrids used in the two studies. The difference could also have been caused because the short length of geogrid specimen used by Ingold did not meet the criteria proposed in the present study.

The lower values of normal stress used in this study, compared with those used by Ingold, are appropriate because the geogrid used in this study had much lower strength than did that used by Ingold.

REFERENCES

1. F. Schlosser and N. T. Long. Recent Results in French Research on Reinforced Earth. *Journal of the Construction Division*, ASCE, No. C03, Sept. 1974, pp. 223–237.
2. J. Binquet. Analysis of Failure of Reinforced Earth Walls. *Proc.*, Symposium on Earth Reinforcement, ASCE, 1978, pp. 232–251.
3. K. L. Lee, B. D. Adams, and J. M. J. Vagneron. Reinforced Earth Retaining Walls. *Journal of the Soil Mechanics and Foundations Division*, ASCE, No. SM10, Oct. 1973, pp. 745–763.
4. F. Schlosser and V. Elias. Friction in Reinforced Earth. *Proc.*, Symposium on Earth Reinforcement, ASCE, 1978, pp. 735–763.
5. R. K. Barrett. Geotextiles in Earth Reinforcement. *Geotechnical Fabrics Report*, Vol. 3, No. 2, March/April 1985, pp. 15–19.
6. R. T. Murray. Fabric Reinforced Walls: Development of Design Equations. *Ground Engineering*, Vol. 13, No. 7. Oct. 1980, pp. 30–36.
7. J. Bacot, M. Itlis, P. Lareal, T. Paumier, and G. Sanglerat. Study of the Soil Reinforcement Friction Coefficient. *Proc.*, Symposium on Earth Reinforcement, ASCE, 1978, pp. 157–185.
8. T. S. Ingold. Some Observations on the Laboratory Measurement of Soil-Geotextile Bond. *Geotechnical Testing Journal*, ASTM, Vol. 5, No. 3/4, Sept./Dec. 1982, pp. 57–67.
9. T. S. Ingold. Laboratory Pull-Out Testing of Grid Reinforcements in Sand. *Geotechnical Testing Journal*, ASTM, Vol. 6, No. 3. Sept. 1983, pp. 101–111.
10. C. J. F. P. Jones. Design and Construction Methods. In *Polymer Grid Reinforcement*. Science and Engineering Research Council and Netlon Ltd., London, England, March 1984.
11. A. McGown, K. Z. Andrews, K. C. Yeo, and D. DuBois. The Load-Strain-Time Behavior of Tensar Geogrids. In *Polymer Grid Reinforcement*, Science and Engineering Research Council and Netlon Ltd., London, England, March 1984.

Publication of this paper sponsored by Committee on Rock and Soil Properties.

Why All Important Pavements Should Be Well Drained

HARRY R. CEDERGREN

During the hours, days, and months that pavements are filled with water, heavy vehicle loads cause severe damaging actions such as erosion and pumping, disintegration of cement-treated bases, stripping of asphalt coatings from bituminous-treated bases and subbases, and overstressing of weakened subgrades. The presence of liberal amounts of water causes or increases non-load-bearing damage such as D-cracking, blow-up, frost action, expansion, shrinkage cracking, accelerated oxidation and loss of flexibility, and general deterioration of pavements and bases. Pavements designed without fast internal drainage can stay filled with water during much of the year while they are also subjected to damaging environmental conditions. If pavements are provided with fast internal drainage, water-related damage is almost entirely eliminated, which increases pavement life substantially and saves billions of dollars a year in the United States alone. Even though the need for good drainage and the benefits it can provide have been known for centuries, few modern pavement designers use it. In this author's view, the best methods available should be used in designing pavements, and in addition every important pavement should be provided with an internal drainage system capable of rapidly removing all water that enters.

When a pavement is filled with water, heavy vehicle loads cause severe damaging actions such as erosion and pumping, disintegration of cement-treated bases, stripping of asphalt coatings from bituminous-treated bases and subbases, and overstressing of weakened subgrades. Also, the mere presence of abundant water causes or accelerates numerous non-load-bearing actions such as D-cracking, blow-up, frost action, expansion, shrinkage cracking, increased oxidation and loss of flexibility, and general deterioration of wearing courses and stabilized bases.

Pavements designed without rapid internal drainage can remain filled with water a number of days or weeks after each saturating rainfall, adding up to several months of damaging environmental conditions each year. When good internal drainage is provided, however, water-related damage can be virtually eliminated or at least greatly reduced. Rapid drainage could probably provide at least 10 times more benefit to pavements than do any of the "modern" design and structural strengthening techniques developed in the past 20 to 30 years.

Even though the detrimental effects of poor drainage have been of concern for centuries and thoroughly documented in several major road tests in the past several decades (*1–3*) and the benefits of good internal drainage have been well documented, few designers even consider good drainage as a viable design concept that can extend pavement life three or four times and save billions of dollars a year. Continued presentation of the facts will, it is hoped, convince more and more designers of the need to return to the good drainage ideas advocated by John L. McAdam nearly 200 years ago.

Designers should use the best methods available to design good, economical pavement systems. In addition, every important pavement should be provided with a drainage system capable of removing free water rapidly instead of over the days and even weeks needed when good internal drainage is not used.

Consulting Engineer, 5245 Eye Street, Sacramento, Calif. 95819.

INTRODUCTION

This paper is a brief review of the historical development of basic philosophies of road design and an explanation of how the modern "undrainage" concept became so popular and is so hard to overcome. The damaging actions that take place in undrained pavements filled with water are reviewed, and estimates are given of the costs of not designing all important pavements as well-drained systems that can rapidly eliminate free water and preserve pavements in a relatively "dry" condition essentially 100 percent of the time.

From historical times road builders have known of the damaging actions of water in structural sections and have tried to design roads that will not fail prematurely because of water. Starting with the Appian Way in 312 B.C., the ancient Romans built their military roads very strong, but they also drained swamps to be crossed by their roads and usually provided a layer of broken slag or tile within the foundation layers, which probably improved internal drainage.

Centuries later, wise road builders such as John L. McAdam (*4*) and Pierre M. Tresaguet of France (*5*, p. 3) warned of the consequences of excess water in structural sections and used open-graded stone or gravel in their construction. Sometimes, when an intervening layer of screenings or fine gravel was not placed on clay subgrades to act as a filter, the soil worked into the stone or gravel with undesirable results.

Because of experiences like this, and with the development of modern "rational" and experimental methods for designing pavements, the pendulum swung to the

extreme of relying on density and strength as complete solutions to all problems and believing that good internal drainage is no longer necessary to achieve long-lasting, trouble-free pavements (*6*). This is the one factor above all others, in my view, that is responsible for the untimely deterioration of modern pavements under both traffic-related and non-load-bearing environmental damaging actions and that results in enormous losses in money, energy, and natural resources.

CHRONOLOGY OF ROAD DESIGN

After enactment of the U.S. Federal Aid Act of 1916, pavements were designed (in the United States) on the basis of soil classification (A-1, A-2, etc.) and the designer's experience and judgment. Since the development of modern soil mechanics methods, pavement designs have been based almost entirely on strength factors obtained by conducting static tests on specimens of base, subgrade, and other layers that have been presaturated for testing.

On and off for centuries road builders have believed in good drainage. Nearly 200 years ago, John L. McAdam (*4*) said, "If water pass through a road and fill up the native soil, the road whatever may be its thickness, loses support and goes to pieces." He also commented, "The erroneous opinion . . . that [by] placing a large quantity of stone under the roads, a remedy will be found for the sinking into wet clay or other soft soils . . . [so] that a road may be made sufficiently strong artificially to carry heavy carriages . . . has produced most of the defects of the roads of Great Britain." After McAdam's time, good drainage was commonly preached as necessary for good roads. One text on road design said, "There are just three things necessary for a good road: drainage, drainage, and more drainage."

However, as modern rational methods came into widespread use for pavement design, many designers developed a high level of confidence in their newfound methods of using static tests to evaluate their materials. However, wheel loads apply dynamic forces to pavements, bases, and subgrades, and these design theories assume intergranular pressure distributions that cannot exist in real-world saturated pavements. The presence of abundant free water also causes or accelerates the previously mentioned non-load-bearing detrimental actions.

Many designers are so sure of the modern methods and so sure that drainage is unimportant that they look with disfavor on anyone who believes in good drainage as a viable design concept. In the course of interviews conducted during development of the FHWA's *Guidelines for the Design of Subsurface Drainage Systems for Highway Structural Sections*(*7*) one state highway engineer in the Great Lakes area said, "I have nothing but contempt for anyone who thinks pavements can be drained." A top pavement designer in a major western state said during those interviews, "But, of course, it is neither necessary, practical, nor economical to drain a pavement."

Since the issuance of the FHWA's pavement drainage guidelines in 1972, some change in the attitude of designers has been taking place, but very slowly. Under the nudging of the FHWA about 40 percent of the states are experimenting with "new" or "improved" drainage systems, and about 10 percent are actually using the high-permeability open-graded drainage layers proposed in the Guidelines. (The drainage systems in the Guidelines use a full-width base drainage layer composed of open-graded aggregate in the range of ¼-in. minimum size to ½- to 1½- in. maximum size protected with suitable bases or "filters" and provided with collector pipes and outlet pipes to ensure positive removal of all water that enters.)

At the present time (1987) most pavement designers are using the rational methods without providing internal drainage, but a few are awakening to the marvelous benefits of good drainage and putting it to work in their designs (*6*, pp. 20–21). Raymond Forsyth of Caltrans has been a prominent advocate of good drainage (*8*). California has, since 1982, required the use of positive rapid drainage on most new pavements on its state system. Drake (*9*), Haughton (*10*), and Craven (*11*) are other North American designers who are making use of good drainage ideas. Particularly noteworthy in my view is the landmark work of Roger Lorin in France who has been designing important airport pavements since 1980 with good built-in drainage (*6*, pp. viii, 20). His approach is in sharp contrast with that of most American airport pavement designers who consider strength and density of paramount importance and drainage unnecessary. In a letter to me dated August 1986, Lorin very aptly expressed the need for drainage of airport pavements: "[W]ith a drainage layer of porous concrete, water will no longer become under pressure when an aircraft is passing over, which avoids high-speed water movements, back and forth, under the slab creating voids by attrition of the cement-treated base. By eliminating pore pressures and water movements, the porous drainage layer eliminates pumping effects." Why all airport designers do not understand the need for rapid elimination of free water is difficult to comprehend when it should be so obvious.

With the help of the FHWA and a few progressive-thinking engineers like the ones just mentioned, the "undrainage" attitude is being slowly overcome. This author hopes that it will be a thing of the past before long.

Figure 1 shows the use of a highly permeable drainage layer in pavement structural sections (k = 10,000 to 100,000 ft/day) to rapidly eliminate free water and prevent or greatly reduce water-related damage to pavements. The figure shows the differences in water conditions in pavements of several designs, both without and with good drainage. In the undrained pavements, all wearing courses, bases, and subbases will be subject to flooding for a minimum of a few weeks a year in arid desert areas and many months a year in rainy climates. In the well-drained designs all layers above the drainage layer will be in a moist or damp condition, not in a fully saturated condition, nearly 100 percent of the time, so the detrimental traffic-related and non-load-bearing damaging actions will be virtually nonexistent. In

my view all important pavements should be given the protection shown in the left half of Figure 1.

DAMAGING ACTIONS OF WATER

Traffic-Related Damage

When a pavement is filled with water, every heavy vehicle load passing over it produces a pore pressure wave that moves along at the speed of the vehicle. Spellman (*12*) found that heavy vehicle impacts caused "violent water actions" at the interface between portland cement concrete (PCC) pavement and a cement-treated base (CTB), which caused erosion of cavities under the PCC pavement and ejection of material from the leading edges and its buildup under trailing edges. This action caused loss of support and produced the uncomfortable "faulting" or "step-off" so common in PCC pavements that are being damaged by traffic impacts and undrained water.

As part of the comprehensive field studies undertaken for the FHWA during development of its pavement drainage guidelines (*7*), holes were drilled in a 12-year-old California Interstate highway constructed with PCC on CTB. Although it was on a fill 40 ft high, this section of pavement was already showing excessive faulting and cracking. A hole drilled into the interior of an uncracked slab directly under the wheelpath in the truck lane revealed that the CTB had completely disintegrated into a cohesionless mass that could easily be removed with a small scoop, or even with fingers. A maintenance supervisor told the investigating engineer that this was a common occurrence along this highway; at every location where he had dug out failed pavements to be replaced with high-early strength PCC patches, the CTB was soft and disintegrated. To verify the condition of the CTB in the central passing lane where

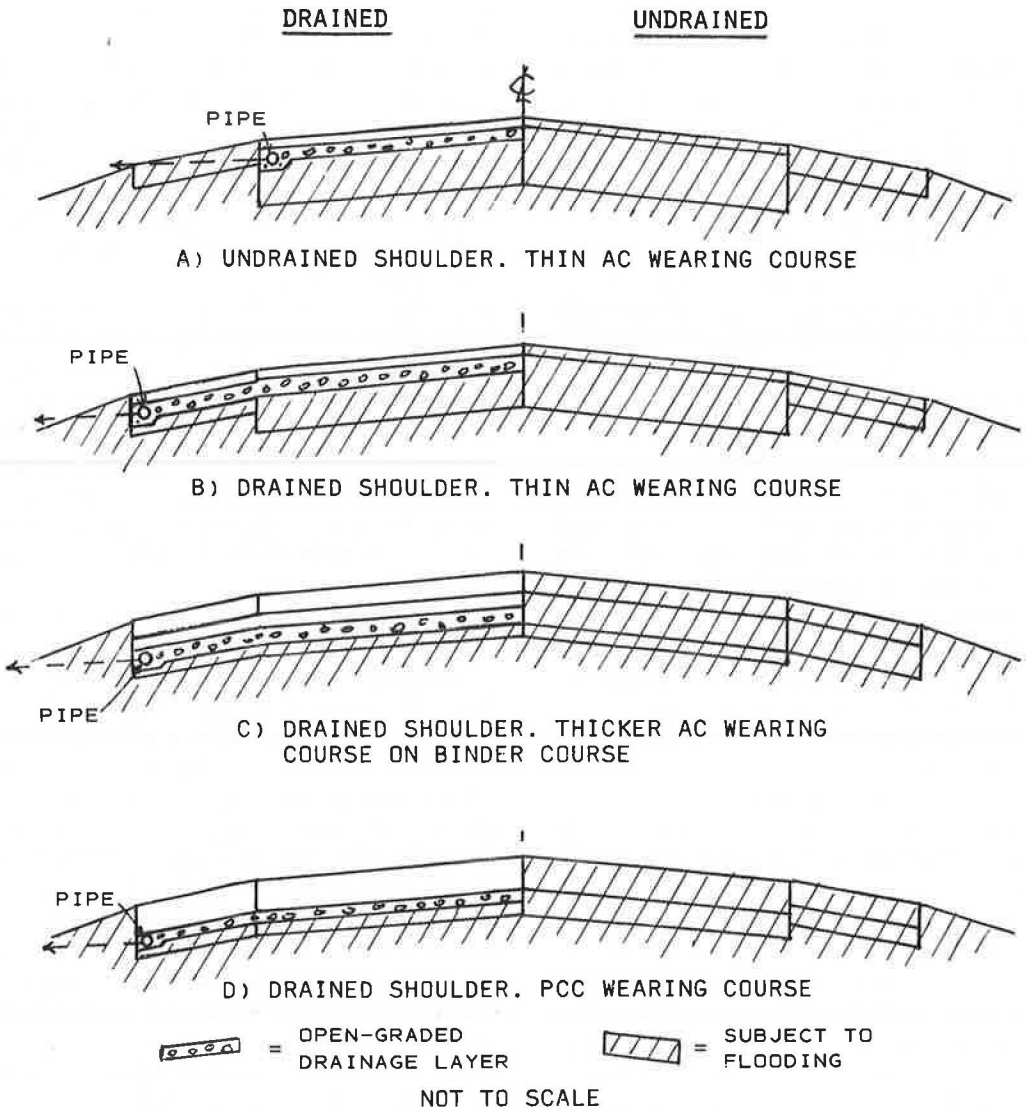

FIGURE 1 Differences in water conditions in drained and undrained pavements.

trucks seldom operated, a hole was drilled into the concrete and a very solid core of CTB was recovered under the PCC core, giving evidence that the CTB had been properly placed.

My explanation of the disintegrated CTB is that pore pressure waves moving under the pavement produce pulsating actions that may leach the cement out of the CTB. At any rate, any benefit from the cement treatment was lost under the truck lanes; the CTB was behaving as a cohesionless sandy base containing fine gravel.

In addition to the kinds of damage just discussed, heavy wheel impacts on water-filled pavements cause stripping of asphalt coatings from bituminous-treated bases and subbases, overstressing of weakened subgrades, increased rates of general deterioration, potholes, break-out of chunks of pavement from wearing courses, losses in safety and comfort to users, and reduced overall serviceability, as well as high repair and replacement costs.

Non-Load-Bearing Environmental Damage

The mere presence of abundant free water in structural sections causes or greatly accelerates non-load-bearing environmental actions that cause premature failure of pavements. Some of these actions do not occur at all in pavements that contain little or no free water.

D-cracking, for example, progresses only in the presence of abundant water. Rapid elimination of free water by the use of the good drainage systems recommended in the FHWA guidelines (*7*) could be very beneficial in reducing D-cracking, but good drainage systems are hardly ever thought of as a primary remedy for this troublesome form of disintegration of concrete pavements. Studies by Verbeck et al. (*13*) for the Portland Cement Association (PCA) on some 4,400 lane miles of pavements in Ohio led to the following statements in their report: "The field and laboratory observations . . . are taken as evidence that D-cracking is caused by stresses generated during the freezing of critically saturated coarse particles. . . . D-cracking is initiated when atmospheric moisture penetrates open joints and cracks, and together with moisture already present beneath the pavement, raises the degree of saturation of the coarse aggregate to a critical level. . . . If allowed to progress, the entire pavement will be converted to an incoherent mass of rubble."

Under Conclusions and Recommendations, the PCA report says, "It is thus recommended that precautions be taken to upgrade the coarse aggregate and reduce the flow of moisture through the joints." Nothing is said about improving internal drainage, although the rapid elimination of free water by good internal drainage systems offers a practical and economical means of reducing damage due to D-cracking. Trying to keep cracks and joints watertight is, of course, virtually impossible.

In a study of drainage needs of airfield pavements for the U.S. Army Corps of Engineers Construction Engineering Research Laboratory (CERL) (*14*), I found that D-cracking was much more severe in the 150-ft-wide runway of a major airfield in the Great Lakes area than in the 75-ft-wide taxiways. Water can drain out of a 75-ft-wide pavement in about ¼ the time needed to drain 150-ft-wide pavements (drainage time increases approximately in proportion to the squares of the widths). The much greater deterioration of the runway than the taxiways is evidence that increased retention time of water leads to greater D-cracking. It also corroborates the concept that good drainage can reduce D-cracking. If water can remain in the runway about four times longer than in the narrower taxiways after each saturating event, it is to be expected that the runway will suffer much greater non-load-bearing environmental damage than the taxiways.

Other kinds of non-load-bearing environmental damage, such as blow-up, frost action, expansion, shrinkage cracking, increased oxidation and loss of flexibility of asphalt concrete pavements and bases, and general deterioration, are related directly to the amount of time per year that structural sections remain in an essentially flooded condition. Hence, all of these kinds of damage can be greatly reduced by good internal drainage systems.

WARNINGS OF MOUNTING PROBLEMS WITH UNDRAINED PAVEMENTS

Collectively, the pavements of the U.S. Interstate system represent the biggest "experimental road test" of all time. Before much of the Interstate system was built, designers reviewed the results of the WASHO Road Test in Idaho (*1*) and the AASHO Road Test in Illinois (*2*), in which not a single one of the hundreds of test pavements contained a good internal drainage system. Although those tests proved that excess water was always the prime factor in failure of the road test pavements, drainage was completely ignored as a viable design option for Interstates or other important roads. As a consequence, the Interstate system was designed on the concept that if the specified kinds of pavement and base materials were used, and appropriate rational design methods were employed, fast removal of water from within structural sections of pavements would not be necessary.

The entire Interstate system (with few exceptions) therefore represents a technology that depends on strength, not on drainage, for performance. It represents the philosophy of most pavement designers. To illustrate, in August 1962 a prominent advocate of the "strength" philosophy and a staunch antidrainage champion told an international gathering of pavement designers (*15*), "The pertinent question should be, What is underneath the pavement?—not what falls on top of it." This attitude, which has been shared by most designers of Interstates and other pavements—even to the present day—is in my view the major reason for the untimely failure of most modern pavements. What has been put under pavements has not been able to handle what has been falling on them.

Those supervising and reviewing the major road experiments, such as the AASHO Road Test, were interested only in developing combinations of pavement and base

that would withstand traffic and environmental conditions without the benefit of good internal drainage. Because of this view, not one of the hundreds of individual designs incorporated internal drainage systems. Likewise, although some pavements of the Interstate system were provided with drains to control groundwater, spring inflow, and the like, not a single mile had a drainage system for rapid removal of infiltrated surface water. The system is therefore an "experimental road test" of undrained pavements. Its performance is a measure of the effectiveness of the design methods used. Many miles of Interstate started to deteriorate in as little as 6 to 10 years, far short of the life that should have been reasonably expected.

One of the early indications of coming problems with the Interstates was a report issued by the General Accounting Office (GAO) to Congress in 1970. As summarized in an article in *Civil Engineering* (*16*), that report says that surveys made of pavements put down before October 1963 indicated that some 2,800 mi of Interstate pavements already needed overlays at an estimated cost of $200 million. A little later an FHWA report (*17*) said that $329 billion out of a total road construction and repair budget of $450 billion would still be needed from 1976 to 1990 "to keep 1975 levels of condition and performance on the nation's highways." As shown later, I have estimated that at least ⅔ of the $329 billion, or $217 billion, could have been saved by good drainage of all important pavements. This is $15 billion a year in the United States alone.

More recent indications of the growing problems with undrained pavements in the United States are given in the Secretary of Transportation's *1985 Needs Report to Congress* on the condition and performance of the nation's highways (*18*). That report says, "Based on data supplied by the State highway agencies, the percentage of the Interstate pavements needing repair increased from 9 percent in 1981 to 14 percent in 1982." The report also says that failing pavements "will result in over 1 million miles of major roadways requiring work to the end of the century."

In my view, if all major pavements constructed in the past 20 to 30 years had been built as well-drained systems, hardly any would be needing more than normal maintenance and a periodic overlay to compensate for normal wear and tear.

The accelerating problems with the national pavement system have alarmed taxpayers, public officials, and the media. Our "magnificent pavement system," which was supposed to represent the best thinking and modern technology and consumed vast amounts of materials, energy, and money, has been falling apart and little can be done but to pour large amounts of money into repair and replacement projects. A *U.S.News & World Report* article (*19*) says that American roads—the most expensive public works undertaking of all time—are being battered to pieces. Numerous other national publications and local media have expressed concern over deteriorating pavements.

ESTIMATED DOLLAR LOSSES CAUSED BY LACK OF DRAINAGE

Estimating the amount of money being wasted by the "undrainage" practice requires reasonable estimates of two factors: (a) the relative rates of damage per load impact to typical undrained, "flooded" pavements and to well-drained or "nonflooded" pavements and (b) the length of time each year the undrained pavements remain full or essentially full of water and thus are in a flooded condition.

Documented information from major experimental road tests (*1, 2*) provides valuable insight into the potential rates of damage to flooded pavements versus nonflooded or well-drained pavements. I use the term "severity factor" to compare damage rates for undrained and drained pavements. Thus, if the rate of damage per heavy wheel impact is 10 times greater under flooded conditions than under nonflooded conditions, the factor is 10, and so on. That is, each flooded impact shortens pavement life 10 times faster than each nonflooded impact for a factor of 10. Table 1 gives a summary of calculated severity factors for the WASHO Road Test, the AASHO Road Test, and experiments conducted by the University of Illinois in its circular test track (*3*). For the AASHO Road Test, severity factors ranged from around 10 to around 40. For the WASHO Road Test, the factor ranged as high as 70,000 (spring thaw conditions). For the tests run at the University of Illinois, the factor was around 200.

In my estimate of the losses caused in the United States by poor drainage, I used a severity factor of 15, which I believe is rather conservative for a nationwide estimate.

Next, to estimate the average length of time pavements in the United States stay filled with water each year, I used the information in Table 2, which was included in the study for the FHWA's *Guidelines for the Design of Subsurface Drainage Systems for Highway Structural Sections* (*7*). At eight state highway sites and one county road site (selected

TABLE 1 SEVERITY FACTORS FOR FLOODED VERSUS DRAINED STRUCTURAL SECTIONS AS ESTIMATED FROM PUBLISHED REPORTS (*14*)

Test	Behavior Reported	Severity Factor
WASHO Road Test (*1*)	Worst damage occurred during frost melt period	70,000:1
AASHO Road Test (*2*, p. 40)	Damaging effects of traffic were more severe in spring frost melt period than in summer and fall	10:1 to 40:1
University of Illinois circular test track (*3*)	Before saturation, 700,000 load applications produced 0.2 in. to 0.5 in. rutting; after saturation, 12,000 additional load applications destroyed the pavements while causing 0.5 in. or more additional rutting	200:1

TABLE 2 ESTIMATED LENGTH OF TIME STRUCTURAL SECTION REMAINS ESSENTIALLY SATURATED AFTER IT STOPS RAINING

Case Study	Estimated Time (days)	Relative Time (Eureka = 1)	Special Notes
California	20	2000	Section is on 50- to 60-ft high clayey fill with some sandy material
Connecticut	15	1500	Section is on shallow fill on low side of superelevated curve; clayey subgrade layers over sandy fill
Eureka (Humboldt Co., Calif.)	0.01	1	Has highly permeable base drainage layer under full width of traveled way, with an outlet pipe
Georgia	12	1200	Section is on clayey sand—silty sand fill
Michigan	0.2 (unfrozen)		
	Infinite (frozen)	20	Section is on sand fill; freezes in winter
Oklahoma	15	1500	Has black base that is not directly drained
Pennsylvania	12	1200	Section is on silty sandy fill; 6-in. underdrain pipe under subbase, which is also daylighted
Utah	8	800	Section is on clayey sand fill; base is daylighted
Washington	5	500	Section has 2-in. porous base with no outlet and is not daylighted

SOURCE: K. O'Brien, J. Arman, and H. R. Cedergren, *Development of Guidelines for the Design of Subsurface Drainage Systems for Highway Pavement Structural Sections,* Final Report, FHWA, U.S Department of Transportation, Feb. 1973. Table 5, p. 68.

by the FHWA and local engineers), holes were drilled and tests run on typical samples of pavement, base, subbase, and subgrade to evaluate conditions at each site. Taking into account all known factors such as permeabilities of structural layers, bases, and subgrade; lengths of drainage distances; slopes; and the like, an estimate was made of the length of time the pavements at each site could remain filled with water after a saturating event. Omitting the Michigan site and the Humboldt County site, which are not typical of normal state highway pavements, the times range from 5 days to 20 days, with an average of 12 days per saturating rainfall. If each location in the United States has as few as 10 saturating rainfalls a year (most areas will have more), its pavements would be essentially flooded at least 4 months a year or 33 percent of the time. Trying to be conservative in my estimate, I assumed that pavements in the United States are filled with water an average of only 20 percent of each year.

If traffic loads with a severity factor of 15 act 20 percent of the time each year and the balance of the year they act with a factor of 1.0, the life cycle of the average pavement will be reduced to less than ⅓ of that experienced with wheel loads that have a severity factor of 1.0 during 12 months each year. On this basis, the losses in serviceability that are being caused by undrained water in the United States are more than ⅔ of the $329 billion the FHWA estimated as necessary to keep the nation's roads in serviceable condition to 1990 (*6*, pp. 60–61; *17*).These losses could have been saved by widespread usage of good drainage—$217 billion for the 14-year period or $15 billion a year (*20*). On a worldwide basis I estimate that the losses caused by the "undrainage" practice could exceed a trillion dollars over a 30- or 40-year period (*21–23*).

SUMMARY AND CONCLUSIONS

During the time pavements are filled with water, heavy wheel impacts cause pore pressures and water-hammer-like actions that erode bases and cause faulting and other detrimental actions that greatly shorten pavement life. Also, abundant free water causes or accelerates numerous non-load-bearing environmental actions that deteriorate pavements.

For centuries road builders have advocated good drainage as a means of counteracting the detrimental effects of water. Unfortunately, very few pavements built in the past 30 or 40 years have been provided with good internal drainage systems, with the result that many start to fail within less than half of a reasonably expected life span.

In the light of documented proof from several major road tests and the high costs of maintaining modern pavements, I urge all designers to "return to McAdam" and put good drainage systems in every important pavement they design.

ACKNOWLEDGMENTS

The author wishes to take this opportunity to thank the FHWA and its project manager, George W. Ring, for allowing him to take part in the extensive investigations of problems with water in Interstates and state highways, which led to the FHWA's *Guidelines for the Design of Subsurface Drainage Systems for Highway Structural Sections*. Also, thanks are extended to the U.S. Army Corps of Engineers Construction Engineering Research Laboratory, Champaign, Illinois, and its project manager, Ernest J. Barenberg, for permitting the author to carry out detailed investigations of problems with water in airfields in the United States. These two studies gave the author a much better understanding of problems with water in pavements of all kinds.

Thanks are also expressed to Raymond A. Forsyth, Chief, Transportation Laboratory, Caltrans, Sacramento, for reviewing a draft of this paper and offering a number of constructive suggestions for its improvement.

REFERENCES

1. *The WASHO Road Test, Part 2: Test Data, Analyses, Findings*. Special Report 22. HRB, National Research Council, Washington, D.C., 1955, 212 pp.
2. *The AASHO Road Test, Report 7: Summary Report*. Special Report 61G. TRB, National Research Council, Washington, D.C., 1962, 60 pp.
3. E. J. Barenberg and O. O. Thompson. *Behavior and Performance of Flexible Pavements Evaluated in the University of Illinois Pavement Test Track*. Highway Engineering Series No. 36; Illinois Cooperative Highway Research Program Series No. 108. Urbana, Ill., Jan. 1970.
4. J. L. McAdam. *Report to the London Board of Agriculture*. 1820.
5. A. G. Bruce. *Highway Design and Construction*. International Text Book Co., Scranton, Pa., 1934.
6. H. R. Cedergren. *Drainage of Highway & Airfield Pavements*. John Wiley & Sons, Inc., N.Y., 1974; Robert E. Krieger Publishing Company, Malabar, Fla., 1987.
7. H. R. Cedergren, K. O'Brien, and J. Arman. *Guidelines for the Design of Subsurface Drainage Systems for Highway Structural Sections*. FHWA, U.S. Department of Transportation, 1972.
8. R. A. Forsyth, G. K. Wells, and J. H. Woodstrom. The Economic Impact of Pavement Subsurface Drainage. In *Transportation Research Record 1121*, TRB, National Research Council, Washington, D.C., 1987, pp. 77–86.
9. E. Drake. New Subbase Design Uses Commercially Available Aggregates. *Highway and Heavy Construction*, Vol. 122, No. 10, Oct. 1979, pp. 106–108.
10. D. R. Haughton. *Open-Graded Aggregate Highway Construction, Pine Pass Project, Canada*. Geotechnical and Materials Branch, Ministry of Transportation and Highways, Victoria, British Columbia, Canada, 1986.
11. Open-Graded Base Course at Portland Airport. *Engineering News-Record*, July 5, 1979.
12. D. L. Spellman, J. H. Woodstrom, and B. F. Neal. Faulting of Concrete Pavements. In *Highway Research Record 407*, HRB, National Research Council, Washington, D.C., 1972, pp. 1–9.
13. G. Verbeck, P. Klieger, D. Stark, and W. Teske. *Interim Report on D-Cracking of Concrete Pavements in Ohio*. Ohio Department of Highways with Portland Cement Association, Research and Development Laboratories, Skokie, Ill., March 1972.
14. H. R. Cedergren. *Methodology and Effectiveness of Drainage Systems for Airfield Pavements*. Construction Engineering Research Laboratory, U.S. Army Corps of Engineers, Champaign, Ill., 1974.
15. *Proc.*, International Conference on the Structural Design of Asphalt Pavements. Civil Engineering Department, University of Michigan, Ann Arbor, 1962, Discussion, Session 1, p. 20.
16. Interstate Pavements Failing Early. *Civil Engineering*, Aug. 1970, p. 83.
17. Nation's Roads Deteriorating Rapidly. *Engineering News-Record*, Nov. 10, 1977, p. 14.
18. Secretary of Transportation. *1985 Needs Report to Congress*.
19. America's Highways Going to Pot. *U.S.News & World Report*, July 24, 1978, pp. 36–38.
20. H. R. Cedergren. Poor Pavement Drainage Could Cost $15 Billion Yearly. *Engineering News-Record*, June 8, 1978, p. 21.
21. H. R. Cedergren. How To Save Highway Dollars. *Sacramento Union*, Dec. 16, 1978, p. D-8.
22. H. R. Cedergren. Overcoming Psychological Hang-Ups Is Biggest Drainage Challenge. *Proc.*, Second International Conference on Geotextiles, Vol. 1, pp. 1–6.
23. H. R. Cedergren. Undrained Pavements: A Costly Blunder. *Civil Engineering*, April 1987, p. 6.

Publication of this paper sponsored by Committee on Environmental Factors Except Frost.

Slope Steepness Factor for Predicting Erosion on Highway Slopes

JEN-CHEN FAN AND C. W. LOVELL

A number of field soil erosion tests were successfully accomplished on newly constructed highway fills at Putnamville and Evansville, Indiana, in 1985 and 1986. The slope steepnesses ranged from 9 to 50 percent. It is possible to use the Universal Soil Loss Equation (USLE), which is widely applied for prediction of soil erosion, for highway slopes. However, the empirical slope steepness factor (*S*) in the USLE has been developed for slopes of from 3 to 18 percent. Because most highway slopes exceed this range, it was necessary to generate original experimental data. The modified rainfall simulator needed to obtain the data and its use are briefly described. The *S* factor reflects the development of rills, and the impact of raindrops, and appears to reach a maximum value of 1.5 at an intermediate value of slope steepness of 20 percent (11.2 degrees). The *S* factor may change with slope length, soil properties, and elapsed time, and accordingly is not an independent factor. In this study, the ratios of total erosion (which consists of the erosion in dry, wet, and very wet runs) to the erosion due to very wet runs are close to a constant. The mean value is 6.348 with a coefficient of variation of 4.90 percent.

Sediment due to soil erosion has been found to be an important factor in water pollution, and construction areas without protective covers have been found to be an important source of sediment (*1*). Further, construction areas with steep slopes and large areas (e.g., highway embankments) can yield much sediment. The steepness of highway slopes usually varies from 0 to 50 percent.

It is possible to use the Universal Soil Loss Equation (USLE) by Wischmeier and Smith (*2*), which is widely applied for prediction of soil erosion, for highway slopes. The USLE is written as follows:

$$A = RKLSCP \tag{1}$$

where

- A = computed soil loss per unit area (tons per acre),
- R = rainfall and runoff factor (hundreds of foot-tonf × inch per acre × hour),
- K = soil erodibility factor (ton × acre × hour per hundreds of acres × foot × tonf ×inch),
- L = slope length factor,
- S = slope steepness factor,
- C = cover and management factor, and
- P = support practice factor.

School of Civil Engineering, Purdue University, West Lafayette, Ind. 47907.

However, the USLE has been developed mainly for agricultural uses. According to Wischmeier and Smith (*2*), the USLE slope steepness varied from 3 to 18 percent, which is less than the usual steepness of highway slopes.

The *S* factor used by Wischmeier and Smith is given by

$$S = 65.41 \sin^2 \theta + 4.56 \sin \theta + 0.065 \tag{2}$$

where θ is the slope angle (degrees).

McCool and George (*3*) suggested that the *S* factor is given by

$$S = (\sin \theta / \sin 5.14^\circ)^{0.7} \tag{3}$$

and the *S* factor used by Foster (*4*) for interrill erosion analysis is

$$S = 2.96 (\sin \theta)^{0.79} + 0.56 \tag{4}$$

The *S* factor proposed by Stein (*5*) for the sites of the Ayrshire mine of Amax Coal Co. is

$$S = 12.784 \sin \theta - 0.146 \tag{5}$$

For the sites of Solar Sources, Inc., the value is

$$S = 10.742 \sin \theta + 0.037 \tag{6}$$

After studying the *S* factors proposed by several researchers, McCool et al. (*6*) recommended that the *S* factor be defined as

$$S = 10.8 \sin \theta + 0.03 \qquad \theta < 5.14 \text{ degrees} \tag{7}$$

$$S = 16.8 \sin \theta - 0.50 \qquad \theta \geq 5.14 \text{ degrees} \tag{8}$$

The curves of the *S* factor versus slope angle (θ) for Equations 2–8 are shown in Figure 1.

All of the data sets used to develop the equations have a slope steepness range of from 0.1 to 18 percent. Application of the equations to slopes greater than 18 percent is an extrapolation beyond the observed data.

In Figure 1, it is obvious that the differences among these curves are very large. The six curves intersect at θ = 5.14 degrees (9 percent slope), where S = 1. For other angles, especially angles greater than 10 degrees (17.6 percent slope), the differences are significantly large.

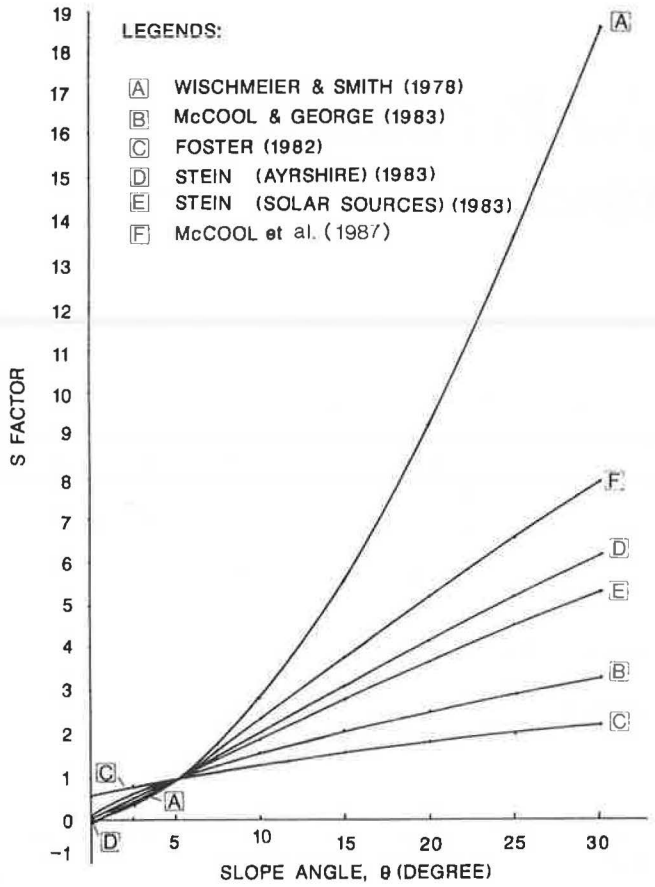

FIGURE 1 *S* **factor versus slope angle.**

Therefore it is necessary to run tests and establish the *S* factor for slopes steeper than 18 percent. To achieve this goal, a rainfall simulator was designed, constructed, and successfully operated on highway slopes with steepnesses of from 9 to 50 percent at Putnamville and Evansville, Indiana, in 1985 and 1986.

RAINFALL SIMULATOR AND ITS USE

The rainfall simulator was designed and constructed by modifying a programmable rainfall simulator that was developed by Foster et al. (*7*). To install and operate the rainfall simulator safely and effectively on highway slopes of from 0 to 50 percent, and to achieve accurate test results, the following modifications were necessary.

1. Wedges (Figure 2) were used to keep the troughs horizontal on all of the test plots.
2. Hinges were added to allow the half U-shaped frames to rotate, and bracings adjustable to different slope steepnesses were used to keep the whole structure vertical and stable.
3. The design wind speed was 20 mph, which is much higher than the previous limiting workable wind speed of 10 mph.

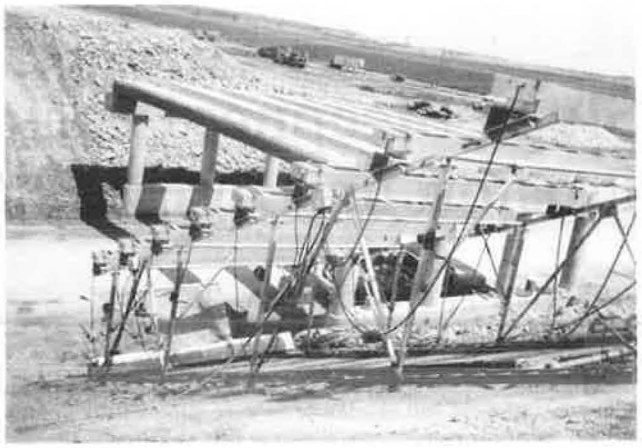

FIGURE 2 Wedges used to keep troughs horizontal on a 2 to 1 slope.

4. Footings were made of aluminum pipes 2 in. in diameter and 4 ft long and were designed to bear the horizontal and uplift load under the application of design wind speed.
5. Bearing plates 1 ft square were designed to connect the legs of the rainfall simulator and the footings and to bear the weight of the entire structure.
6. The rainfall simulator was assembled on highway shoulders and then lifted to selected positions by a crane.

Figures 3–5 show details.

FIELD EROSION TESTS

Three test plots at Putnamville, Indiana, and 12 test plots at Evansville, Indiana, were selected for field erosion tests. The test plots were on newly constructed highway slopes without any cover, management, or support practice.

The three test plots at Putnamville had 50 percent slopes. Each plot was 10 ft wide and 35 ft long along the slope.

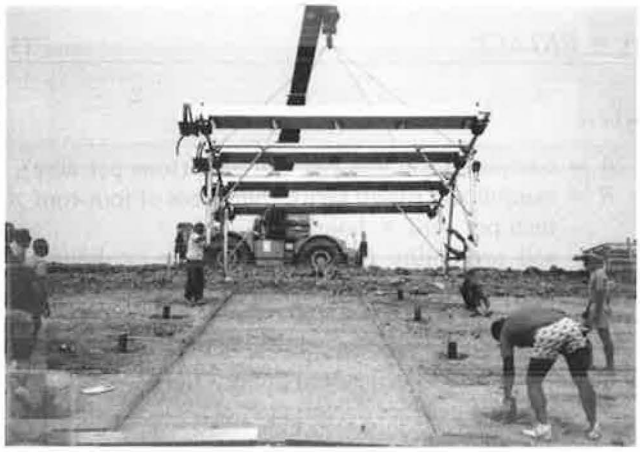

FIGURE 3 Crane lifting rainfall simulator from highway shoulder to test plot on 3 to 1 slope.

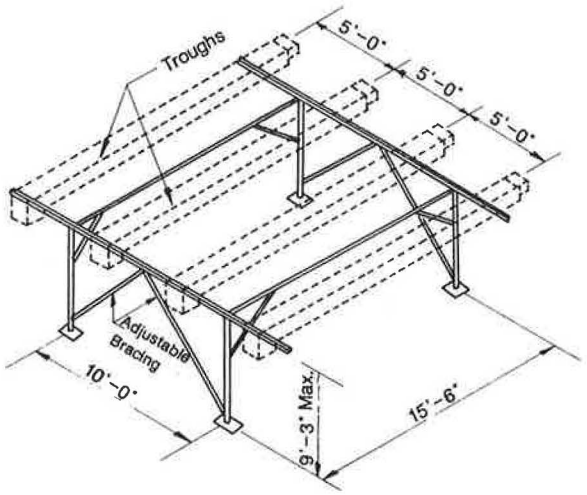

FIGURE 4 Overview of rainfall simulator.

There were four test sites at Evansville, each of which had three test plots. The slope steepnesses at Sites 1–4 were 50, 33.3, 16.7, and 9.1 percent, respectively. The test plots of Site 3 were 10 ft wide by 15 ft long along the slope, and the other test plots were 10 ft wide by 35 ft long along the highway slopes.

The soil conditions of the test plots at Putnamville, such as the source of the soil, field density, and water content, were controlled to be approximately the same. The soil conditions of the test plots at Evansville were also controlled to be essentially constant. As a result, the soil erodibility factor was essentially constant. For the sites at Evansville, the slope steepness was designed to be the only variable so that the slope steepness factor could be established for slopes of from 9 to 50 percent.

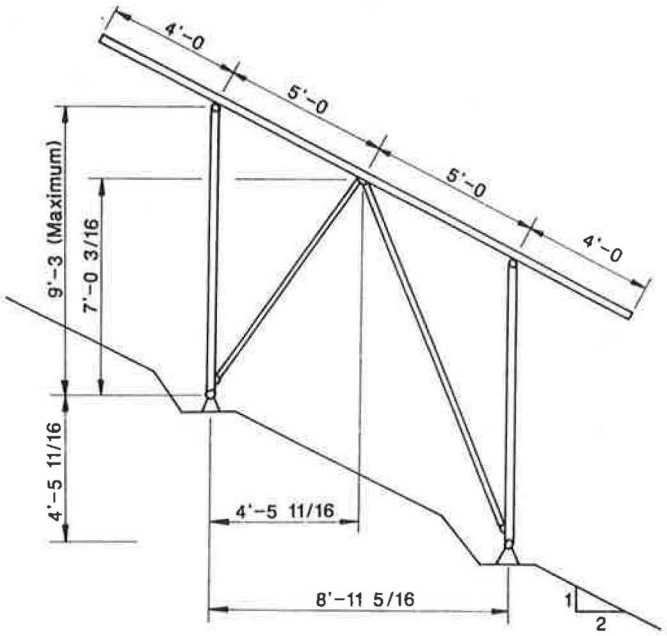

FIGURE 5 Side view of rainfall simulator on 2 to 1 slope.

All plots were covered by plastic sheets to prevent both plant growth and erosion from natural rainfall before the rainfall simulation tests. During the heat of the day, the plastic sheets were removed to allow evaporation and to reduce the initial moisture content.

For each erosion test in the field, the sequence of rainfall simulation consisted of a 1-hr "dry run," a 30-min "wet run," a 30-min "very wet run," and a 40-min "extra inflow run." The targeted intensity for each run was 2½ in./hr. The dry and wet runs were separated by a 1-hr wait, and the wet, very wet, and extra inflow runs by a 15-min data collection period. The extra inflow run was to study rill erosion by adding clear water at three successively higher rates to the top of the plot. After an initial 10-min simulated rain (2½ in./hr), each inflow rate was successively applied for 10 min. The height of water-spraying nozzles in the troughs was set at 8 ft vertically above the ground of the test plots.

DATA ANALYSIS AND RESULTS

General Data and Results of Field Erosion Tests

After field erosion tests were run, the samples collected in the field were tested in the laboratory, and the data were then analyzed. Soil properties of the test sites at Evansville and Putnamville are given in Table 1. The data and results from the erosion tests are given in Table 2 in which Items 1 through 9 and Item 13 are measured data. Item 10, the rainfall and runoff factor (R), is calculated using the equation proposed by Meyer and McCune (*8*):

$$R = 800 \times V \times I/100 \tag{9}$$

where

R = rainfall and runoff factor (hundreds of foot-tonf × inch per acre × hour),
V = amount of rain (inches), and
I = rainfall intensity (inch per hour).

Equation 9 is used because the spraying system of the rainfall simulator used in this research is the same as that used by Meyer and McCune (*8*).

For Item 11, the lengths of slopes are considered to be horizontal lengths; that is, the length on a horizontal base (l_h) is

$$l_h = l_s/(1 + s^2)^{0.5} \tag{10}$$

where l_s is slope length along the slope and s is slope steepness. This is consistent with rainfall intensities, because rainfall intensities are also considered to be on horizontal bases. Except for the slope lengths along Site 3 at Evansville, which are 15 ft, the lengths are 35 ft.

For Item 12, the slope length factor (L) is calculated using the equation by Wischmeier and Smith (*2*):

$$L = (\lambda/72.6)^m \tag{11}$$

TABLE 1 SOIL PROPERTIES OF TEST SITES

Item of Test / Location of Site and Site No.		Evansville				Putnamville
		1 (2 to 1 slope)	2 (3 to 1 slope)	3 (6 to 1 slope)	4 (11 to 1 slope)	(2 to 1 slope)
Specific Gravity		2.754	2.776	2.762	2.773	2.712
Atterberg Limits	Liquid Limit (%)	38.9	38.6	36.7	41.3	30.9
	Plastic Limit (%)	24.3	24.5	22.1	22.6	20.7
	Plastic Index (%)	14.6	14.1	14.6	18.7	10.2
Grain Size Distribution (% Finer)	4.76 mm (#4)	100.	100.	100.	100.	97.
	2.00 mm	100.	100.	100.	100.	94.
	0.100 mm	91.	91.	85.	88.	67.
	0.074 mm (# 200)	89.	88.	80.	84.	63.
	0.05 mm	85.	84.	77.	81.	60.
	0.002 mm	36.	31.	29.	32.	17.
Organic Matter (%)		1.0	1.0	0.8	1.0	0.5
Soil Classification	USCS	CL	CL	CL	CL	CL
	AASHTO	A-6 (close to A-7)	A-6 (close to A-7)	A-6 (close to A-7)	A-7 (close to A-6)	A-4 (close to A-6
	USDAC	Silty Clay Loam (close to Clay Loam)	Silty Clay Loam (close to Clay Loam)	Clay Loam (close to Silty Clay Loam)	Silty Clay Loam (close to Clay Loam)	Loam

where

λ = slope length in feet,
m = 0.5 when the slope is 5 percent or more,
m = 0.4 when the slope is 3.5 to 4.5 percent,
m = 0.3 when the slope is 1 to 3 percent, and
m = 0.2 when the slope is less than 1 percent.

Item 14, areas of test plots on horizontal bases (A_h) is calculated by multiplying the widths of test plots (10 ft) by Item 11, slope lengths on horizontal bases.

For Item 15, the cover and management factor (C) is 1.0 by definition because none of the test plots was covered or managed.

For Item 16, the support practice factor (P) is also 1.0 by definition because none of the test plots had any support practice.

Calculation of the *S* Factor

To calculate the soil erodibility factor (K), the equation by Wischmeier et al. (*9*) is applied:

$$K_{ave} = \frac{13\,A_d + 4\,A_w + 3(A_w + A_v)}{13\,EI_{30d} + 4\,EI_{30W} + 3(EI_{30w} + EI_{30v})} \quad (12)$$

where

K_{ave} = average soil erodibility of all runs (ton × acre × hour per hundreds of acres × foot × tonf × inch)
$A_{d,w,v}$ = adjusted rate of dry, wet, and very wet runs (tons per acre);
E = total storm energy by Wischmeier and Smith (*2*) (foot-tonf per acre); and
$I_{30d,w,v}$ = maximum 30-min intensity of dry, wet, and very wet runs (inch/hour).

The term EI_{30} is the R factor. Therefore the term EI_{30} can be replaced by the R factor of Equation 9. Assume the rainfall intensities (I), the slope length factor (L), the slope steepness factor (S), and the area of the test plot on a horizontal base (A_h) are the same in dry, wet, and very wet runs. Then, Equation 12 can be written as follows:

$$K_{ave} = \frac{\frac{13 \cdot T_d}{L \cdot S \cdot A_h \cdot C \cdot P} + \frac{7 \cdot T_w}{L \cdot S \cdot A_h \cdot C \cdot P} + \frac{3 \cdot T_v}{L \cdot S \cdot A_h \cdot C \cdot P}}{18 \cdot R} \quad (13)$$

where

$T_{d,w,v}$ = total erosion in dry, wet, and very wet runs (tons);

TABLE 2 DATA AND RESULTS FROM EROSION TESTS

Item No.	Items			Evansville				Putnamville
				Site 1	Site 2	Site 3	Site 4	
1	Field Density (PCF)			109.0	110.5	108.3	109.9	106.8
2	Dry Run (60 minutes)		(a) Erosion (lb) (b) Discharge (lb)	185.41 (3538.7)	197.24 (3297.2)	83.57 (1483.8)	190.70 (3548.3)	454.81 (3406.3)
3	Wet Run (30 minutes)		(a) Erosion (lb) (b) Discharge (lb)	43.54 (1781.8)	80.34 (1782.9)	27.73 (777.4)	58.66 (1803.2)	105.45 (1801.9)
4	Very Wet Run (30 minutes)		(a) Erosion (lb) (b) Discharge (lb)	44.13 (1849.5)	49.62 (1792.1)	20.94 (756.3)	51.14 (1802.8)	97.16 (1877.7)
5	Extra Inflow Run	1st 10 min.	(a) Erosion (lb) (b) Discharge (lb)	10.48 (619.9)	9.14 (501.9)	5.29 (237.9)	16.25 (608.7)	33.69 (571.0)
6		2nd 10 min.	(a) Erosion (lb) (b) Discharge (lb)	27.07 (1494.1)	34.14 (1660.4)	20.65 (994.1)	38.63 (1576.1)	77.65 (1564.9)
7		3rd 10 min.	(a) Erosion (lb) (b) Discharge (lb)	50.45 (2126.2)	79.93 (2272.9)	34.40 (1220.6)	63.93 (2241.7)	113.82 (2494.5)
8		4th 10 min.	(a) Erosion (lb) (b) Discharge (lb)	124.78 (3764.8)	155.65 (3403.2)	46.52 (1595.8)	109.37 (3913.3)	82.44 (3951.1)
9	Rainfall Intensity, I (in/hr)			2.500	2.175	2.389	2.203	2.720
10	Factor of Rainfall & Runoff for One Hour Rain, R			50.00	37.85	45.66	38.83	59.19
11	Length of Slope on Horizontal Base, l_h (ft)			31.273	33.203	14.809	34.843	31.338
12	Factor of Slope Length, L			0.6563	0.6763	0.4516	0.6928	0.6570
13	Slope Steepness, s (%)			50.3	33.3	16.1	9.4	49.7
14	Area of Test Plot on Horizontal Base, A_h (sq. ft.)			312.73	332.03	148.09	348.43	313.38
15	Factor of Cover & Management, C			1.0	1.0	1.0	1.0	1.0
16	Factor of Support Practice, P			1.0	1.0	1.0	1.0	1.0
17	Previous Approx. of S Factor (Assume S = 1.0, when slope steepness = 9.419%)			0.853	1.187	1.354	1.0	
18	Factor of Slope Steepness, S			0.880	1.222	1.395	1.03	

$$R = EI_{30d} = 2;$$
$$EI_{30w} = 2\,EI_{30v}; \text{ and}$$
$$A_{d,w,v} = \frac{T_{d,w,v}}{L \cdot S \cdot A_h \cdot C \cdot P}$$

Because the C and P factors are 1.0 for all of the cases in this study, Equation 13 can be written as follows:

$$K_{ave} = \frac{1}{18R \cdot L \cdot S \cdot A_h}(13T_d + 7T_w + 3T_v) \qquad (14)$$

When the data in Table 2 are used, Equation 14 becomes

$$K_{ave} = \frac{1}{18R \cdot L \cdot S \cdot A'_h}(13\,T'_d + 7T'_w + 3\,T'_v)21.78 \qquad (15)$$

where

K_{ave}, R, L, S = same as those in Equations 12–14
A'_h = area of test plot on horizontal base (square feet);
$T'_{d,w,v}$ = total erosion in dry, wet, and very wet runs (pounds); and

$$1\ \frac{\text{lb}}{\text{ft}^2} = 21.78\ \frac{\text{tons}}{\text{acre}}$$

Assuming that $S = 1.0$ when slope steepness is 9.4 percent, soil erodibility is then calculated using Equation 15:

$$K_{ave} = \frac{13 \times 190.70 + 7 \times 58.66 + 3 \times 51.14}{18 \times 38.83 \times 0.6928 \times 1.0 \times 348.43} \times 21.78$$

$$= 0.3928\ (\text{ton} \cdot \text{acre} \cdot \text{hour per hundreds of acres} \cdot \text{foot-tonf} \cdot \text{inch})$$

From Equation 15, the slope steepness factor can be calculated as follows:

$$S = \frac{1}{18 \cdot R \cdot L \cdot K_{ave} \cdot A_h'}(13\,T_d' + 7\,T_w' + 3\,T_v') \times 21.78 \qquad (16)$$

Assuming that the soil erodibility factors are the same in all of the sites at Evansville, the previously approximated S factors for the other slopes are calculated and given under Item 17 of Table 2.

These data are used to establish a curve representing the relationship between the previously approximated S factor and slope steepness (Figure 6).

The S factor at a slope steepness of 9 percent has been chosen to be unity by researchers for years. To be consistent with this, from Figure 6, the S factor of 9.4 percent is adjusted to 1.03.

By applying Equation 15, the soil erodibility of Site 1 at Evansville is then found to be 0.3814. Again, assuming that the soil erodibility factors are the same in all of the sites at Evansville, the S factors for the other slopes are calculated and given under Item 18 of Table 2. These data are used to establish a curve showing the relationship between the S factor and the slope angle (Figure 7).

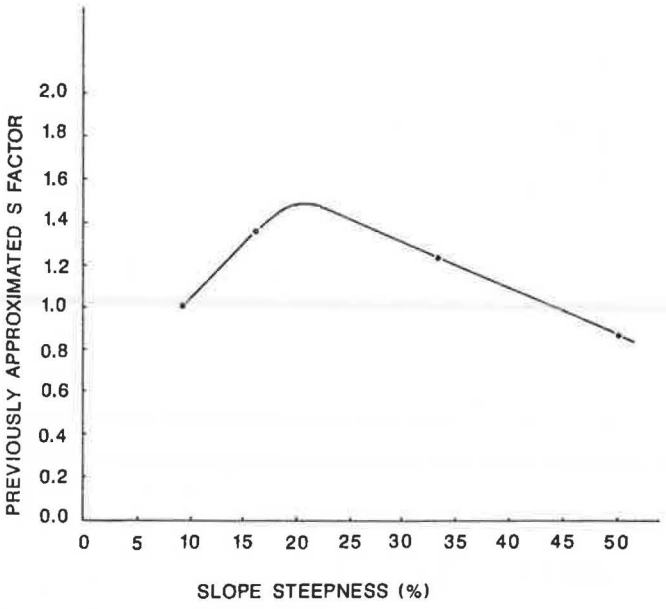

FIGURE 6 Previously approximated S factor versus slope steepness.

Analysis of Erosion Due to Extra Inflow

The main purpose of extra inflow runs is to simulate runoff from upper slopes to the test plots, from which the relationships between discharge rate and erosion rate may be obtained. It is assumed that the average erosion rate occurs at the middle of the test plot and that the average discharge rate includes only the discharge passing by the middle line of the test plot.

Therefore the data in Table 2 can be used to obtain average erosion rates (lb/ft² × hr) (D), average discharge rates (lb/ft × sec) (q), values of sin θ, and rainfall intensities (Table 3). The relationship between erosion rate and discharge rate for different slopes is plotted in Figure 8. The lower part of Figure 8 is plotted according to erosion theories proposed by Hussein and Laflen (*10*) and Foster (*4*).

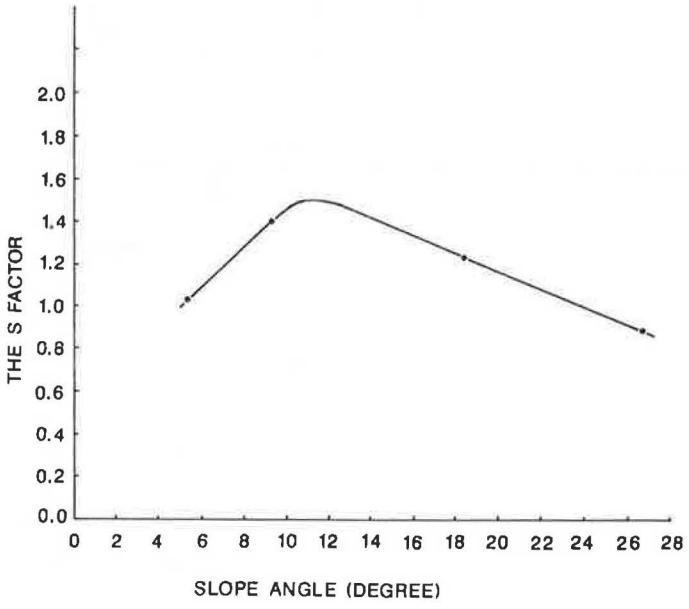

FIGURE 7 S factor versus slope angle.

TABLE 3 DATA FOR ANALYSIS OF EROSION DUE TO EXTRA INFLOW

Sites at Evansville	Erosion Rate D_2 (lb/ft^2·hr)	Discharge Rate q (lb/ft·sec)	Sin θ	Rainfall Intensity I (inch/hr)
	0.201	0.0517	0.449	2.500
Site 1	0.519	0.1974	0.449	2.500
(2 to 1 Slope)	0.968	0.3027	0.449	2.500
	2.394	0.5758	0.449	2.500
	0.165	0.0418	0.316	2.175
Site 2	0.617	0.2349	0.316	2.175
(3 to 1 Slope)	1.439	0.3370	0.316	2.175
	2.246	0.5254	0.316	2.175
	0.215	0.0198	0.159	2.389
Site 3	0.837	0.1459	0.159	2.389
(6 to 1 Slope)	1.394	0.1836	0.159	2.389
	1.885	0.2462	0.159	2.389
	0.280	0.0507	0.094	2.203
Site 4	0.665	0.2120	0.094	2.203
(11 to 1 Slope)	1.101	0.3229	0.094	2.203
	1.883	0.6015	0.094	2.203

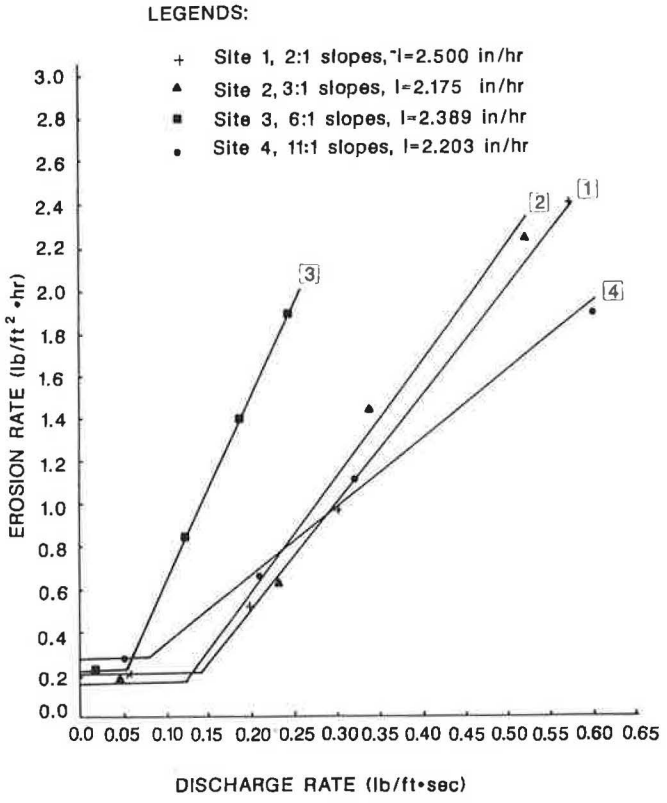

FIGURE 8 Erosion rate versus discharge rate.

Hussein and Laflen (*10*) found that, for soils with zero critical shear stress, the erosion rate increases linearly with the simulated length for extra inflow from upper areas.

Foster (*4*) proposed an equation for rill erosion. According to the equation, a critical shear stress exists for a given soil. For shear stresses below the critical value, the erosion rate increases very little or does not increase at all with shear stress, but beyond the critical value, the erosion rate increases markedly with shear stress.

Soil Erodibility from the Nomograph of Wischmeier et al.

Wischmeier et al. (*9*) proposed a nomograph for estimation of soil erodibility. The nomograph is shown in Figure 9. The data given in Tables 1 and 2 and the nomograph are used to find the soil erodibilities of the sites at Evansville and Putnamville (Table 4). In this table, soil structures and permeabilities are estimated from data from site investigations and the *Soil Survey Manual* of the U.S. Department of Agriculture (*11*).

Relationship Between Total Erosion and Erosion Due to Very Wet Runs

Total erosion means the total amount of erosion in dry, wet, and very wet runs. The relationship between total

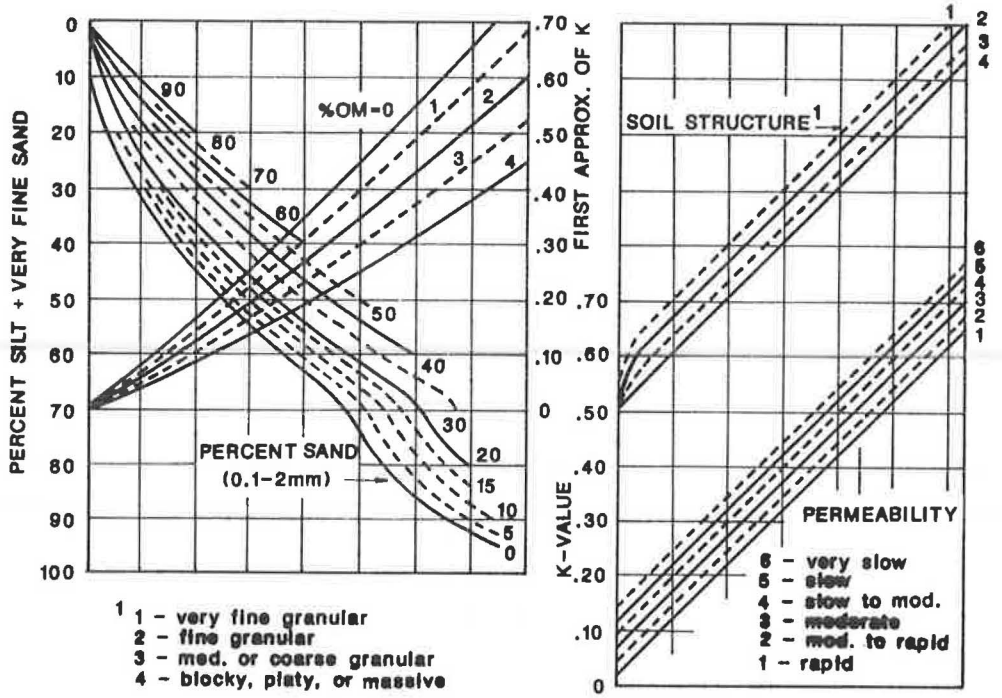

Procedure: With appropriate data, enter scale at left and proceed to points representing the soils % sand (0.10-2.0mm), % organic matter, structure and permeability, in that sequence. Interpolate between plotted curves.

FIGURE 9 Soil erodibility nomograph (*9*).

TABLE 4 SOIL ERODIBILITY OF SITES ACCORDING TO NOMOGRAPH AND FIELD EROSION TESTS

	Evansville				Putnamville
	Site 1 (2:1)	Site 2 (3:1)	Site 3 (6:1)	Site 4 (11:1)	
% Silt (0.002-0.05 mm)	49	53	48	49	43
% Very Fine Sand (0.05-0.1 mm)	6	7	8	7	7
% Silt + Vfs	55	60	56	56	50
% Sand (0.10-2.0 mm)	9	9	15	12	27
% OM	1.0	1.0	0.8	1.0	0.5
First Approximation of Soil Erodibility	0.27	0.32	0.32	0.30	0.32
Soil Structure	4	4	4	4	4
Permeability	6	6	6	6	6
Soil Erodibility from Nomograph	0.42	0.46	0.46	0.44	0.46
Soil Erodibility from Erosion Tests	0.381	0.381	0.381	0.381	-

TABLE 5 RELATIONSHIP BETWEEN TOTAL EROSION AND EROSION DUE TO VERY WET RUNS

Item No.	Amount of Erosion (lb) / Sites / Runs	Evansville Site 1 (2:1)	Evansville Site 2 (3:1)	Evansville Site 3 (6:1)	Evansville Site 4 (11:1)	Putnamville (2:1)
1	Dry Run	185.41	197.24	83.57	190.70	454.81
2	Wet Run	43.54	80.34	27.73	58.66	105.45
3	Very Wet Run	44.13	49.62	20.94	51.14	97.16
4	Total (1)+(2)+(3)	273.08	327.20	132.24	300.50	657.42
5	Item 4 / Item 3	6.188	6.594	6.315	5.876	6.766

erosion and erosion of very wet runs is given in Table 5, using the data in Table 2.

DISCUSSION OF RESULTS

General Soil Properties

According to the data given in Tables 1 and 2, soil properties of the four sites at Evansville are reasonably close. The soil properties include specific gravity, Atterberg limits, grain size distribution, organic matter content, and field density. The results of grain size distribution show that the soil of Site 3 is a little bit coarser. Nevertheless, according to soil classification methods of the Unified Soil Classification System (USCS), AASHTO, and U.S. Department Agriculture Classification (USDAC), they are about the same. Therefore the soil conditions and soil erodibilities of the tested plots at Evansville are considered to be the same.

S Factor

In Figure 7, for slope steepness less than 18 percent, the *S* factor is between that defined by McCool and George (*3*) and that defined by Foster (*4*) in Figure 1. But for slope steepness greater than 18 percent, the *S* factor reaches a maximum value of 1.5 at an intermediate value of slope steepness of 20 percent (11.2 degrees) and then decreases. This means that interrill and rill erosion do not continue to increase with slope steepness. This is quite different from previous researchers' extrapolations of the *S* factor. The following reasons are advanced to explain the differences:

1. Under the conditions of this study, interrill erosion dominates total erosion;
2. Interrill erosion decreases with slope steepness; and
3. During dry runs, hydraulic tractive force is considered important for transporting the loose particles on soil surfaces.

The results plotted in Figure 8 may be considered supporting evidence for Reason 1. Figure 8 shows that when the discharge rate is less than a certain amount, the erosion rate increases very little, or not at all, with the discharge rate. Discharge rate is directly related to length of slope. This means that the slope lengths of the tested plots are too short to allow marked rill erosion to occur. Indeed, during the field erosion tests at Evansville, no rill development was found in the dry, wet, and very wet runs.

Figure 8 and the data in Table 3 can be applied to support Reason 2. In extra inflow runs, the runs of the first 10 min for different slopes are considered to have negligible erosion due to rill erosion. There was only rain, no extra inflows, in these runs.

A basic equation for interrill detachment (*4*) is

$$D_i = 0.0138\, K_i \times I^2 \tag{17}$$

where

D_i = interrill detachment rate (kg/m^2 × hr),
K_i = soil erodibility factor for detachment by raindrop impact (kg × hr/N × m^2), and
I = rainfall intensity (mm/hr).

Equation 17 can be rewritten as

$$D_i = 9.77\, K_i \times I^2 \tag{18}$$

where

D_i = interrill detachment rate (lb/ft^2 × hr),
K_i = soil erodibility factor of detachment by raindrop impact (lb × hr/lbf × ft^2), and
I = rainfall intensity (in./hr).

By using Equation 18 and the data in Table 3, interrill erosion rates can be adjusted on the basis of rainfall intensity of 2.5 in./hr (Table 6). In this table, the adjusted interrill erosion rate decreases with slope steepness.

As Poesen (*12*) pointed out, the following mechanisms may explain this:

- Steeper slopes have smaller amounts of raindrop impact when rain falls vertically;
- The normal component of raindrop impact decreases with increasing slope steepness (cosine effect); and
- Low slopes offer more opportunity for the occurrence of a thin water layer covering the soil surface through

TABLE 6 ADJUSTED INTERRILL EROSION RATE FOR RAINFALL INTENSITY OF 2.50 in./hr

Sites at Evansville	Interrill Erosion Rate D_i (lb/ft^2·hr)	Discharge Rate q (lb/ft·sec)	Slope Steepness (%)	Sin θ	Rainfall Intensity I (inch/hr)	Adjusted Interrill Erosion Rate (lb/ft^2·hr)
Site 1 (2 to 1 Slope)	0.201	0.0517	50.3	0.449	2.500	0.201
Site 2 (3 to 1 Slope)	0.165	0.0418	33.3	0.316	2.175	0.218
Site 3 (6 to 1 Slope)	0.215	0.0198	16.1	0.159	2.389	0.235
Site 4 (11 to 1 Slope)	0.280	0.0507	9.4	0.094	2.203	0.361

which the compactive force of the impacting raindrops is increased.

Before dry runs, the soil surfaces were naturally dry and had some quantity of loose particles on them. During dry runs, low slopes (e.g., 9.4 percent) may not be able to transport all of the loose particles and those detached by raindrop impact, even though their interrill detachment may be more. Therefore slopes with steepnesses of 16.1 and 33.3 percent may have more erosion. However, steep slopes (e.g., 50.3 percent) have the least erosion. Though their hydraulic tractive forces are high enough to transport the loose particles, their interrill detachments are too small.

Figure 10 is plotted to explain this qualitatively. The measured data under Item 2 of Table 2 for the Evansville sites support this. These data indicate that the erosion rate increases and reaches a maximum value and then decreases. After the loose particles on dry soil surfaces were totally eroded in dry runs and wet runs, the erosion rates in very wet runs are expected to be less for steeper slopes. The measured data given under Item 4 of Table 2 support this. Aside from the loose particles on soil surfaces, another reason why dry runs have much higher erosion rates than wet and very wet runs may be the slaking of dry soils during dry runs.

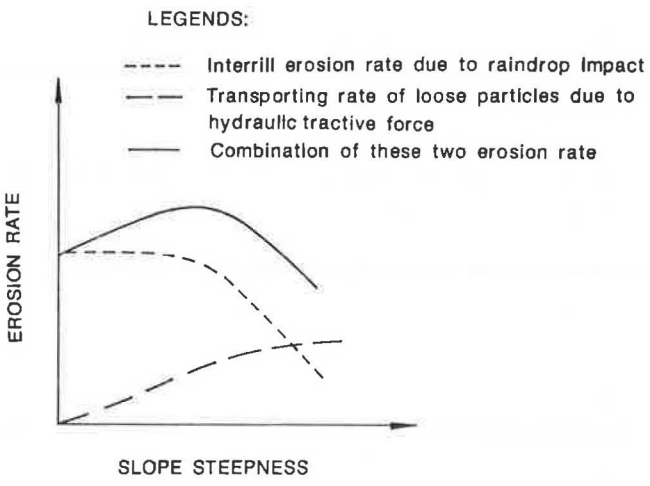

FIGURE 10 Erosion rate versus slope steepness during dry run.

Relationship Between Erosion Rate and Other Factors

According to Figure 8, erosion rate is very sensitive to discharge rate, but not sensitive to slope steepness. When the discharge rate is lower than a certain value, the erosion rate does not increase much with the discharge rate. Therefore a critical discharge rate or a critical slope length is expected for a given soil and slope steepness. Beyond that range, erosion rate increases markedly with discharge rate or slope length.

Comparison of Soil Erodibility by Measurement and by Nomograph

For the sites at Evansville, the average soil erodibility from the nomograph (*9*) is 0.445. However, the measured soil erodibility from erosion tests is 0.381, which is 85.6 percent of that obtained from the nomograph. This effect may be due to compaction of the soils on highway slopes. The nomograph was mainly developed for agricultural uses. Therefore data on compacted soils were not included in this nomograph. It is recommended that, for compacted cohesive soils of highway slopes, the soil erodibilities from the nomograph be multiplied by a factor of compaction to obtain the true soil erodibility.

S Factor of the Site at Putnamville

If the *S* factor of Wischmeier and Smith (*2*) is used to analyze the data on the sites at Putnamville, the value of *S* is calculated to be 15.07 using Equation 2. Then soil erodibility (*K*) is calculated to be 0.0457 (ton × acre × hour per 100 acres × foot-tonf × inch). This is not reasonable because this value is much less than that of the sites at Evansville, and the soils of Evansville are more cohesive and dense. When Equation 8 for the *S* factor (*6*) is applied, the value of *S* is 6.981. Then the *K* value is 0.0987, which is unreasonably low for the same reasons. The upper bound of the *K* factor for the site at Putnamville is 0.46, according to the nomograph. The lower bound is 0.394, which is the multiplication of 0.46 and 0.856, the compaction factor of the sites at Evansville. That is to say,

the lower and upper bounds of the *S* factor of the site at Putnamville are 1.50 and 1.75, respectively. In any case, the *S* factors proposed by previous researchers are too high to be applicable in this case.

The *S* factor of the site at Putnamville is a little bit higher than the *S* factor obtained from the tests at Evansville. The *S* factor may change with soil properties.

Relationship Between Total Erosion and Erosion Due to Very Wet Runs

Before dry runs, the test plots were naturally dry. It is somewhat difficult to simulate soil conditions in laboratory tests from which some indicators may be obtained to relate soil erodibilities and other factors. It is much easier to simulate soil conditions before and during very wet runs because the soils are nearly fully saturated. However, the relationship between total erosion, which consists of the total amount of erosion in dry, wet, and very wet runs, and erosion due to very wet runs should be found. Otherwise, the indicators obtained from the tests on fully saturated soils would be of little use.

Item 5 of Table 5 represents the division of total erosion by the erosion due to very wet runs. The mean value is 6.348 with a standard deviation of 0.311 and a coefficient of variation of 4.90 percent. This means that the relationship between total erosion and the erosion due to very wet runs is rather constant.

CONCLUSIONS

From the field erosion tests on highway slopes at Evansville, the *S* factor is extended to 50 percent from 18 percent as shown in Figure 7. The *S* factor reflects the development of rills, and the impact of raindrops, and appears to reach a maximum value of 1.5 at an intermediate value of slope steepness of 20 percent (11.2 degrees). This means that erosion due to interrill and rill erosion does not continue to increase with slope steepness.

The *S* factor of the site with a slope steepness of 49.7 percent at Putnamville is estimated to be 1.50 to 1.75, which is much less than that proposed by previous researchers but close to the *S* factor proposed in this paper.

For cohesive and compacted soils of the highway slopes at Evansville and Putnamville, total erosion is quite sensitive to discharge rate or slope length, but not sensitive to slope steepness.

For the erosion tests at Evansville, a critical discharge rate or a critical slope length appears to exist for a given slope steepness. When the discharge rate is less than this critical value, the erosion rate increases very little or not at all with the discharge rate. Beyond this critical value, erosion rate increases markedly with discharge rate.

The *S* factor changes with slope length, soil properties, and elapsed time. Accordingly, the *S* factor is not an independent factor.

For cohesive and compacted soils in this study, the soil erodibility factor is less than that from the nomograph of Wischmeier et al. (*9*). This effect may be described as the factor of compaction, which is less than 1.0.

For the field erosion tests in this study, the ratios of total erosion (which consists of dry, wet, and very wet runs) to erosion due to very wet runs are close to a constant. The mean value is 6.348 with a standard deviation of 0.311 and a coefficient of variation of 4.90 percent.

REFERENCES

1. K. M. Morgan and R. Nalepa. Application of Aerial Photographic and Computer Analysis to the USLE for Area Wide Erosion Studies. *Journal of Soil and Water Conservation*, Vol. 6, 1982, pp. 347–350.
2. W. H. Wischmeier and D. D. Smith. *Predicting Rainfall Erosion Losses*. Handbook 537. Science and Education Administration, U.S. Department of Agriculture, 1978, 58 pp.
3. D. K. McCool and G. O. George. A Second Generation Adaption of the Universal Soil Loss Equation for Pacific Northwest Drylands. Paper 83-2066. American Society of Agricultural Engineers, St. Joseph, Mich., 1983, 20 pp.
4. G. R. Foster. Modeling the Erosion Process. In *Hydrologic Modeling of Small Watersheds* (C. T. Hann, H. P. Johnson, and D. L. Brakensiek, eds.), ASAE Monograph 5, American Society of Agricultural Engineers, St. Joseph, Mich., 1982, Chapter 8, pp. 297–380.
5. O. R. Stein, Jr. *Erodibility and Related Soil Properties of Three Reclaimed Surface Mined Soils*. Master's thesis. Purdue University, West Lafayette, Ind., 1983, 133 pp.
6. D. K. McCool, L. C. Brown, G. R. Foster, C. K. Mutchler, and L. D. Meyer. Revised Slope Steepness Factor for the Universal Soil Loss Equation. Submitted for Publication in *Transactions of the American Society of Agricultural Engineers*, 1987.
7. G. R. Foster, W. H. Neibling, and R. A. Nattermann. A Programmable Rainfall Simulator. Paper 82-2570. Presented at 1982 Winter Meeting, American Society of Agricultural Engineers, 20 pp.
8. L. D. Meyer and D. L. McCune. Rainfall Simulator for Runoff Plots. *Agricultural Engineering*, Vol. 10, 1958, pp. 644–648.
9. W. H. Wischmeier, C. B. Johnson, and B. V. Cross. A Soil Erodibility Nomograph for Farmland and Construction Sites. *Journal of Soil and Water Conservation*, Vol. 26, No. 5, 1971, pp. 189–193.
10. M. H. Hussein and J. M. Laflen. Effects of Crop Canopy and Residue on Rill and Interrill Soil Erosion. *Transactions of the American Society of Agricultural Engineers*, Vol. 25, No. 5, 1982, pp. 1310–1315.
11. *Soil Survey Manual*. Handbook No. 18. U.S. Department of Agriculture, 1951, 503 pp.
12. J. Poesen. Surface Sealing as Influenced by Slope Angle and Position of Simulated Stones in the Top Layer of Loose Sediments. *Earth Surface Process and Landforms*, Journal of the British Geomorphological Research Group, Vol. 11, 1986, pp. 1–10.

Publication of this paper sponsored by Committee on Environmental Factors Except Frost.